New Horizons

HEC Approved Y-Category

Vol:# 81-82 Upto June 2014

ISSN 2226-3659

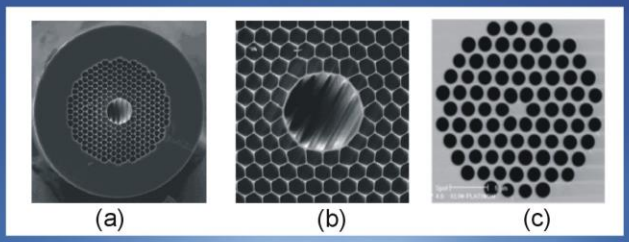

P.40

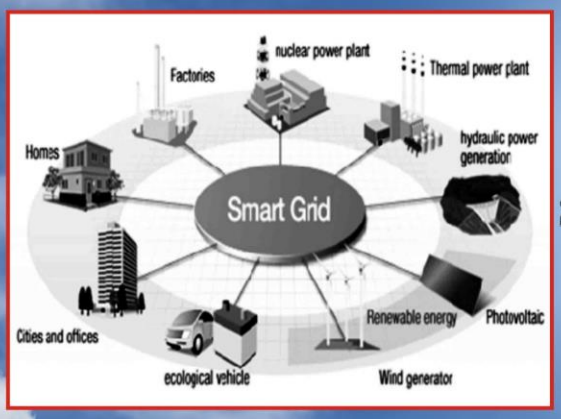

P.3

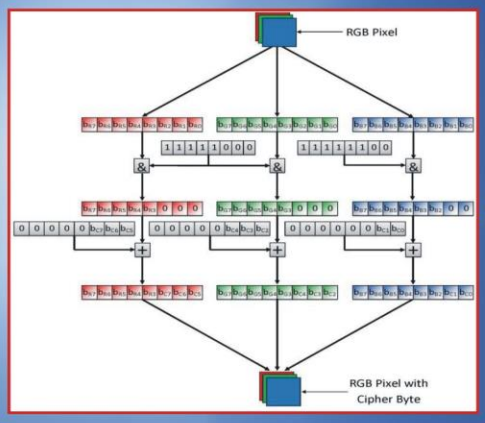

P.31

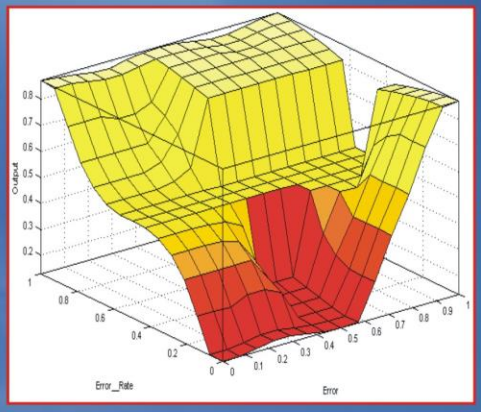

P.36

IEEEP

Journal of The Institution of Electrical and Electronics Engineers Pakistan

"New Horizons"

Journal of
The Institution of
Electrical & Electronics
Engineers Pakistan

VOL # 81-82 Upto June 2014

4-Lawrence Road, Lahore. Ph:(042) 36305289
Fax: (042) 36360287 Email:info@ieeep.org.pk
Website:www.ieeep.org.pk

CONTENTS

EDITORIAL

Continuing our mission of dissemination of knowledge to our engineering community, we are bringing to you some latest research and development papers in various fields of technology. Presently, as we all know, our country is facing extreme power shortages. Therefore, we encourage engineers to write papers with focus on possible techniques to help reduce this crisis. In this regard an informative paper describing "Smart Grid Capabilities" has been included. This emphasizes the need to integrate existing traditional sources of supply and the renewable sources in order to establish a new energy system which would help overcome existing and future challenges in a cost effective manner.

Another excellent paper studies "Hollow Core Fiber Design". Presently, photonic crystal fiber is a new technology of optical fiber which has provided secure and managed data transfer with low dispersion properties and confinement loss because of which it can be utilized in Wavelength Division Multiplexing Systems.

With the passage of time data protection is the most evolving topic of Information Technology. One included paper discusses this subject and proposes the technique of securing data by first using cryptology and then encodes the encrypted data using steganography. This makes it almost impossible for any individual to intrude the hidden message. This scheme can be used to transmit data securely and covertly over wired as well as wireless media.

Also included is a paper describing a computer aided program for "Designing an Optimized Current Transformer" and another article showing "Applications of a Dummy Load for Output Voltage Regulation".

There has been lot of delay in processing of Technical Papers especially from our Referees' side. We are trying our best to minimize these delays. Please see the back-page of this journal to clearly understand our "Time-Line for Papers Processing for IEEEP Quarterly Journal". Our respected Authors and Referees are requested to cooperate with us so that we can publish this Journal in a timelier manner.

Increase your knowledge from the technical papers presented in this journal.
God bless you; Allah hafiz!

Chief Editor.

Smart Grid Capabilities, Infrastructure, Impact on Power Suppliers/Consumers and Concerns

Riaz Ahmad Rana, Dr. Umar Tabrez Shami, Muhammad Saleem and Nabeel Khalid

ABSTRACT

This paper dwells on the need to integrate existing traditional sources of supply and the renewable sources in order to establish a new energy system which is energy efficient, reliable, controllable, secure, compatible, economical and sustainable. Smart grid can overcome existing and future challenges in a cost effective manner. In this paper, the main focus is on the smart grid infrastructure, its capabilities, communication scenarios, technologies and energy management. The implementation of the vision of modernized intelligent smart grid can overcome problems and challenges of traditional electricity grids and utilities. The paper also focuses on the services and factors that attract the consumers and utilities to change the way they operate in order to improve the current services. Various measures are proposed to help in implementation and adoption of smart grid vision in Pakistan. Finally, paper presents smart grid research programs, deployments, issues and concerns.

KEYWORDS – smart grid, renewable sources, load patterns, infrastructure, utilities, compatible, sustainable, scenarios.

1. INTRODUCTION

The term smart grid refers to the next generation electrical power grid in which information, communication and control technologies are used to collect process and transfer data/information between utility companies and customers in an automated manner with negligible delays [1]. A fully automated smart grid as shown in figure-1 has the following benefits over a traditional electric grid:

- Power flow is bi-directional in smart grid while uni-directional in traditional grid [2].
- Power generation is distributed in smart grid while centralized in traditional grid.
- Customers participate in smart grid as against in the traditional grid.
- Smart grid accessibility is expandable while of traditional grid is limited. e.g., enabling transition to plug-in-vehicles [3]
- Smart grid is environmental friendly as against that traditional girds.
- Power storage is possible in case of smart grid.
- Smart grid offers real time communication between suppliers, consumers, smart devices and regulating authorities as compared to traditional grid.
- Reliability, stability, controllability, efficiency and economics of smart grid is higher than that of traditional grid.
- Smart grid uses sensors throughout the network as against in traditional grid.

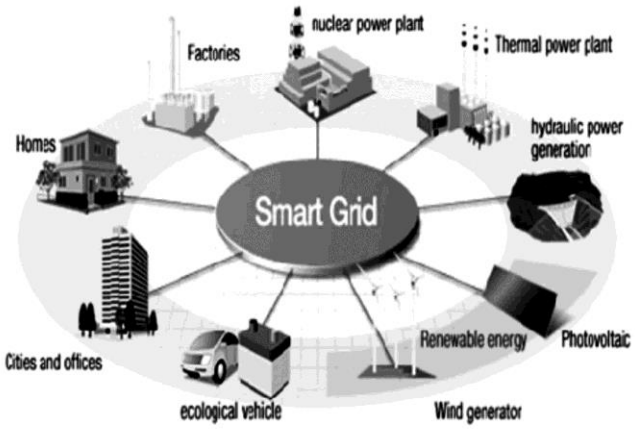

Figure-1: Pictorial Concept of Automated Smart Grid [4]

2. CAPABILITIES OF SMART GRID

Reliability: Smart grid ensures the reliability of the system. It detects and removes electrical faults automatically. *Network Flexibility & Integration*: Smart grid facilitates centralized as well as distributed energy sources. Traditional energy generation units and distributed generation units like solar systems, fuel cells, wind turbines, pumped hydroelectric power plants and superconducting magnetic coils may be integrated to improve system efficiency and flexibility [5].

Transmission Enhancement: : Smart grid uses FACTS (Flexible AC Transmission Systems), HVDC (High Voltage DC Systems), DLR (Dynamic Line Rating Technology) and HTS (High Temperature Superconductors) to improve transmission efficiency [6].FACTS and HVDC technologies are used to enhance the controllability of transmission line and optimize power transfer capability.DLR indentifies current carrying capability of a section of a network and optimizes utilization of existing transmission assets.HTS are used to reduce transmission losses and limit fault currents.

Load Management: In smart grid, efficiency of the power usage can be increased by managing the load at consumer side. Power plants do not need to produce extra energy during peak-load hours.

Demand Response Program: Smart devices installed at utility side and consumer side share information with each

other using communications technologies and remote switching is made in accordance with the consumer choice.

Utility companies can reduce consumption by communicating directly to devices installed at consumer end in order to prevent system overloads [7].

Power Quality: Smart grid provides different grades and prices of power to different customers. Customers get uninterrupted supply with better rates. Faults can be cleared in short time.

Environmental Capabilities: Smart grid helps to reduce greenhouse gases and other pollutants by reducing generation from inefficient energy sources and supporting renewable energy resources. It also replaces gasoline-powered vehicles with plug-in-electric vehicles.

3. HARDWARE INFRASTRUCTURE

Advanced Metering Infrastructure (AMI): Smart meter is usually an electrical meter that records consumption of electric energy in intervals of hours or less and communicates that information at least daily back to the utility for monitoring and billing purposes. AMI performs the following functions:[8]

- Demand Response Program (DRP) to consumers to reduce energy bills
- Smart metering to collect, store and report customer energy consumption data to control centers for bill generation
- Detection of losses and thefts
- Connection and disconnection of supply

Distributed Energy Storage Infrastructure: Distributed energy sources like wind, solar, biomass etc are integrated with traditional energy sources. Energy of renewable sources is stored in batteries and used for dc as well as ac loads. Addition of this energy optimizes efficiency, reliability and stability of the power supply system. . Main obstacle for employing additional flexible storage solutions such as batteries or pumped storage is their relatively high cost.

Electric Vehicle (EV) Charging Infrastructure: EV infrastructure of smart grid handles charging, billing and scheduling of electric vehicles. An electric vehicle is defined as a vehicle with an electric battery that can be charged from the network, i.e. Plug-in-Hybrid electric vehicles.

Home Energy Management Systems (HEMS):Smart appliances such as refrigerators ,air-conditioners, fans, washing machines, etc offer great control and reduce overall electricity consumption. Digital signal controllers deliver precise control of all smart appliances. HEMS are the interface between smart grid and domestic energy objects. Home energy management collects real time energy consumption data from smart meter and from various house objects. Consumers can see how their energy usage affects their costs and they can change their behavior.

Communication Infrastructure: Communication infrastructure used in smart grid includes:

1. Wide Area Network
2. Field Area Network
3. Home Area Network

When control centers are located away from consumers and substations, then wide area network (WAN) is used to transport real-time measurements of electronic devices to/from control centers and between different IEDs (Intelligent Electronic Devices). Smart devices are installed along power transmission lines, distribution lines, intermediate stations and substations to get messages/information and activate control as well as protection commands received from control centers. IEDs are micro-processor based smart electronic devices used for protection, local and remote monitoring and controlling a power station.

Field area network (FAN) is used to share and exchange information between applications and control centers that cover distribution domain. Field based applications like transmission lines, transformers, circuit breakers, relays, sensors, voltage regulators, etc use SCADA for exchange of information or data.

Customer based applications (houses, buildings, industrial users, etc) use AMI, DR (Demand Response), LMS (Load Management System), MDMS (Metering Data Management System), etc. for information and data exchange [5].

Home area networks (HAN) monitor and control smart devices in the customer domain. In customer domain, ESI (Energy Service Interface) is used between the utility and the customers to share information. Customer devices like fan, refrigerator, air-conditioner, etc are connected to smart meter via ESI and smart meter communicates with the utility to exchange information.

4. COMMUNICATION TECHNOLOGIES

Different communication technologies are used for message and data transfer in transmission, distribution and customer domains of smart grid. The available network technologies are:

1. Power line communication technology
2. Dedicated wire line communication technology
3. Wireless communication technology

In power line communication, power lines are utilized for electrical power transmission as well as data transmission. Typically data signals cannot propagate through transformers and hence the power line communication is limited within each line segment between transformers.

Dedicated wire-line cables separate from electrical power lines are used for data transmission. Dedicated transmission medium may be copper wire, coaxial cable, SONET, SDH, Ethernet and DSL. SONET (Synchronous Optical Network) is the international transmission standard for optical networks which gives much more data rates. SONET speeds are classified as optical carriers 1 (OC-1) to optical carriers 192 (OC-192).

Wireless communication networks are generally employed for short distance communication and transfer data at low rate. A number of wireless network standards are available to transfer data from utility to consumer and vice versa. The standard802.11 is widely used for LAN which transfers data at 150 Mbps up to 250 m. The standard 802.16 is used for broadband wireless internet communication. It sends data packets at data rate of up to 100 Mbps and covers 50 Km area. WiFi and ZigBee networks are used for home applications [9].

5. COMMUNICATION SCENARIOS

Communication scenarios represent data flow in smart grid infrastructure that may help for energy management. Following communication scenarios are illustrated:

Substation Control Scenario: Real-time monitoring and control of substation is achieved using local area networks (LAN), wireless WAN and Ethernet as depicted in figure-2 [10]. Special sensors are installed to take the equipment status samples, these samples are processed, digitized and sent to control center of substation for appropriate action. Each switch processes information and sends processed message to control center. Network delay for maintenance purpose is about 1 sec, for real-time monitoring and control is about 10 ms and for equipment fault information is about 3 ms.

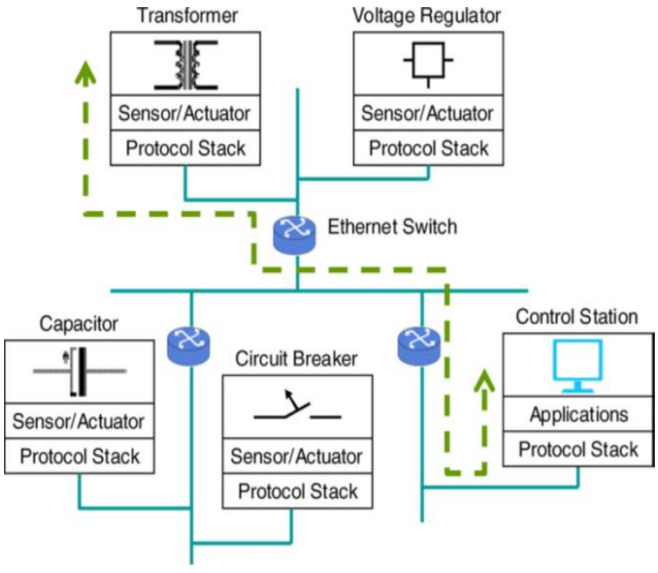

Figure-2: Substation Control Scenario

Transmission Line Monitoring Scenario: Sensors installed along power lines collect real-time data for line monitoring and control as laid out in figure-3 [10]. Data is digitized and transmitted to control center through wide area network. Transmission delay for fault message should not exceed 3 ms.

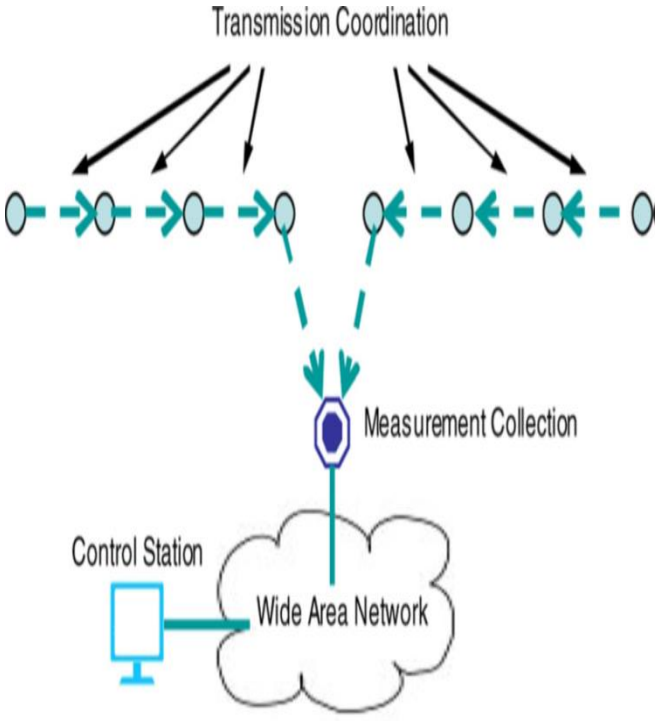

Figure-3: Transmission Line Monitoring Scenario

Automatic Meter Reading Scenario: Smart meters send meter readings automatically to utility companies over network for customer bill generation as shown in figure-4. Communication delay for meter readings is acceptable for few seconds.

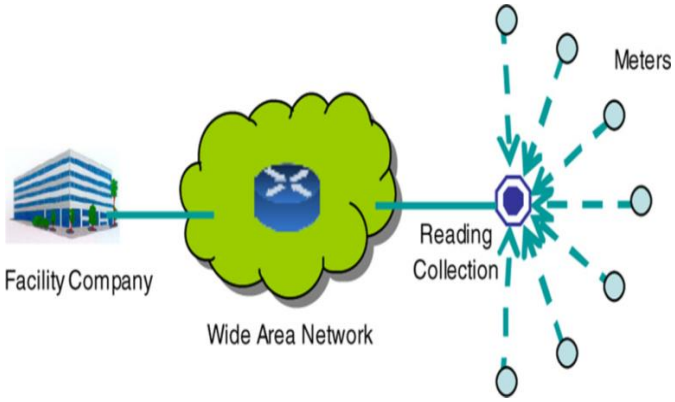

Figure-4: Automatic Meter Reading Scenario

Demand Response Decision Making Scenario: In smart grid, communication network will facilitate suppliers and customers for energy trading as shown in figure-5[10]. Network delay of a few seconds is acceptable to catch up with dynamic market states.

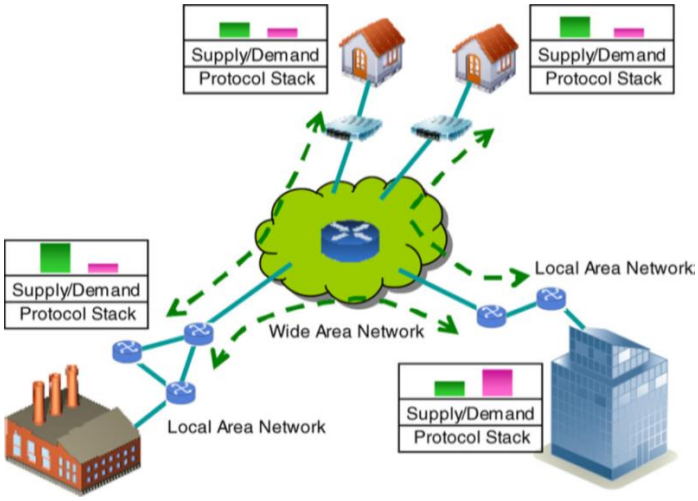

Figure-5: Demand Response Decision Making Scenario

Energy Usage Scheduling Scenario: Customers can take advantage of dynamic energy prices to reduce energy cost by scheduling time of low energy prices. Prices are low at night because demand of energy decreases when factories, schools, universities and office buildings are closed. Prices are high during daytime because electricity is largely used. This scenario is depicted below in figure-6 [10].

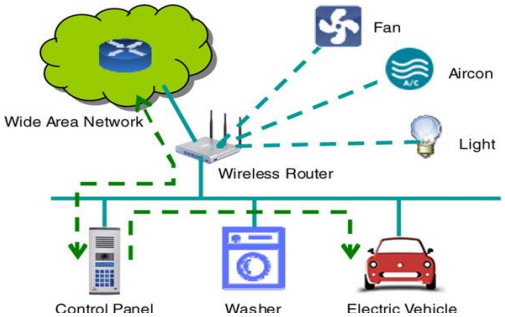

Figure-6: Energy Usage Scheduling Scenario

6. IMPACT OF OPTIMIZED AUTOMATED SMART GRID ON SUPPLY COMPANIES

- Real time status monitoring of network and smart devices
- Quick fault detection, location and troubleshooting
- Network self restoration and reconfiguration
- Direct reduction of energy usage having direct control on consumer appliances
- Increased capability of distributed generation
- Reduced transport losses
- Reduction of carbon emissions
- Usage of energy storage options
- Increasing network power load factors

7. IMPACT OF AUTOMATED SMART GRID ON POWER SUPPLY CONSUMERS

- Availability of uninterrupted quality supply
- Promotion of energy usage scheduling
- Plug-in-charging of hybrid vehicles
- Pollution free environment
- Mitigation of energy thefts

8. MAJOR RESEARCH PROGRAMS

IntelliGrid Program (U.S): Started by EPRI to replace traditional grid system by smart grid in order to improve quality, availability and controllability of supply delivery system. IntelliGrid provides funds worldwide to promote global research efforts and is also supplier of smart grid components [11].

MGI - Modern Grid Initiative(U.S): A number of bodies like DOE, NETL, utility companies, customers, and researchers are doing efforts to develop a fully automated modern smart grid [12].

Grid 2030 (U.S) Program: Joint program of government and non-government bodies to improve existing grids including generation, transmission, distribution and utilization. The vision of Grid 2030 program is to develop a more flexible, reliable, controllable and efficient electric power delivery system for United States. Universities, research laboratories, R&D departments, industries, government departments and investors are doing efforts to meet smart grid targets [13].

GridWise Program (U.S): This program facilitates utility companies and consumers to modernize electric power delivery system. It is a joint effort started by different government and non-government departments to implement the vision of smart grid in America. It provides funds, technology, software and hardware infrastructure and assistance to improve electric power delivery system [14].

GridWise Architecture Council (GWAC): Made by U.S, DEO to enhance interoperability between different smart devices in the electric supply system. GWAC provides consultancy to industry and utility companies regarding improvements in electric power delivery system [15].

GridWorks Program (U.S): The aim of this program is to improve efficiency, reliability, controllability, availability and safety of power electric system by optimizing the grid components. GridWorks emphasis on high quality cables, supper conductors, modern substations, reliable protective systems, harmonic free power electronic devices, flexible distribution systems, reliable transmission systems, distributed integrated technologies and energy storage technologies [16].

9. DEPLOYED SMART GRIDS

Enel (Italy) Smart Grid:1st smart grid project, Completed in 2005, project cost – 2.1 billion euro, annual saving – 500 million euro [17].

Austin, Texas (U.S) Smart Grid: Working since 2003, currently managing 500,000 real-time devices, servicing 1million consumers & 43000 businesses [18].

Boulder, Colorado Smart Grid:1st phase completed in August 2008 [19].

Hydro One Smart Grid: Ontario – Canada, servicing 1.3 million customers since 2010 [20].

10. ISSUES & CONCERNS

- New and immature technology
- Shortage of experts to implement smart grid
- High initial implementation cost
- No consumer privacy
- Complex (variable) rate systems
- Remotely-controlled supply concerns
- Emission of RF signals from smart meters

11. PROPOSALS FOR IMPLIMENTATION OF SMART GRID VISIONIN PAKISTAN

Government of Pakistan has initiated various projects on solar, wind and biomass power generation at different areas to meet demands of increasing loads and this distributed generation is to be added to national grid. In order to implement vision of smart grid, following points needs to be considered:

- Government must make effective and clear policies on future energy supply.
- National and international investors must be encouraged and facilitated in all respects to import infrastructure, technology and standards.
- Small projects regarding renewable energy (solar, wind, biomass, etc) be initiated and integrated to overcome existing and future power shortage crisis.
- Power energy departments be headed by qualified, eligible, dedicated, devoted and experienced persons to manage and implement vision of smart grid.
- Tax free import of hardware and technology be ensured.
- Universities, researchers and R&D departments be funded to carry out research projects to improve power delivery system using smart grids.

12. CONCLUSIONS

It is concluded that smart grid is expected to relieve the energy shortage problems by integrating renewable energy resources and two-way communication network may help for cost effective energy management.

Further, the issues of aging power infrastructure, work manpower, power theft, pollution free environment, electric power quality, availability, stability and controllability can be solved by deploying smart grids.

Smart grid infrastructure, communication technologies, communication scenarios, impact on utilities and consumers, research programs and smart grid deployments have produced new issues and concerns.

This work summarizes that fruitful collaborative efforts are still required from industrialist, transmission and distribution companies, power researchers, power monitoring bodies, government officials, power traders, policy makers, consumers, power equipment manufacturers and software experts to integrate and optimize emerging technologies for implementation of smart grid.

13. REFERENCES

[1] Ye Yan, "A survey on smart grid communication infrastructure: Motivations, Requirements and Challenges" IEEE communications surveys & tutorials, vol. 15, NO. 1, First Quarter 2013

[2] Xi Fang, "Smart Grid – The New and Improved Power Grid" IEEE communications surveys & tutorials, vol. 14, NO. 4, Fourth Quarter 2012

[3] Fangxing Li, "Smart Transmission Grid: Vision and Framework" IEEE transaction on smart grid, Vol.1, September 2010.

[4] Xiang Lu, "An Empirical Study of Communication Infrastructures towards the Smart Grid", IEEE transaction on smart grid, Vol-4, NO. 1, March 2013

[5] Xi Fang, "Smart Grid – The New and Improved Power Grid" " IEEE communications surveys & tutorials, vol. 14, NO. 4, Fourth Quarter 2012

[6] Chun-Hao Lo, "The Progressive Smart Grid System from Both Power and Communications Aspects" IEEE communications surveys & tutorials, vol. 14, NO. 3, Third Quarter 2012

[7] Chun-Hao Lo, "The Progressive Smart Grid System from Both Power and Communications Aspects" IEEE communications surveys & tutorials, vol. 14, NO. 3, Third Quarter 2012

[8] Daojing H, "An Enhanced Public Key Infrastructure to Secure Smart Grid Wireless Communication Networks" IEEE networks January/February 2014

[9] Zhong Fan "Smart Grid Communications: Overview of Research Challenges, Solutions, and Standardization Activities" IEEE communications surveys & tutorials, vol. 15, NO. 1, First Quarter 2013

[10] Wenye Wang, Yi Xu, Mohit Khanna "A survey on the communication architectures in smart grid", computer networks 55 (201) 3604-3629, www.elsevier.com

[11] "Electric Power Research Institute (EPRI)" www.epri.com/IntelliGrid(online)

[12] U.S. Department of Energy, National Energy Technology, Modern Grid Initiative, www.netl.doe.gov (online)

[13] U.S. Department of Energy, Office of Electric Transmission and Distribution, "Grid 2030" www.oe.energy.gov

[14] U.S. Department of Energy, Office of ElectricityDelivery and Energy Reliability, GridWorkswww.gridwise.org

[15] GridWise Architecture Council Interoperability Context Setting Framework, www.gridwiseac.org

[16] U.S. Department of Energy, Office of Electricity Delivery and Energy Reliability, GridWorks www.oe.energy.gov

[17] NETL Modern Grid Initiative-Powering Our 21 st Century Economy, www.netl.doe.gov

[18] "Building for the future": Interview with Andres Carvallo, CIO-"Austin Energy Utility"www.nextgenpe.com

[19] Betsy Loeff (2008-03), "AMI Anatomy: Core Technologies in Advanced Metering" Ultrimetrics Newsletter, www.mvv.de

[20] Best Loeff, Demanding Standards: Hydro One aims to leverage AMI via interoperability www.elp.com

14. BIOGRAPHIES

Riaz Ahmad Rana is an Assistant Professor in Electrical Engineering Department, University of Central Punjab Lahore Pakistan. He has eighteen years field as well as academic experience. His research interest includes electrical machines, renewable energy resources and smart grid. rana.riaz@ucp.edu.pk

Dr. Umar Tabrez Shami is an Assistant Professor in the department of Electrical Engineering, University of Engineering & Technology (UET) Lahore Pakistan. He received his Ph. D. degree in Power Electronics from Tokyo Institute of Technology Japan. His research interest includes electrical machines, power electronics, renewable energy resources and smart grid. ushami@ucp.edu.pk

Muhammad Saleem is currently working as lecturer in Electrical Engineering Department, University of Central Punjab Lahore. He received his M. Sc. degree in power engineering from University of Darmstadt Germany. His research interest includes power systems, energy storage technologies, renewable energy resources and smart grid. He has been working on smart grid project at HSE Germany. m.saleem@ucp.edu.pk

Nabeel Khalid is a lecturer in department of Electrical Engineering, University of Central Punjab Lahore. His research interest includes electrical machines, renewable energy resources, instrumentation & process control and smart grid. nabeel..khalid@ucp.edu.pk

****

Current Transformer Design Optimization

Muhammad Umar Aziz[1], Tahir Izhar[2] and Sohail Mumtaz Bajwa[3]

[1,3]National Transmission and Despatch Company Limited (NTDCL)
WAPDA, Lahore, Pakistan

[2]Department of Electrical Engineering,
University of Engineering and Technology, Lahore, Pakistan

Abstract

This paper devises a computer-aided program to design an optimized Current Transformer (CT) not only fulfilling the basic requirements of the user/client but also presents the most economical design. In the first step, basic equations for designing the CT have been set up and a computer program has been developed. Then a numerical optimizing technique i.e. pattern search has been used for determining the most economical design for a certain rating of a CT. To evaluate the workability and practicability, a CT has been designed and manufactured using the results obtained from the program. The results of this work have been then compared with the locally manufactured CT of same rating. Computer application has been developed using MS Excel with background coding in Visual Basic (VB).

Keywords— *Current Transformer, CT Design, Optimization, Computer, Visual Basic,*

I. INTRODUCTION

A CT in many ways differs from a normal transformer. It is connected in series with a circuit, whose current is needed to measure, and its primary and secondary currents are independent of the burden and these currents are of prime interest. The voltage drops are only of interest for determining exciting currents [1] - [3].

There are two types of CTs based on their application in power system [1], [4], [5]:

i. Measuring CT to feed the current to meters / energy meters

ii. Protection CT to feed current to protective relays.

The IEEE papers referred at [2] and [3] published in recent year i.e. 2007 and 2011 respectively, only discusses the performance and behaviour of a current transformer under different operating conditions while the papers at [6] and [7] published fifty years back, provide the basics calculation of CT parameters.

In the forthcoming sections, the basic theory relating to a current transformer, equations involved in the design process and the outline of algorithm employed to obtain the optimized solution will be discussed. In last two sections, the physical and electrical parameters of the CT designed using the developed program shall be compared with the CT manufactured locally to conclude viability of the work-done.

For the purpose of this research work, a 12 kV, 800/5 A metering current transformer of accuracy class 0.5 has been selected. This type of CT is commonly used in 11 kV incoming and outgoing feeders' panel in NTDC/ Distribution Companies' systems. In the first step, design equations for the current transformers have been step up then the numerical optimization technique has been used to obtain the most economical design. The computer application has been developed in a macro enabled EXCEL workbook.

II. BASICS OF CURRENT TRANSFORMER

A. Working Principle of a Current Transformer

For a short circuited CT [1], [2], [8], the simplified equivalent model of the CT is:

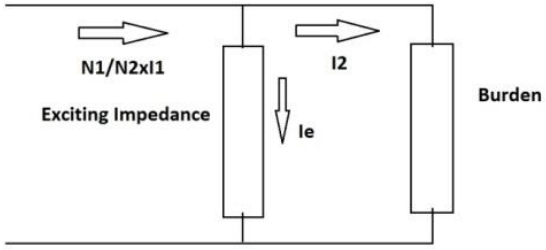

Figure 1: Simplified equivalent model of CT [1].

According to above,

$$I_2 = \frac{N_1}{N_2} I_1 - I_e \qquad (1)$$

I_1 = Primary current
I_2 = Secondary current
N_1 = Number of primary turns
N_2 = Number of secondary turns

Also, vector diagram for 1:1 current transformer, describing the relation between current, voltage and flux may be represented as follow:

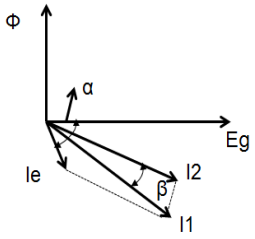

Eg = Induced Secondary Voltage
Φ = Flux
I1 = Primary Current
I2 = Secondary Current
Ie = Excitation Current
α = angle of excitation current
β = phase angle

Figure 2: Vector diagram showing the relation between current, voltage and flux in a current transformer [9].

B. Determination of Ratio and Phase Errors

Ratio and phase error introduced by a CT in the secondary current, are the function of the magnetizing

current I_e. The error produced in magnitude is due to the watt loss component of the excitation current I_e and the phase error is proportional to the reactive component of this current.

The phase error being the function of reactive component of the excitation current which varies widely over the current range, take the top priority in the design consideration of the current transformer [8].

A vector diagram between primary and secondary of 1:1 current transformer is shown in Fig. 3 with making two assumptions [1] and [8]:

a) The leakage reactance of the current transformer is neglected

b) The burden is purely resistive.

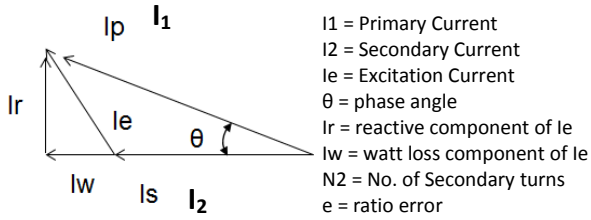

Figure 3: Vector diagram showing relation between primary and secondary current [1] & [8].

For above vector diagram;

$$sin\theta = \frac{I_r}{I_1} \quad (2)$$

$$i.e. \quad \theta = sin^{-1}\frac{I_r}{I_1} \quad (3)$$

However, in actual θ is so small that [8]

$$\theta \approx \frac{I_r}{I_1}\ (radian) \quad (4)$$

Also

$$I_1 = \sqrt{[(N]_2 I_2 + I_w)^2 + Ir^2} \quad (5)$$

Since θ is so small, hence the approximation [8]

$$I_1 \approx N_2 I_2 + I_w \quad (6)$$

and the ratio error as

$$e = \frac{I_w}{I_1}\ \mathbf{x\ 100\ (\%)} \quad (7)$$

III. CURRENT TRANSFORMER DESIGNING

The designing process of a CT consists of the following step:

A. Core Design

It is first and the most essential design parameter of a CT. Ratio and phase errors of a CT are directly dependent on this.

For toroidal cores, following three parameters are selected by the designer:

i) Internal diameter of the core (ID)

ii) Outer diameter of the core (OD)

iii) Step thickness or axial height of the core (HT)

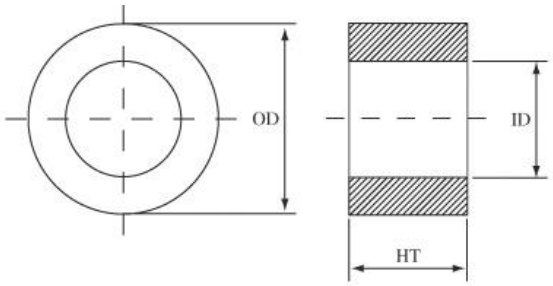

Figure 4: Geometry of toroidal core

The selection of internal diameter (ID) of the core is function of primary conductor size and Insulation class of CT.

B. Winding Design

The designing of winding in the case of CTs is quite straight forward and easy task as the maximum current flowing through the secondary winding is independent of VA burden on the current transformer.

The normally used secondary current ratings are of 1 A or 5 A, therefore, selection of the conductor depends upon the type of insulation used i.e. oil type or cast resin and the short circuit current capability of CT.

C. Error Calculation

After finalizing the core and winding design, the ratio and phase error shall be calculated for the designed core-coil assembly. The results should meet the error limits mentioned in the IEC 60044-1. The steps involved in the calculation are:

i. Calculation of secondary induced emf E_{si}(V):

$$E_{si} = I_s\ \mathbf{x}\ \text{[illegible]} \quad (8)$$

where

Z is total secondary impedance

$$Z = \sqrt{(R_b + R_{wind})^2 + X_b^2} \quad (9)$$

Where

R_b = Resistance of Burden in Ohm

R_{wind} = Resistance of Winding at 75°C

X_b= reactance of Burden in ohm

ii. Determination of Flux density B_m(T) required to induce E_{si}

$$B_m = \frac{E_{si}}{4.44 \mathbf{x} f \mathbf{x} N_2 \mathbf{x} A_{core}} \quad (10)$$

Where

f = frequency in Hz

N_2 = number of secondary turns

A_{core} = core area in mm^2

iii. Calculation of reactive and watt loss current

The reactive (H_r) and watt-loss (H_w) component of magnetizing force necessary to induce the flux density B_m can be obtained from the magnetizing curve of the core and consequently the I_r and I_w can be found as under:

$I_r = H_r \text{ x } L_m$ & $I_w = H_w \text{ x } L_m$ (11)

Where L_m = mean length of core in m.

iv. Determination of Ratio and phase errors

The error then calculated using equations (4) and (7).

D. Calculation of Instrument Security Factory (ISF)/ Accuracy Limit Factor (ALF)

The instrument primary current limit of metering CT is the value primary current beyond which CT core becomes saturated while the accuracy limit primary current of protection CT is the value of primary current up to which CT does not saturate. The ISF or ALF can be found using following relations:

i. Calculation of secondary limiting EMF and corresponding flux density:

$E_{limit} = \text{ISF x } I_s \text{ x Z or ALF x } I_s \text{ x Z}$ (12)

$$B_m = \frac{E_{limit}}{4.44 \mathbf{x} f \mathbf{x} N_2 \mathbf{x} A_{core}} \quad (13)$$

ii. Determination of I_e(A) and subsequently calculation of ISF/ALF:

$I_e = H_o \text{ x } L_m$ (14)

For measuring core:

$$\frac{I_e}{(I_2 \ x \ ISF)} \ x \ 100 \geq 10 \quad (15)$$

For protection core:

$$\frac{I_e}{(I_2 \ x \ ALF)} \ x \ 100 \leq composite\ error \quad (16)$$

IV. METHODOLOGY

Since it has been discussed in the above section, the core design is the first and the most important step as it directly affects the ratio and phase errors, therefore independent variables which affect the CT performance are ID, OD and HT. Other variable may be the diameter of the secondary conductor, but this does not have much effect on the performance of CTs. Only core design parameters have been considered while writing the optimization code.

The algorithm used for the optimization uses the basic blueprint of pattern search [10]. The flow chart of the working of the algorithm is shown below:

Step-1: **Input** data

⇩

Step-2: **Estimate** an initial design and stores it as optimum solution and corresponding material cost as minimum cost

⇩

Step-3: **Generate** discrete sets of each independent variable using some step value $X=\{\ldots,x_i+\Delta, x_i, x_i-\Delta,\ldots\}$

⇩

Step-4: **Using** discrete sets of Step-3, generate unique combinations independent variables

⇩

Step-5: **Do** design calculations for each combination

⇩

Step-6: **Find** the combination giving minimum cost and meeting requirement

⇩

Step-7: **while** *material cost obtained in Step-6 <>material cost of Step-2* material cost obtained in Step-6 is new optimum solution and go to Step-3

⇩

Step-8: **Output** the result

V. SIMULATION

Algorithm has been developed using macros of MS EXCEL. The macro consists of three Sub routine. First sub routine returns the initial solution, second Sub routine do the calculations of the combinations while in third Sub routine, main code is implemented. The graphical user interface has been developed using worksheets of MS EXCEL.

As it mentioned in above sections, we have selected the CT having characteristics as mentioned below:

i. Transformation ratio = 800 A / 5 A
ii. Type of CT = Metering (cast resin Box Type)
iii. Voltage class = 12kV
iv. Accuracy class = 0.5
v. Instrument security factor = 10
v. Short time withstand current = 12.5kA

In order to obtain the results from the program developed, following steps are performed:

Step1: The above data is entered in the worksheet name "Input". Also the other necessary inputs like clearance, size of primary conductor, rate of copper and core are also entered.

Step2: After providing the necessary inputs, push the button "Run optimization", and the 'opt' worksheet is appeared on which different calculation are being done by the main code.

Step3: When the program finds the optimum solution, it terminates the loop and the 'output' sheet appears.

The snapshot of 'output' sheet is shown below:

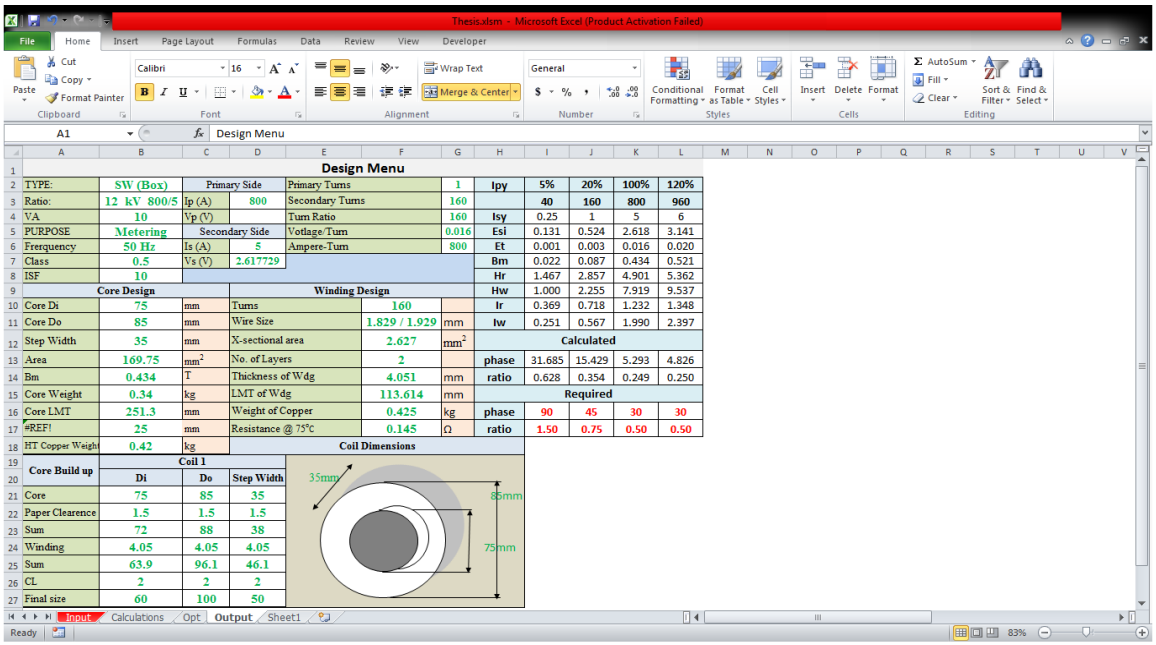

Figure 5: Snapshot of "Output" Worksheet

The output result obtained using this program is as under:

Table 1 PHYSICAL DIMENSION AND WEIGHTS

Dimensions in mm	ID	OD	HT
	75	85	35
	ID_final	OD_final	HT_final
	60	100	50
Weights in kg	Wcore	Wcond	Wcore+coil
	0.35	0.422	0.772

Table 2 Errors calculation

Ip	5%	20%	100%	120%
	40A	160A	800A	960A
Is	0.25A	1A	5A	6A
CALCULATED				
Phase	31.748'	15.463'	5.304'	4.839'
Ratio	0.628%	0.356%	0.250%	0.251%
REQUIRED				
Phase	90'	45'	30'	30'
Ratio	1.50%	0.75%	0.50%	0.50%

VI. VERIFICATION OF RESULTS & COMPARISON

Based upon output results, the core coil assembly of the CT was manufactured and tested using the CT accuracy test equipment in order to ascertain the viability of the devised program for real world implementation.

Figure 6: Picture of designed CT core and coil assembly

The physical dimensions and results of manufactured core coil assembly are summarized below:

Table 3 Physical Dimension and weights

Dimensions in mm	ID	OD	HT
	75	85	35
	ID_final	OD_final	HT_final
	62.4	106.3	43
Weights in kg	Wcore	Wcond	Wcore+coil
	0.40	0.43	0.830

The graphical representation of ratio and phase errors' allowable limit, their calculated and measured value are shown Figure 7 & 8.

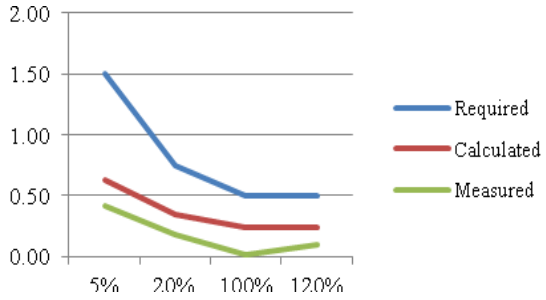

Figure 7: Percentage rated primary current Vs % Ratio error

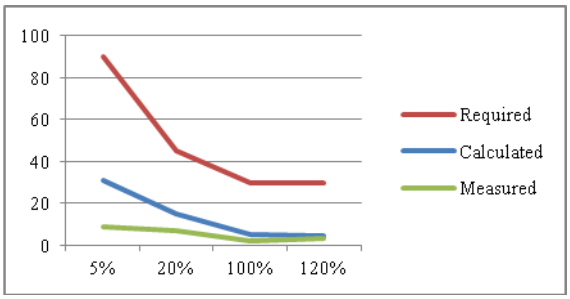

Figure 8: Percentage rated primary Current Vs % Phase error

The weights and material cost of the designed CT has been compared with the CT of same type manufactured locally. The comparison showed that the cost of designed CT's core coil assembly is 80% less than the locally manufactured CT. The summary of the comparison made is shown below:

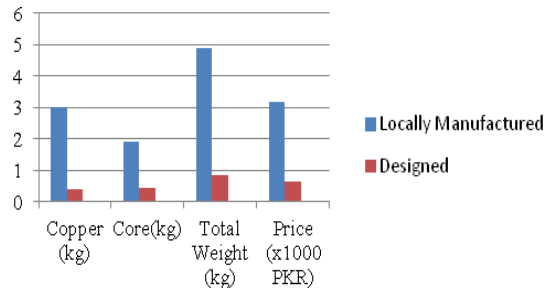

Figure 9: Graphical representation of weight and Price Comparison

It should also be noted that above comparison only considers the saving in secondary core coil assembly cost. The saving in primary conductor and volume of epoxy resin has not been considered in the comparison. If these are also taken into consideration, it may be established that the designed CT is not only economical but also it provides saving in volume/ space.

VII. CONCLUSION

The devised computer aided program for the designing of CT is not only easy and time saving but also provides the best economical design possible keeping in view all the practical constraints. The results obtained by using this program not only conform to experimental data but also provides economical solution as the saving in the copper and core is 85 % and 75 % respectively as compared to the locally manufactured CT which results in the cost of reduction of more than 80%.

The program developed can be improved by considering the industrial practices and also by including other features which are not included in this work like consideration of insulating resin and primary turn selections and its size and their consideration in selection of optimal solution. This program with slight change can also be applicable for protection type current transformer.

This paper is based upon the Master's thesis submitted in the Eletrical Engineering Department University Of Engineering And Technology Lahore.

REFERENCES

[1] Instrument Transformer Application Guide, ABB AB, High Voltage products Department Marketing & Sales Sweden

[2] M. Yahyavi, F. V Brojeni, M. Vaziri "Practical Consideration of CT Performance" 60th Annual Conference for Protective Relay Engineers, Texas A&M University 27-29 March, 2007

[3] H. E. Mostafa, A. M. Shalltoot & K..M. Youssef "Evaluation of Current Transformer Performance in the Presence of Remnat Flux and Harmonics" IEEE Jordan Conference on Applied Electrical Engineering and Computing Technology (AEECT), 6-8 Dec 2011

[4] Instrument transformer Part-1 Current Transformer, IEC Standard 60044-1, Edition 1.2, 2003-02.

[5] IEEE Standard Requirements For Instrument Transformers, IEEE standard C.57.13,1993.

[6] J. Meisel, Member IEEE "Current Instrument Transformer Error Calculations" IEEE Transaction on Power Apparatus and System, pp. 63-103, DEC. 1963.

[7] E.C Wentz, Associate AIEE, "A Simple Method For Determining Of Ratio Error And Phase Angle In Current Transformers," AIEEE Transaction, vol. 60, OCT. 1941.

[8] Wound Cores-A transformer Designer Guide, 1st Edition by WILTAN TELMAG

[9] Manual of Instrument Transformers - Operation Principles and Application Information, General Electric Edition GET-97D

[10] Virginia Torczon, Pattern Search Method for Non-Linear Optimization (2014) The College of William & Mary [Online]. Available: http://www.cs.wm.edu/~va/articles/

***

Creep force analysis at wheel-rail contact patch to identify adhesion level to control slip on railway track.

Zulfiqar Ali Soomro* PhD Scholar (Mech;Engg)
Imtiaz Hussain Kalwar Asstt.prof (Electronics)
Bhawani Shanker Chowdhary Emeritous Professor (Electronics)

Mehran University of Engineering and Technology Jamshoro (Sind) Pakistan

.Abstract:

Creep forces and creepage has a huge weightage in railway vehicle transport and wheel;-rail contact dynamics for detecting adhesion level to avoid the slippage of wheels from track for smooth running. In this paper, the wheelset dynamics comprising the longitudinal, lateral and spin moment creepage and creep forces along with their respective creep co-efficient has been enumerated and its mathematical modeling has been framed. The creep forces and creepage are analyzed under different adhesion levels to detect slip and slide of railway wheelset to prevent derailment.

Keywords: creep, adhesion, creepage, slip

1. INTRODUCTION

The interactive forces of the rail and the wheel have a significant effect on the dynamical behavior of the rail vehicle. The creep, Adhesion and wear can significantly affect the railway vehicle dynamics. The adhesion depends on the rough surfaces and environmental conditions upon rail runway. The concerned Creep forces depend on the dimensional profile of the rail and the wheel like the materials of the wheel and the rail. In order to calculate the sliding forces on the wheel/rail contact mechanics must be studied.[1]

There are various rolling contact theories in the literature that calculate longitudinal and lateral creep forces at the wheel/rail interface. Some of the more useful theories are Kalker's linear theory, Kalker's empirical theory, Johnson and Vermeulen's model, and the Heuristic nonlinear model [2]. Kalker's theories are often used for rail dynamics studies. Johnson and Vermeulen's theory is less accurate but has greater simplicity [1].

Wheel/rail contact creepages and creep forces are important in understanding the railway vehicle dynamics. For safe train operations, wheel/rail adhesion conditions are very important to consider when studying creep forces in order to avoid wheel skid during braking. In [3], The Polach (researcher) observed an advanced model of creep force for railway dynamic vehicle when running on proper adhesion limitation. He considered in his study, the influence of lateral, longitudinal, spin creepages, and the shape of the elliptical contact on the railway vehicle dynamic system. He also considered the friction co-efficient for dry and wet conditions and it is assumed that it is fixed for each simulation.

*corresponding: zulfiqarali_s@yahoo.com.

In [4] rolling contact phenomena, creepages on wheel/rail contact, and creep force models for longitudinal train dynamics are presented. Matsumoto, Eguchi and awamura [5] have presented a re-adhesion control method for train traction. Watanabe and Yamashita [6] have presented an anti-slip re adhesion control method using vector control without speed sensor.

Mei, Yu, and Wilson have proposed a new approach for wheel slip control [7]. The study is based on the detection of torsional vibration of a wheelset when slipping. Considering the shaft elasticity, a simplified model that consists of dominant modes of the wheelset is developed to investigate slip detection and re-adhesion scheme.

The de Beer et al. [8,9] searched a similar theoretical model based upon the excitation by unstablity lateral creepage. They have also invented an experimental rig based on a reduced scale wheel and roller representing the rail dynamics [10,11].

The Lateral creepage is thus likely to exist in combination with longitudinal creepage and the influence of longitudinal creepage on the mechanism of squeal noise behavior specifically the creepage/creep force relationship is of interest to learn. This paper presents some experimental results obtained for combined longitudinal, lateral and spin creepage. The correlation has been simulated to investigate the relationship between creepages and creep forces in the presence of 3-D creepages. Some of the simulated results from this investigation are presented and discussed below.

2. RAIL WHEELSET DYNAMICS

2.1 Creepage Computation

The Creepages can be formed when the two bodies do not have the exact same velocities. The term creepage or creep is used to define the slip ratio. These creepages can be, longitudinal creepage, lateral creepage and spin creepage.

Figure-1 below shows the graphical representation of creepages and associated creep forces in longitudinal, lateral and vertical directions. Since the wheel and rail are elastic bodies, the contact ellipse has a slip region and adhesion region.

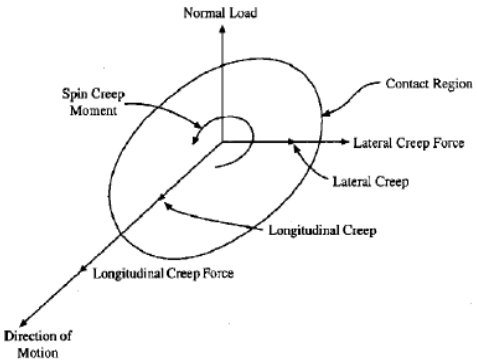

Figure-1 creep and forces acting on wheelset

Sliding occurs when the contact ellipse entirely becomes a slip region. In other words, when there is not enough adhesion between the two bodies, they will slip with respect to each other [2].

Following are the mathematical formulation is framed on each wheel depending upon its dynamics in terms of creep forces and total creepage of rail wheelset system.

2.1.1 Longitudinal creep on Rail wheelset

In case of rolling without slipping, the distance traveled by the wheel in one revolution is equal to the circumference of the wheel. But when torque is applied to the wheel, the distance traveled by the wheel in the forward direction is less than the circumference [12].

$$W_R = \frac{v}{r_R} and\ v = W_R * r_R$$

$$W_L = \frac{v}{r_L + ro} and\ v = W_L * ro$$

Above are angular/forward wheel velocities

Creepage of left wheel $= \lambda_L = \frac{r_o \omega_L - v}{v}$ (1)

Creepage of right wheel= $\lambda_R = \frac{r_o \omega_R - v}{v}$ (2)

Total longitd; creepage $= \lambda_x = \lambda_L + \lambda_R$ (3)

2.1.2 Lateral creep on Rail wheelset

The Lateral creepage is likely to exist in the combination with longitudinal creepage and the effect of longitudinal creepage on the mechanism for created squeal noise behavior, specifically the creepage and creep force relationship, is of interest to study and work on. [13].

lateralvel=$\dot{y}$= $v * \Psi$ Where $\Psi = 0.9250\ rad$

Creepage of left wheel (4)

Creepage of right wheel=Creep of left wheel

Total lateral creepage $= \lambda_y = \lambda_L + \lambda_R$ (5)

2.1.3 Spin/moment creep on left/right wheels

The longitudinal creepage λx is related with the difference between the rolling forward velocity and the circumferential velocity |V − Vcir|, the lateral creepage λy characterize the non alignment of the wheel with respect to the rail, while the spin creepage λsp is related with the concity of the wheel [14].

Spin$_L$(Ω_L $= \frac{w_L}{V}$ and spin$_R$ $(\Omega_R) = \frac{wr}{}$

Total spin creepage $(\Omega) = (\Omega L + \Omega R)$ (6)

Thus combining all above creepages we get total creepage of rail wheelset as under.

$$\lambda = \sqrt{\lambda_x^2 + \lambda_y^2 + \Omega} \quad (7)$$

2.2 Tangential contact forces

It may be possible to compute the tangential contact forces using one of the models available in the literature with the knowledge of the normal contact forces that procure between the wheel and rail and its creepages, i.e., the relative velocities. Three models arc presented here in order to allow for a comparative study between them to be developed. The Kalker linear evaluates the longitudinal and lateral components of the creep force and the spin creep moment, that develop in the wheel-rail contact region. The figure-2, displays the forward (v), lateral velocity (y) along with yaw motion (ψ), which have been used in calculating the creep analysis above. The creep forces acting upon left and right of rail wheelset in longitudinal, lateral and spin moment creep directions have been shown and calculated as under.

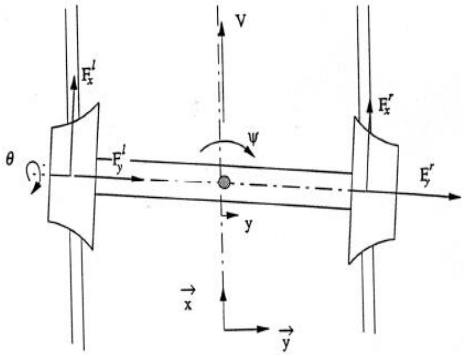

Figure-2 creep forces on left & right wheels

The longitudinal creep forces on right/left wheel are $F_{xR} = f_{11}\lambda_{xR}$ and $F_{xL} = f_{11}\lambda_{xL}$

The lateral creep forces on right/left wheel are $F_{yR} = f_{22}\lambda_{yR}$ and $F_{yL} = f_{22}\lambda_{yL}$

The Spin moment creep forces on right/left wheel are $F_{\Omega R} = f_{23}\lambda_{\Omega R}$ and $F_{\Omega L} = f_{23}\lambda_{\Omega L}$

Total creep forces = $Fx + Fy + F\Omega$

Where f_{11}, f_{22} and f_{23} are the creep coefficient of longitudinal, lateral and spin moment.

The tangential contact problem resolves the tangential creep forces acting on the contact patch. A deviation from pure rolling motion of the wheelset is caused by acceleration, traction, braking and the presence of lateral forces acting on the wheel-rail interface.

3. SIMULATION RESULTS

The mathematical model of wheelset dynamics presented in section-2 has been simulated and the simulation results are given as under

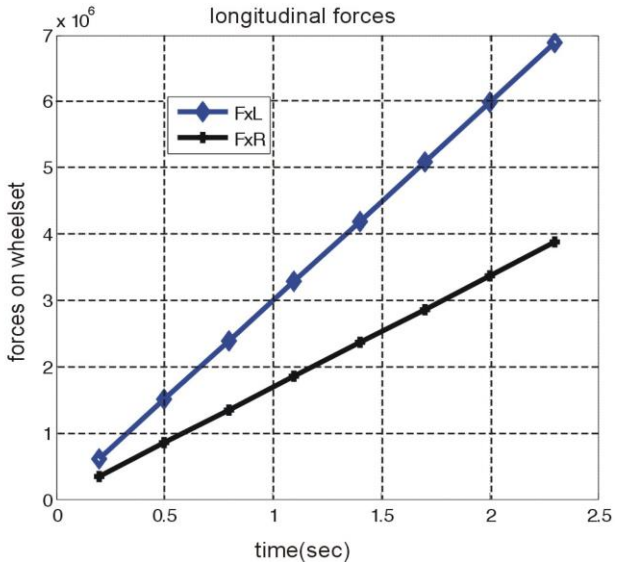

Fig-3 longitudinal forces on left/right wheels

In above figure-3, the relationship of longitudinal creep forces on each left and right wheels of railway wheelset contact have been shown. In this figure, left wheel creep force denoted by blue diamond reacts upper the black+ representing right wheel creep force. Both lines start from same origin point below 1 mN, then left wheel force increases upward and ends on 7 mN, while right wheel force increases but lower than that of left wheel ending at 4*10^6 N.

In the figure-4, the behavior of the lateral creep forces relationship for left and right rail wheelset has been denoted as under. Here lateral forces of left and right wheels start nearly below 0.2 mN to $1.8*10^{-9}$ N. These both lines overlap eachother as the lateral forces for left and right wheels is same as their creepages are also same.

The spin moment forces of left and right wheels relationship has been described as under.

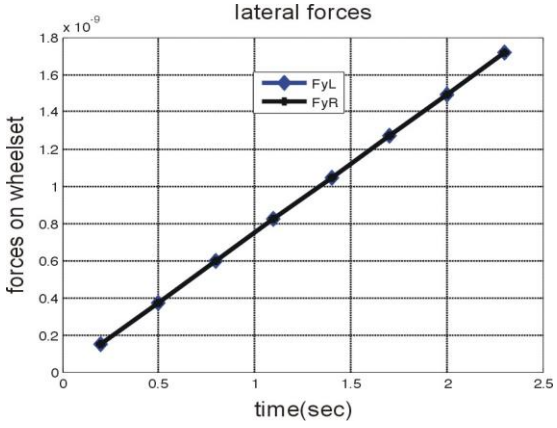

Figure-4 lateral forces on left/right wheels

Here spin force of right wheel denoted by black+ line of right wheel increases above spin force of left wheel increment. Both start below 1000 mN, whereas creep force of right wheel ends upto 6000 mN, while creep force ends 2000mN. From this diagram, it resembles differently as that of longitudinal creep forces for right and left wheels, where left wheel creep force is increasing above left wheel. While here in spin creep force of right wheel is replacing it

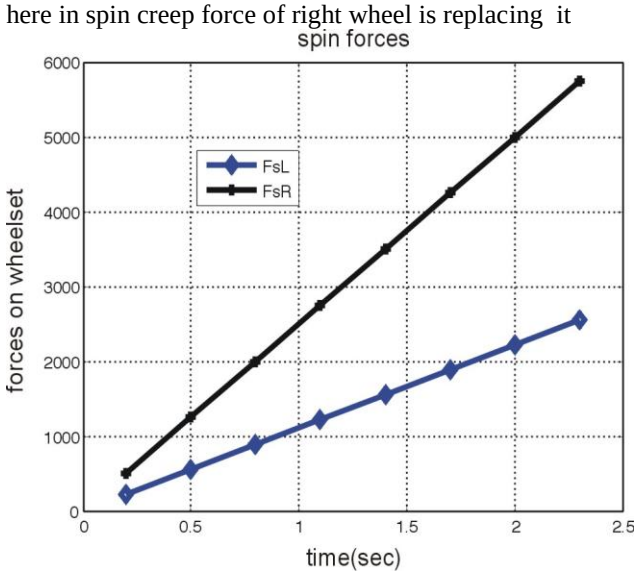

Fig-5 Spin moments on left/right wheels

In above fig-6, the total creep forces are compared with total creepage.

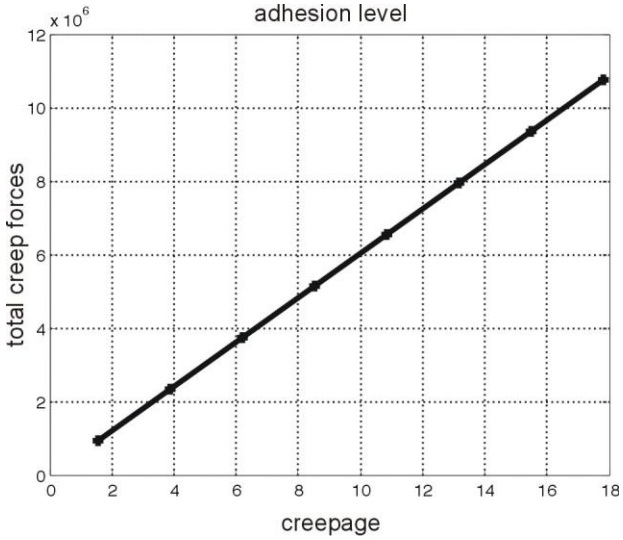

Fig-6 Relation of total creep force/creepage

Here the behavior of both has been shown in straight line, which shows that there is no tension of slippage which is ideal condition. Here total creep forces are increasing upward vertically with rise of total creepage horizontally.

CONCLUSION

In this paper, the creep forces acting upon each wheel of railway wheelset has been discussed, calculated and simulated by its expected results. These creep forces are

determined by applying concerned creep coefficient $f_{11}= f_{22}=$ 6.728e6 for longitudinal and lateral creepages while that of spin creep co-efficient as 1000 N/m^2. The correlation of these forces has been graphed and determined. However the fig-6 is shows apparent importance as it enumerates that creep forces and creepage behave linearly. This linearity of curve shows that there is no any slip due to sufficient adhesion level. This linear line proves the maximal of columb's law of motion which states that if the tangential forces (creep forces) are equal or greater than normal forces (creepage,μN). This creepage is perpendicular to creep forces giving relation creep coefficient.

REFERENCES

[1] Garg, V. K., & Dukkipati, R. V. *Dynamics of Railway Vehicle Systems*. Ontario, Canada:Academic Press, 1984.

[2] Dukkipati, R. V. *Vehicle Dynamics*. Boca Raton, Florida: CRC Press, 2000.

[3] Polach, O., "Creep Forces in Simulations of Traction Vehicles Running on Adhesion Limit," Elsevier, *Wear* 258, pp. 992 – 1000, 2005.

[4] Kung, C., Kim, H., Kim, M. & Goo, B., "Simulations on Creep Forces Acting on theWheel of a Rolling Stock." International Conference on Control, Automation and Systems, Seoul, Korea. Oct. 14 – 17, 2008.

[5] Matsumoto, Y., Eguchi, N.& Kawamura, A. "Novel Re-adhesion Control for Train Traction Systems of the 'Shinkansen' with the Estimation of Wheel-to-Rail Adhesive Force." The 27th Annual Conference of the IEEE Industrial Electronics Society. Vol. 2, pp. 1207 – 1212, 2001.

[6] Watanabe, T. & Yamashita, M. "Basic Study of Anti-slip Control without Speed Sensor for Multiple Drive of Electric Railway Vehicles." Proceedings of Power Conversion Conference, Osaka, IEEE Vol. 3, pp. 1026 – 1032, 2002.

[7] Mei, T., Yu, J. & Wilson, D. "A Mechatronic Approach for Effective Wheel Slip Control in Railway Traction." Proceedings of the Institute of Mechanical Engineers, Journal of Rail and Rapid Transit, Vol. 223, Part. F, pp.295-304, 2009.

[8] F.G. de Beer, M.H.A. Janssens, P.P. Kooijman, Squeal noise of rail-bound vehicles influenced by lateral contact position, Journal of Sound and Vibration (267) 497–507, 2003.

[9] F.G. de Beer, M.H.A. Janssens, P.P. Kooijman, W.J. van Vliet, Curve squeal of rail bound vehicles—part 1: frequency domain calculation model, Vol. 3, Proceedings of Inter noise, Nice, France, pp. 1560–1563 2000.

[10] P.P. Kooijman, W.J. van Vliet, M.H.A. Janssens, F.G. de Beer, Curve squeal of railbound vehicles—part 2: set-up for measurement of creepage dependent friction coefficient, Vol. 3, Proceedings of Inter noise, Nice, France, pp. 1564–1567, 2000.

[11] M.H.A. Janssens, P.P. Kooijman, W.J. van Vliet, F.G. de Beer, Curve squeal of rail bound vehicles—part 3: measurement method and results, Vol. 3, Proceedings of Internoise, Nice, France, pp. 1568–1571, 2000.

[12] A. A. Shabana, R. Chamorro, and C. Rathod. A multi-body system approach for finite-element modelling of rail flexibility in railroad vehicle applications. Proc. IMechE, Part K: Journal of Multi-body, 222(1), 2008.

[13] A. D. Monk-Steel, D. J. Thompson, F. G. de Beer, and M. H. A. Janssens. An investigation into the influence of longitudinal creepage on railway squeal noise due to lateral creepage. Journal of Sound and Vibration, 293, 2006.

[14] J. J. Kalker. A fast algorithm for the simplified theory of rolling-contact. Vehicle System Dynamics, 11(1), 1982.

****

Hand Structure Analysis for Finger Identification and Joints Localization

Mujtaba Hassan, Muhammad Haroon Yousaf

ABSTRACT

The development of kinematic model of hand can play a vital role in hand gesture recognition and Human Computer Interaction (HCI) applications. This paper proposes an algorithm for finger identification and joints localization, thus generating the kinematic model of human hand by means of image processing techniques. Skin tone analysis and background subtraction is carried out for hand detection in the workspace. Geometric features of hand are used for hand identification (left or right), finger identification and joints localization. Proposed algorithm is tested for diverse hand poses and remarkable results are produced. Algorithm not only generates the kinematic model for the different orientations of the hand but also have very low computational cost.[1]

Index Terms — Gesture Recognition, Hand Kinematic model, Finger detection, Joints Localization.

KEYWORDS – smart grid, renewable sources, load patterns, infrastructure, utilities, compatible, sustainable, scenarios.

I. INTRODUCTION

The hand has always been of significant importance to humans. In everyday life many interactions are performed by hand including object grasping, message conveying, and numerous other tasks. Keyboard and mouse are currently the main interfaces between man and computer. In recent years, the application of hand gesture has become an important element in the domain of Human Computer Interaction (HCI) [1, 2, and 3] or Human Machine Interaction.

Two general approaches can be applied to classify and analyze the hand gestures for HCI: contact and non-contact .Contact-based approach consists of mounting a device (usually gloves) to the hand which can capture the poses as hand moves. However there are issues associated with almost all glove - based techniques like portability, high cost, and calibration or low resolution. A detailed analysis and review has been done of glove-based techniques in [4] .The non contact or vision-based techniques are glove-free and can be divided into the three-dimensional (3-D) and the two-dimensional (2-D) approaches. In the 3-D approach, 3-D model of the human hand is developed and the parameters are derived to classify hand gestures. As 3- D hand models are quite complicated, as a consequence such models are computationally extensive which makes real-time classification difficult. Compared with 3-D models, the 2D models are relatively less complex. However, 2-D models are generally used with static hand gestures as they do not contain information regarding hand and finger movement for the classification of complex dynamic hand gestures.

Issues and problems related to 2D vision based hand gesture classification have been discussed, resolved and presented in [5]–[8]

In virtual world, the role of human hand interaction with virtual environment is escalating. A reasonable and precise model of hand may be required to be applied in virtual reality, medical simulation, animation, virtual prototyping, special-effects and games. However, modeling an accurate and realistic virtual human hand has always been a challenging task, as great skills are required since the human hand has a complex shape with many degrees of freedom (DOF)

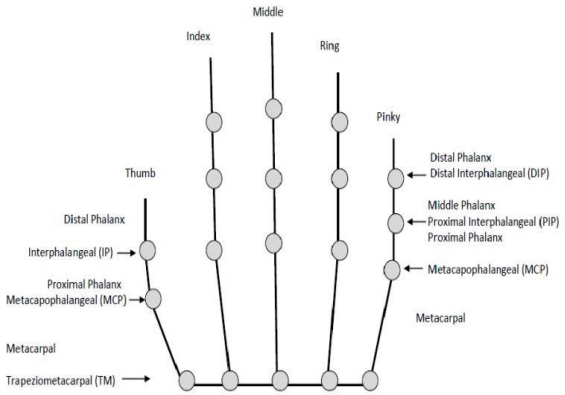

Fig. 1. Kinematic Model of Hand

Fig. 1 represents the kinematic model of hand, which illustrates the naming and localization of fingers and joints. As all ten fingers can take part in producing hand gestures, so these fingers are named according to their anatomical names as pinky, ring, middle, index and thumb. Joints in the human hands are named according to their location on the hand as metacarpophalangeal (MCP), Proximal interphalangeal (PIP) and Distal interphalangeal (DIP). Fig. 1 shows that thumb has only metacarpophalangeal (MCP), interphalangeal (IP) joints.

Many hand models are developed for HCI using vision-based approaches. Rhee et. al. [9] developed a 3D hand model from hand surface anatomy in which hand creases were used to detect hand fingers and joints. Parida et. al. [10] developed hand model for multi-fingered robotic hand in which kinematic modeling and analysis has been done [10]. Wu et. al. [11] contributed in detailed analysis of various hand models.

This paper aims to describe a fast and reliable algorithm, how kinematic model of hand based on 2D vision can be developed. Algorithm helps to identify and tag hand (right or left), hand

This work was supported by the Directorate of Advance Studies, Research and Technological Development, University of Engineering and Technology Taxila, Pakistan and Higher Education Commission of Pakistan

Mujtaba Hassan is a Lecturer in Electrical Engineering Department, NWFP UET Peshawar (Kohat Campus), Pakistan (Email: engr.mujtabahassan@gmail.com)

Muhammad Haroon Yousaf is Assistant Professor working with Video and Image Processing Laboratory, Department of Computer Engineering, University of Engineering and Technology Taxila, Pakistan. (E-mail: haroon.yousaf@uettaxila.edu.pk).

fingers (pinky, ring, middle, index and thumb), finger joints (MCP, PIP and DIP) and finger tips which can be used for the analysis of hand structure. Such kind of hand structure analysis can be utilized in developing hand gesture recognition applications.

II. Proposed Methodology

Proposed algorithm for development of kinematic model of hand is divided into six subunits. Flow chart shown in Fig. 2 presents the brief description of these sub-units. Sub-units are further discussed comprehensively in the subsequent sub-sections.

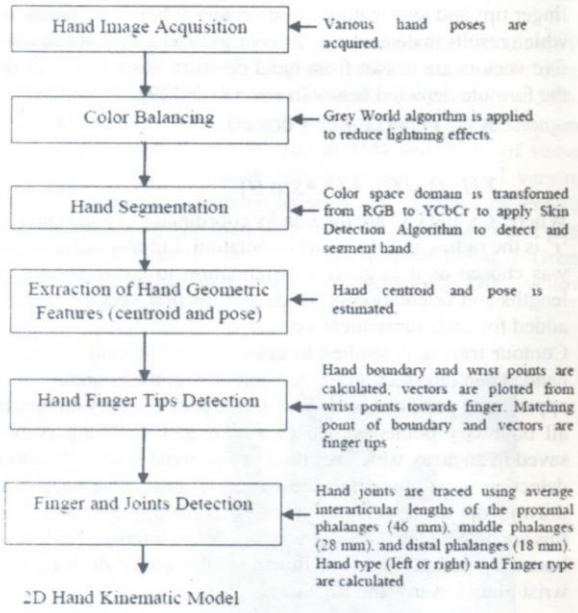

Fig. 2: Flow Chart of Proposed Methodology

A. *Hand image Acquisition*

Input comprises of image of hand captured in daily life illumination conditions in non-cluttered environment using a CCD/CMOS camera on a flat surface. Fig. 3 (a) shows the image of right hand captured at approximately 90° orientation.

B. *Color balancing*

Before proceeding to hand segmentation it is necessary to smooth input image in order to reduce the lightning effects imposed by the environment. Grey World Algorithm (GWA) [12] is selected for this purpose. The particular lightning effect can be removed by applying the gray world assumption on the image which results in color image that is very close to original scene. Gray World algorithm is based on the assumption that given an image with sufficient amount of color variations, the average value of the R, G, and B components of the image should be average to a common gray value.

$$R_{avg} = G_{avg} = B_{avg}$$

By scaling α, β and γ in the R, G and B color channels, illuminated color changes can be modeled as mentioned in [13].The algorithm provides solution which is independent of color luminance by dividing each color channel by its average value as shown in the following formula:

$$(\alpha R, \beta G, \gamma B) \rightarrow \left(\frac{\alpha R}{\frac{\alpha}{n}\sum_{i}^{n} R}, \frac{\beta G}{\frac{\beta}{n}\sum_{i}^{n} G}, \frac{\gamma B}{\frac{\gamma}{n}\sum_{i}^{n} B} \right) \quad (1)$$

Fig. 3(b) shows the results after applying Grey World algorithm. Smoothing variation can be observed as compared to original image.

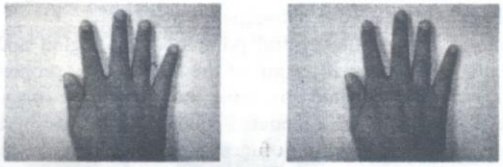

Fig. 3. (a) Input image (b)Input image after color balancing

C. *Hand Segmentation*

Image segmentation and hand detection work as foundation for modeling human hands. Segmentation is essential because it proceeds towards the extraction of the required hand region from the image background. Various algorithms and methods have been proposed to detect and segment visual features like shape, skin color, motion and anatomical models of hands. Performance of various hand segmentation techniques is already discussed in [14].

Detecting hand region in color image is fairly easy as skin color has its own unique property .Many color models exist to detect skin in image e.g. the RGB, HS (Hue, Saturation), normalized RGB and HSV (Hue, Saturation, Value), and YCbCr color spaces were employed in [15], [16], [17] and [18, 19] respectively. As luminance effects skin color so RGB model may impact as false skin color detection. So, YCbCr color model is opted in proposed algorithm to detect skin color in image .The input image after color balancing is transformed from RGB to YCbCr color space and then background is subtracted .A pixel is classified as skin pixel if it falls in certain ranges in YCbCr color space .The ranges are given below.

$$(Cb>=77 \ \& \ Cb<=127 \ \& \ Cr>=133 \ \& \ Cr<=173)$$

The input image is transformed from RGB to YCbCr color space and then all those pixels which fall in above mentioned range of YCbCr color space are denoted as marked pixels by assigning value "1" and unmarked pixels by assigning value "0", thus subtracting the background. Skin color detection and background subtraction results are shown in Fig. 4(a) and 4(b).

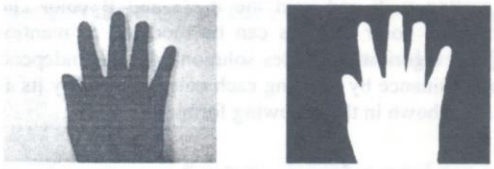

(a) (b)

Fig. 4: (a) Skin Color Detection (b) Hand Segmentation using background subtraction

D. Hand Geometric Features

After hand segmentation, geometric features of hand such as centroid and pose orientation are calculated. These geometric features will be used in subsequent stages.

Centroid depicts the central point of hand region and pose orientation tells the direction of the hand. Many properties of image can be calculated by using moment of the image [20]. These moments are calculated using regional properties of hand. For a 2D continuous function $f(x,y)$, moment is defined as

$$M_{pq} = \int_{-\infty}^{\infty} \int_{-\infty}^{\infty} x^p y^q f(x,y) dx dy \qquad (2)$$

The first order moment in x and y, normalized by the area, gives the centroid feature of hand region:

$$\bar{x} = \frac{M_{10}}{M_{00}}, \bar{y} = \frac{M_{01}}{M_{00}} \qquad (3)$$

$\bar{x}$ and $\bar{y}$ in eq. (3) returns the centroid of the hand region. Fig. 5 shows the centroid for the hand region in Fig. 4(b). Pose orientation is the angle between the x-axis and the major axis of the ellipse that has the same second-moment as the region. It can be processed by fitting an ellipse to the region by matching first- and second-order moments [20]. Principal Major and minor axis passes through centroid .Their direction is given by expression:

$$\frac{1}{2}\left(\frac{\mu_{02}-\mu_{20}}{\mu_{11}}\right) \pm \frac{1}{2\mu_{11}}\sqrt{\mu_{02}^{\ 2} - 2\mu_{02}\mu_{20} + \mu_{20}^{\ 2} + 4\mu_{11}^{\ 2}} \qquad (4)$$

Where

$$\mu_{11} = M_{01} - \bar{x}M_{01}$$
$$\mu_{20} = M_{20} - \bar{x}M_{10}$$
$$\mu_{02} = M_{02} - \bar{y}M_{01}$$

The moments can be estimated as mentioned below using intensities.

$$M_{00} = \sum_x \sum_y I(x,y) \qquad (5)$$

$$M_{10} = \sum_x \sum_y xI(x,y) \qquad (6)$$

$$M_{01} = \sum_x \sum_y yI(x,y) \qquad (7)$$

Fig. 5: Hand Centroid and Orientation (90°)

E. Hand Finger Tips Detection

This sub-unit focused on finger tips detection that is essential for finger identification and joints localization. Algorithm proceeds as drawing of five vectors from hand wrist towards finger tips and terminating those vectors at boundary points and which results in detection of finger tips. To take points on wrists five vectors are drawn from hand centroid towards wrist using the formula depicted below in eqs. (8) and (9):

$$X(i,j) = Cx + (r * \cos\theta) \qquad (8)$$

$$Y(i,j) = Cy + (r * \sin\theta) \qquad (9)$$

Where 'Cx and Cy' are the x and y coordinates of hand centroid, 'r' is the radius and 'Θ' is the orientation. Initially radius of 400 was chosen as it is good approximation to cover hand of all lengths and orientation of 70 degree for first vector and 12° is added for each subsequent vector.

Contour tracing is applied to draw contour around segmented hand. Then intersection of the vectors with the boundary at the appropriate positions is observed. It is performed by comparing all boundary points with each vector and matching point is saved in an array which resulted in five wrist points. Results of detecting wrist points are shown in Fig. 6(a). Five vectors are drawn from those wrist points towards hand fingers and finger tips are detected in the same way as vectors intersect the farthest boundary points. Fig. 6(b) illustrates the vector drawing from wrist pints towards the fingertips.

Fig. 6: (a) Hand Wrist Points Detection (b) Finger Tips Detection

F. Joints Localization and Finger identification

This sub-unit proceeds as tagging of hand type (Left or Right), identification of fingers, and localization of finger joints. In order to identify hand type, length of all five vectors drawn in Fig. 6(b) is calculated using formula given below:

$$L = \sqrt{(y_2 - y_1)^2 + (x_2 - x_1)^2} \qquad (10)$$

These lengths are than normalized and stored for future use. Simple logical analysis decides the tagging of hand. If the length of first vector is greater than fifth then it is right hand else it is left hand under the assumption that all four fingers and thumb are present in image.

Tagging of hand let the finger identification process quite simplified. In case of right hand then first vector will be representing pinky finger, similarly second, third, fourth and fifth vector represent the ring, middle, index and thumb respectively. For left hand the assigning order of fingers would be reversed.

Hand dimensions vary largely among humans. However, the progression of each finger approximately follows the Fibonacci sequence as seen by the average interarticular lengths of the proximal phalanges (46 mm), middle phalanges (28 mm), and distal phalanges (18 mm). [21]. As per this approximation, five vectors representing four fingers and thumb are segmented with ratios given below to find out the approximate location of joints in each finger and thumb.

It was found out that for fingers, metacarpophalangeal (MCP) joint, proximal interphalangeal (PIP) joint and distal interphalangeal (DIP) joint was located approximately at 55% , 73% and 86 % of vector length and for Thumb interphalangeal (IP) joint and MCP was located at 45% and 70 % of vector length .This approximation may work for hands of varying lengths. All detected characteristics and features by criteria mentioned above are than mapped to original hand and thus completing 2D hand kinematic model as shown in Fig. 7. Green markers represent finger tips, red represents DIP, yellow represents PIP and blue represents MCP.

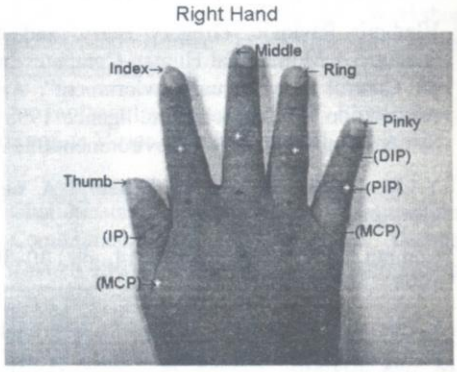

Fig .7: Kinematic Model of Hand Showing Identification of Fingers and Localization of Joints.

III. Experimental Results

Hand images with different poses were captured in daily-life conditions for the testing of the proposed algorithm. Fig. 8 shows the three poses for each hand i.e. (a) right hand pose at 90° (b) right hand pose at 60°(c) right hand pose at -60°(d) left hand pose at 90°(e) left hand pose at 60°(f) left hand pose at -60°.

Proposed algorithm of section II was applied to these images and result for color balancing, skin color detection, hand segmentation and centroid estimation, finger tip detection and finger identification and joints localization can be seen in Fig. 9, 10, 11, 12 and 13 respectively.

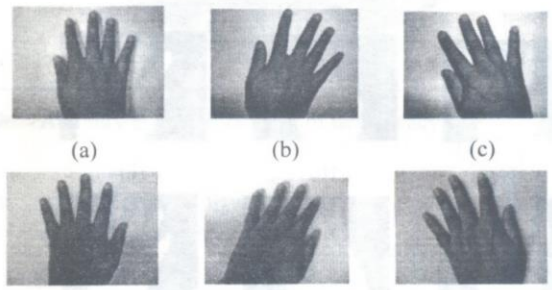

Fig. 8: Input images at different poses (a) right hand pose at 90° (b) right hand pose at 60°(c) right hand pose at -60°(d) left hand pose at 90°(e) left hand pose at 60°(f) left hand pose at -60°.

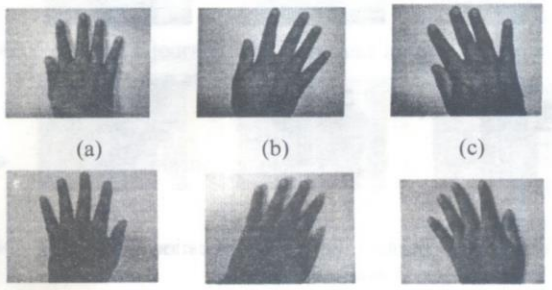

Fig. 9: Input hand Images after implying color balancing.

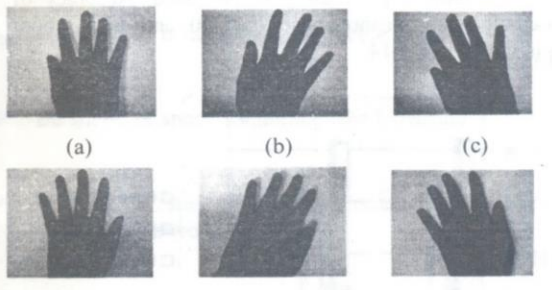

Fig. 10. Marked skin pixels

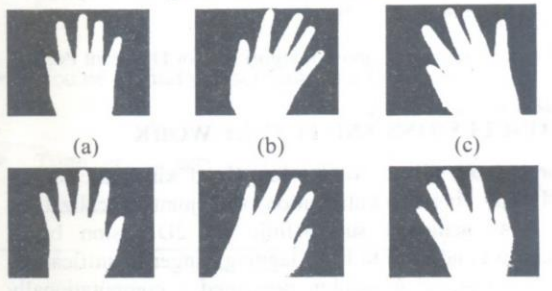

Fig. 11: Hand Segmentation with Centroid and Orientation

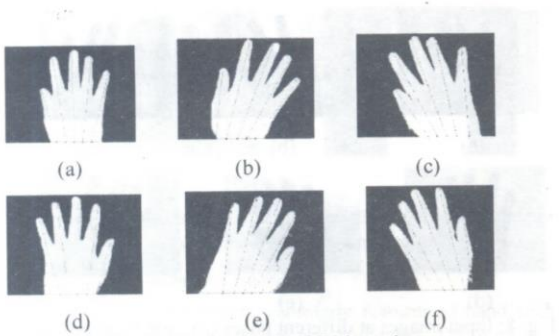

Fig. 12: Finger tips and Wrist points

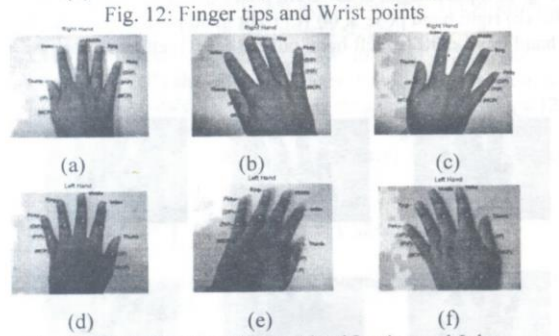

Fig 13: Hand Tagging, Finger Identification and Joints Localization Results

Proposed algorithm was tested on hands with varying dimensions. For this purpose hand images of approximately 50 different persons were acquired, tested and very acceptable results were produced for all poses of hand. Accuracy of proposed algorithm for three poses (60˚, 90˚ and -60˚) of both hands is shown in Fig 14.

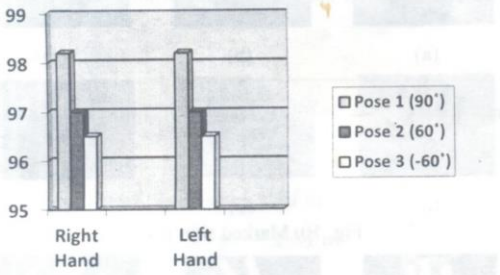

Fig.14. Accuracy of Proposed Algorithm for Different Poses

IV. CONCLUSIONS AND FUTURE WORK

Research work aimed to develop Hand kinematic model (HKM) for finger identification and joints localization, which was achieved successfully. A 2D vision based approach was adapted to hand tagging, finger identification, joints localization. Algorithm presented a computationally fast mechanism for the development of kinematic model for static hand poses. Reliable results were observed by apply algorithm on different hand poses of various persons.

In future, research work will be focused on developing kinematic model of hand under diverse backgrounds, cluttered environments and varying lightning conditions. Finger identification and joints localization can be employed in various hand recognition applications and can be taken into account in HCI application as well. Research work can be deployed in developing mechanism for non-contact mouse, controlling of home appliances, vision based virtual keyboard and in-car applications etc. Use of thermal images or bone scans of hands for structural analysis can lead to better medical diagnosis for the patients. Deployment of joint shape and motion information of hands may reveal new dimensions in human activity recognition.

ACKNOWLEDGMENT

Authors are thankful to Dr. Hafiz Adnan Habib for his immense guidance. Authors are also thankful to the peers involved in the images dataset collection for the project.

REFERENCES

[1] J.K.Aggarwal, Q.Cai, “Human Motion Analysis: A Review,” IEEE proc. Nonrigid and Articulated Motion Workshop’97, pp90-102, 1997.

[2] R.Kjeldesn, J.Kender, ”Toward the Use of Gesture in traditional User Interfaces”, IEEE Automatic Face and Gesture Recognition, pp151-156,1996.

[3] Vladimir Pavlovic, Gregory Berry, and Thomas Huang, ”A Multimodal Human-Computer Interface for Control of a Virtual Enviornment”, American Association for Artificial Intelligence 1998 Spring Symposium on Intelligent Environments, 1998.

[4] Y. D. J. Sturman and D. Zeltzer, “A survey of glove-based input,” IEEE

Comput. Graph. Appl., vol. 14, pp. 30–39, Jan. 1994.

[5] J. Lee and T. L. Kunii, “Model-based analysis of hand posture,” IEEE

Comput. Graph. Appl., pp. 77–86, Sept. 1995.

[6] B. Moghaddam and A. Pentland, “Probabilistic visual learning for object recognition,” IEEE Trans. Pattern Anal. Machine Intell., vol. 19, pp.696–710, July 1997.

[7] T. Staner, J. Weaver, and A. Pentland, “Real-time American sign language recognition using desk and wearable computer based video,”IEEE Trans. Pattern Anal. Machine Intell., vol. 20, pp. 1371–1375, Dec. 1998.

[8] Y. Cui and J. Weng, “A learning-based prediction-and-verification segmentation scheme for hand sign image sequence,” IEEE Trans. Pattern Anal. Machine Intell., vol. 21, pp. 798–804, Aug. 1999.

[9] Taehyun Rhee ,Ulrich Neumann , J.P. Lewis “Human Hand Modeling from Surface Anatomy ” ,ACM SIGGRAPH Symposium on Interactive 3D Graphics and Games,2006.

[10] Parida, P K Biswal, B B Khan, M R , "Kinematic Modeling and Analysis of a Multifingered Robotic Hand ",Advanced Materials Research Vols. 383-390 , pp 6684-6688 ,2012

[11] Ying Wu, Thomas S. Huang "Hand modeling, analysis and recognition ", Signal Processing Magazine, IEEE , Volume: 18 , Issue: 3 ,Page(s): 51 – 60 ,2001.

[12] G.D. Finlayson, B. Shiele and J.L. Crowley. Comprehensive colour normalization Proc. European Conf. on Computer Vison (ECCV). Vol. I, 475-490, Freiburg, Germany. 1998

[13] Jose M. Buenaposada; Luis Baumela , "Variations of Grey World for face tracking" ,International Conference on Computer Analysis of Images and Patterns. Vol. 7, no 3-4, 2001 .

[14] M.Cote,P. Payeur, and G. Comeau. Comparative study of adaptive segmentation techniques for gesture analysis in unconstrained environments. In IEEE Int. Workshop on Imagining Systems and Techniques, pages 28 to 33, 2006.

[15] J. Fritsch, S. Lang, M. Kleinehagenbrock, G. A. Fink and G. Sagerer, IEEE Int. Workshop OIL Robot and Human Interactive Communication, September 2002.

[16] N. Tanibata, N. Shimada and Y. Shirai, Proc. oflnt. Conf on Virion Interface, pp.391-398.2002.

[17] N. Soontranon, S. Aramvith and T. H. Chalidabhongst, lntcmatiorial Symposium on Communications and Information Technologies 2M14 (ISCLT 2004) Sapporo, Japan, October 26-29, 2004.

[18] R. L. Hsu, M. Abdel-Mottaleh and A. K. Jain, , IEEE Tram. on Pattern Airalysir and Machine Intelligence,vo1.2, NOS, pp.696-706, May 2002.

[19] J. Yang and A. Waibel, Proc. of Third Workshop OII Applications of Computer Vision, 1996, pp.142-147.

[20] Haralick and Shapiro, Computer and Robot Vision vol. 1, Appendix A, Addison-Wesley ,1992.

[21] Johan M. F. Landsmeer Fadi J. Beijjani. "Basic Biomechanics of the Musculoskeletal System". In: ed. by M Nordin and VH Frankel. Lea & Febiger, Chap. Biomechanics of the hand, pp. 275 to 304, 1989.

****

Quotations

- Adultery is the application of democracy to love.
  H.L. Menchen
- There's nothing like a good dose of another woman to make a man appreciate his wife.
  Clare Boothe Luce
- No act of kindness, no matter how small, is ever wasted.
  Aesop
- All cruelty springs from weakness.
  Seneca the Younger
- Peace is a journey of a thousand miles and it must be taken one step at a time.
  Lyndon B. Johnson
- Nothing can bring you peace but yourself.
  Ralph Waldo Emerson
- Peace hath her victories, no less renown'd than war.
  John Milton
- Peace, like charity begins at home..
  Franklin D. Roosevelt
- Superstition is the religion of feeble minds.
  Edmund Burke
- Be silent, or speak something worth hearing.
  Thomas Fuller
- Nothing so stirs a man's conscience or excites his curiosity as a woman's silence.
  Thomas Hardy
- You can never give complete authority and overall power to anyone until trust can be proven.
  Bill Cosby
- You never find yourself until you face the truth.
  Pearl Bailey
- Truth, like surgery, may hurt, but it cures.
  Han Suyin

Applications of a Dummy Load for Output Voltage Regulation of a Self-Excited Induction Generator for Hydroelectric Power Generation

Shariq Raiz[1], Umar T. Shami[2], and Tahir Izhar[3]

[1,2,and 3] Electrical Engineering Dept., University of Engineering and Technology, Lahore.

ABSTRACT

This research paper presents a technique to regulate the output voltage of self-excited induction generators. The self-excited induction generators output terminals are normally equipped with parallel connected excitation capacitors. A mismatch occurs when the load on the SEIG changes and thereby creating voltage deregulation. This research paper presents the connection of a three-phase dummy load for voltage regulation purposes. The dummy loads are equipped with IGBT based switching for becoming on-load or off-load. Simulation of SEIG with the dummy load is presented.

Keywords- Self-excited induction generators, Hydroelectric Power Generation, variable load.

I. INTRODUCTION

Although the self-excited induction generators (SEIG) were invented many decades ago. However, in recent times the use of SEIG systems for producing electric energy from non-traditional sources, has gained considerable strength [1]-[3]. Nevertheless, SEIG systems have unstable frequency, output power, and output voltage problems. On the centenary, synchronous generators are mostly successful in producing electricity in large bulk due to the volume and cost.

The scope of this paper is to show a method to regulate SEIG output voltage. The technique presented is based on the fact that SEIG output voltage remains stable as long as the load remains same. A change in the load will shift the operating properties of the SEIG and the voltage will deregulate. If a dummy load is connected along with the actual load, then by adjusting the dummy load counter to the load changes, the voltage can be regulated [3].

In our work, a SEIG is coupled with a hydroelectric turbine. Hydroelectric power is the source of generation of electricity in this case. It is assumed that the hydroelectric turbine provides constant amount of power. The primary objective is to solve for SEIG output voltage regulation.

TABLE 4. Parameter Definitions

Parameter	Definition
R_s	Stator resistance
$L_s=L_m + L_{ls}$	Stator inductance
R_r	Rotor resistance
$L_r=L_m+L_{lr}$	Rotor inductance
C	Excitation Capacitance
ω_r	Rotor speed
L_m	Magnetizing inductance
i_{ds}	d-axis stator current
i_{qs}	q-axis stator current
i_{dr}	d-axis rotor current
i_{qr}	q-axis rotor current
R	Load resistance

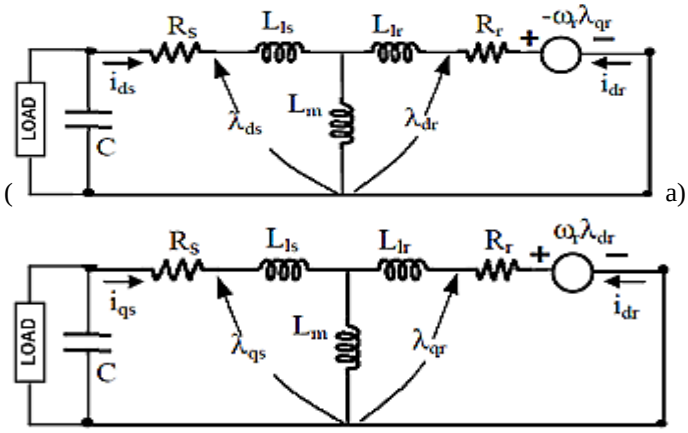

Fig. 1 The SEIG machine stationary reference frame models (a) d-axis model. (b) q-axis model.[1-4]

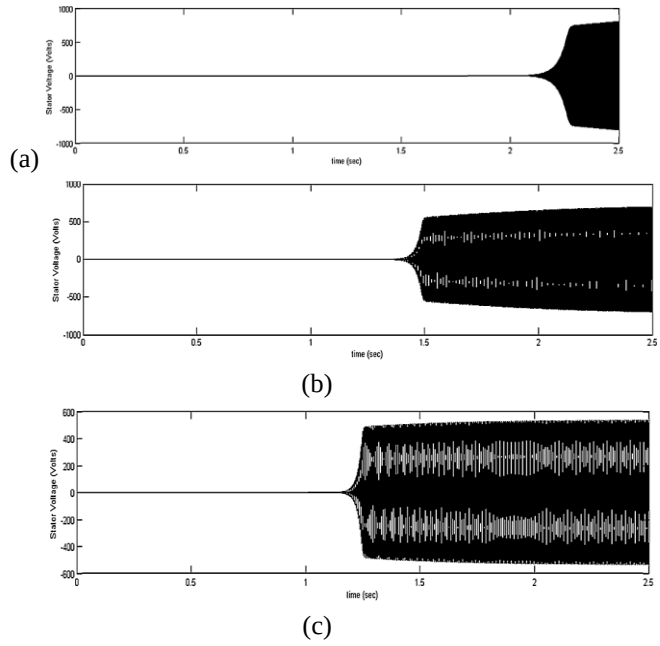

Fig.2 Shows the voltage generation process with respect to time for (a) C=10μF (b) C=30μF, and (c) C=50μF.

II. THE TRADITIONAL SEIG MODEL

The traditional d-q model of a SEIG machine in the stationary reference frame is shown in fig. 1 [4]-[6]. Such a model will be used during the simulation stage of the proposed system. Various parameters of the d-q model are defined in Table-I. The external capacitance C connected across the load is used to voltage generation and will be dealt in a preceding section.

The d-q model of the SEIG can be expressed mathematically by the following matrix [3],[4],[5],[6], i.e.,

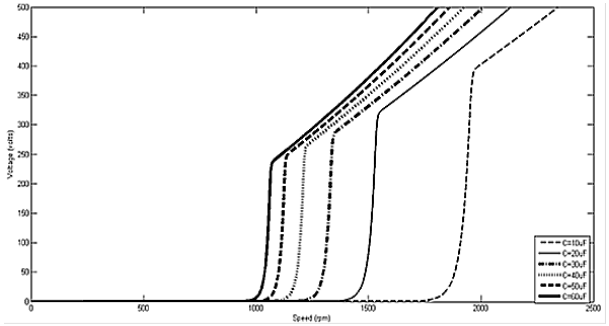

Fig. 3 SEIG output voltage as a function of rotor speed for changing values of excitation capacitance C.

$$\begin{bmatrix}0\\0\\0\\0\end{bmatrix}=\begin{bmatrix} R_s+sL_s+\dfrac{1}{sC} & 0 & sL_m & 0\\ 0 & R_s+sL_s+\dfrac{1}{sC} & 0 & sL_m\\ sL_m & -\omega_r L_m & R_r+sL_r & -\omega_r L_r\\ \omega_r L_m & sL_m & \omega_r L_r & R_s+sL_s\end{bmatrix}\begin{bmatrix}i_{qs}\\ i_{ds}\\ i_{qr}\\ i_{dr}\end{bmatrix} \quad (1)$$

The expansion of (1) leads to an eighth order differential equation, shown as follows, i.e.,

$$\left[As^4+Bs^3+Cs^2+Ds+E\right]^2+\left[Gs^2\right]^2=0 \quad (2)$$

Where,

$$A=L_r^2L_sC-L_m^2CL_r \quad (3)$$

$$B=L_r^2R_sC+2R_rL_rL_sC-L_m^2CR_r \quad (4)$$

$$C=L_r^2+2R_sR_rL_rC+(R_r^2+\omega^2L_r^2)L_sC-L_m^2C\omega^2L_r \quad (5)$$

$$D=2RrLr+(R_r^2\omega^2L_r^2)R_sC \quad (6)$$

$$E=R_r^2+\omega^2L_r^2 \quad (7)$$

$$G=L_m^2C\omega R_r \quad (8)$$

III. SEIG VOLTAGE GENERATION PROCESS

The rotors of most SEIG are permanent magnetics (residual flux) in addition to rotor windings. The residual flux aids in inducing an EMF(electro-motive force) on the stator windings. The induced EMF is feedback to the rotor windings, thus creating a positive feedback and the stator voltages tends to increase. The external capacitance C connected across the load plays vital role during the build-up process of the output voltage. However, when the lagging VARs required by the SEIG machines is equal to the VAR of the external capacitor C, the stator voltage will be saturated. At this point the system has reached to equilibrium. Such a voltage generation process is unique to SEIG machines and it is the reason why SEIG machines are used in remote small scale electrical generation units.

Since the early invention of the SEIG machines, it is a known fact that larger the value of the excitation capacitance C, the larger the generation of SEIG output voltage will be obtained at a lower rotor speed [3] and [7].

Similar results were obtained when the above mentioned system was simulated in MATLAB computer simulation software.

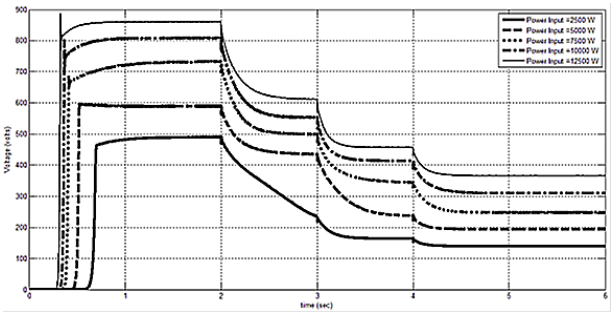

Fig. 4. SEIG output voltage for changing load and changing values of input power.

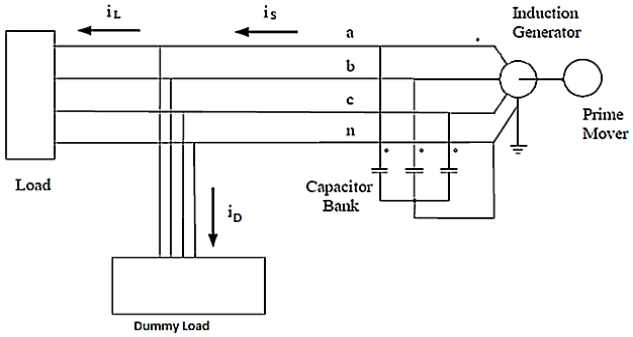

Fig. 5. Connection scheme of the dummy load to the SEIG system.

TABLE 2. Parameter Values

Parameter	Values
Number of poles	= 4
Rated voltage	= 230V
Rated frequency	= 50Hz
Stator resistance R_s	= 0.44Ω
Rotor resistance R_r	= 0.82
Stator Inductance L_S	= 73mH
Rotor inductance L_r	= 73mH
Magnetizing inductance L_m	= 80mH

Capacitance values selected for the simulations were as, 10μF, 30μF, and 50μF. Table-II presents the values of parameters of the SEIG to be simulated.

In all simulation test, the initial speed of the SEIG was set to zero and the machine was run with a constant power. Fig. 1 displays the electrical voltage generation process for C= 10 μF is shown in Fig.2(a) , for C=30μF is shown in fig. 2(b) , and for C=50μF is shown in fig.2(c) .

In addition, fig. 3 shows the simulation results of the SEIG output voltage as a function of rotor speed. Here again the external excitation capacitance C was varied from 10μF to 60μF, in equal steps.

Furthermore, to observe how SEIG output voltage changes as the output load changes, three different loads were applied to the machine after equal intervals. As shown in fig. 4, for a varying output power, the loads were applied in such a way that initially the machine was energized (machine starts at time *t = 0s*) at no load condition. After 2 seconds from start a load of 300W per phase was applied, at time *t = 3s* a load of 500W was added per phase, and finally at time *t = 4s* a load of

500W was added. It was observed that the SEIG output voltage does not remain constant for varying load.

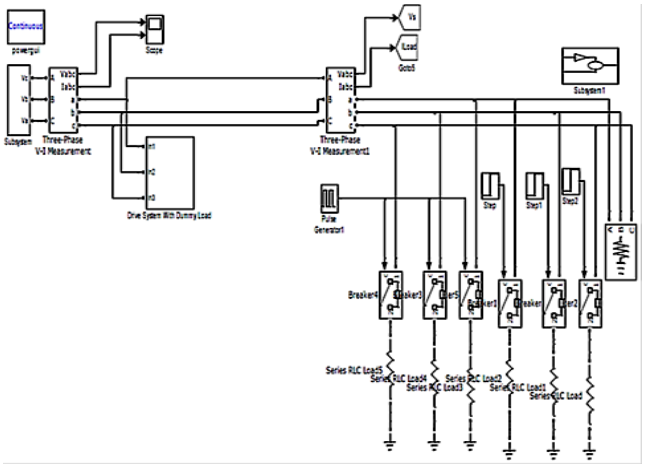

(a)

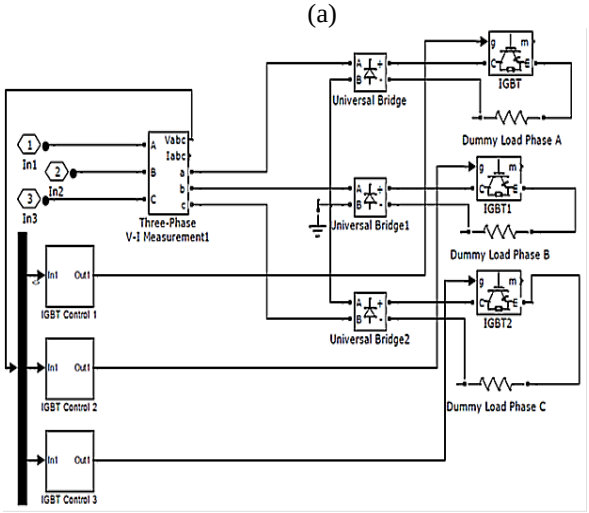

(b)

Fig. 6 (a) SEIG system configuration for constant output voltage (b) Dummy load controller using IGBTs.

A careful inspection of fig. 1, 2, 3 shows an interesting problem associated with SEIG when used as generators. It is observed that the SEIG output voltage changes with external capacitance C, rotor speed, and output load. The above mentioned results indicate that the SEIG cannot be used in the present form because for example if the consumer loads changes, then the output voltage may also change. Hence for SEIG output voltage regulation additional circuits will be required.

IV. DEPLOYMENT OF A DUMMY LOAD FOR VOLTAGE REGULATION

An inspection of fig. 4, shows that the SEIG output voltage remains almost same for a fixed load. Therefore, if a dummy load could be connect across the actual load. This dummy may be brought into the circuit or be removed from the circuit with help of power semiconductor IGBT switches. The dummy load will compensate the changes in the actual load in such a way that as the actual load decreases the dummy load may be increased and similarly as the actual increases the dummy load value may be decreased. By this way the load as seen by the SEIG machine would remain constant. Fig. 5 presents the circuit scheme to deploying the dummy load.

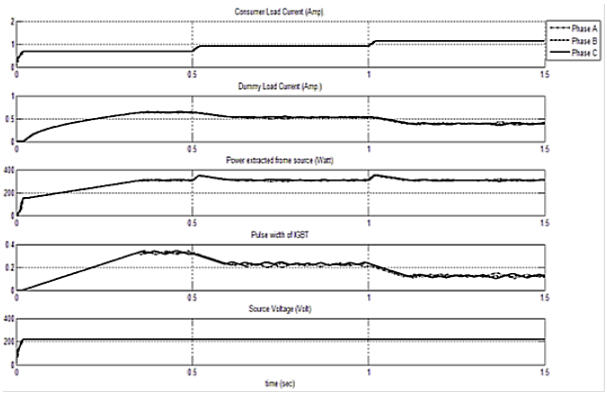

(a)

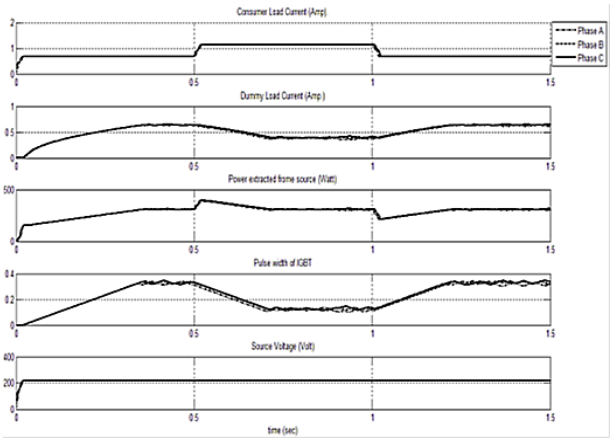

(b)

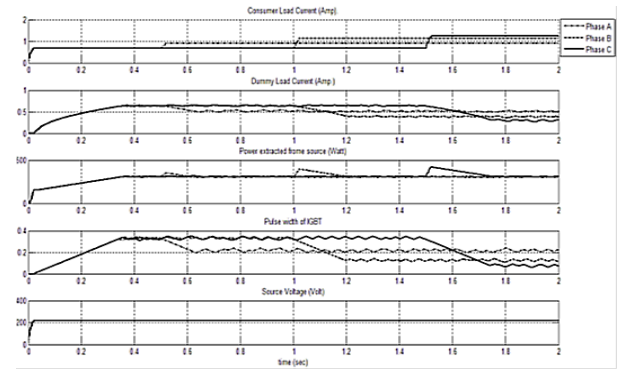

(c)

Fig. 7. Result of the SEIG system deploying IGBT based dummy load controller (a) for increasing consumer loads (b) for increasing and decreasing consumer load (c) for asymmetric consumer loads.

Fig. 6(a) SEIG simulation system implemented in MATLAB software with the dummy load, whereas fig.6(b) shows the details of the IGBT based dummy load controller. The constant voltage is achieved from the information of the output voltage.

V. RESULTS

The SEIG output voltage variation using the actual load along with the dummy load was studied in three different cases. In the first case, the actual load was increased by adding 50W per phase after equal time intervals of 0.5s. The results were studied in terms of load consumed, current consumed by the dummy load, power extracted from the load, pulse width of the IGBT (i.e., the amount of time the dummy load is put in the circuit), and the

SEIG output voltage. Fig. 7(a) shows the observation for increasing loads.

In the second case, the initial load presented on the SEIG system, equal loads on all phases, from time t=0s to 0.5s was 150W, from time t=0.5s to 1s an additional load of 100W was added, and from time t=1s to 1.5s the presented load was again 150W. Fig. 7(b) shows the observations for increasing and decreasing loads.

In the third case, the load presented on the SEIG system was 150W per phase. However, at time t=0.5s a load of 50W was added to phase A. At time t=1s a load of 100W was added to phase B and at time t=1.5s a load of 125W was added to load phase C. Fig. 7(c) shows the observations for varying loads on different phases. In all cases, the dummy load proves to aid to keep the SEIG output voltage regulated.

VI. DISCUSSION

Careful observation of Fig. 6 shows that the proposed dummy load scheme has effectively regulated SEIG output voltage. The IGBT dummy load controller is robust with simple operation. However, one drawback of the dummy load is the constant loss of power dissipated through it when it is in use. Extension of the work includes regulation of the SEIG output frequency and delivery of constant power. Future work may include inductive resistive e.g., an induction motor as the load. In such case the nature of dummy load may have to changed i.e., the RLC circuit.

This system has shown the successful working of a simple IGBT controlled resistive dummy load. However improvements could be made to increase the response time and settling times by the use of PID controller for tracking faster load changes. Furthermore use of IGBTs will add a number of higher order unwanted harmonics which could be eliminated by LC or LCCL filters.

VII. CONCLUSIONS

This research paper has presented the simulations of regulating the output voltage of a SEIG system using three-phase dummy loads. At first the results of SEIG system without a three-phase dummy load were presented followed by the application of three-phase dummy load. The results were encouraging. Despite the fact that three-phase dummy load introduced heat losses, however, the requirement of voltage regulation was achieved with less number of circuit component. The overall system was robust.

VIII. ACKNOWLEDGMENTS

The authors would like to acknowledge the electrical engineering department, University of Engineering and Technology, Lahore, for providing access to the laboratory.

IX. REFERENCES

[1] R. C. Bansal, T. S. Bhatti, and D. P. Kothari, “A bibliographical survey on induction generators for application of nonconventional energy systems,” IEEE Trans. Energy Convers., **18(**3): 433-439, 2003.

[2] M. G. Simões and F. A. Farret, “Alternative Energy Systems: Design and Analysis with Induction Generators, Taylor & Francis, December 2007.

[3] Shariq Riaz , “Design and Implementation of Low Cost and Minimum Maintenance Micro Hydel Power Generation System” Master of Science Thesis, Electrical Engg. Dept., U.E.T., Lahore, 2012.

[4] K. S. Sandhu, “Steady State Modeling of Isolated Induction Generators,” WSEAS Transactions on Environment and Development, **4**(1): 66-77, 2008.

[5] D. Seyoum, C. Grantham, and F. Rahman. "Analysis of an isolated self-excited induction generator driven by a variable speed prime mover," Proc. AUPEC, **1**: 49-54, 2001.

[6] A. Kishore, R. C. Prasad, and B. M. Karan. "Matlab simulink based DQ modeling and dynamic characteristics of three phase self excited induction generator." In Proceedings of the Progress in Electromagnetics Research Symposium, Cambridge (USA), 312-316, 2006.

[7] E. Levy and Y. W. Liao, “An Experimental Investigation of Self-excitation in Capacitor Excited Induction Generators,” Electric Power System Research, 53(1): 59-65, 2000.

****

Data Security using Combination of Steganography and Cryptography

Muhammad Omer Mushtaq, Yasir Saleem, Muhammad Fuzail,
Muhammad Khawar Bashir, Binish Raza

Department of Computer Science & Engineering University of Engineering & Technology, Lahore, Pakistan

Abstract

With the passage of time data protection is the most evolving topic of Information Security. However steganogarphy is less used, Cryptography is employed worldwide extensively in this area. Combination of both is very effective which is discussed in this paper. This paper proposes the technique of securing data by first using cryptology and then encodes the encrypted data using steganography. This makes it almost impossible for any individual cryptanalyst or a steganalyst to intrude the hidden message unless existence of hidden communication as well as encryption technique is known to the intruder. This scheme can be used to transmit data securely and covertly over wired as well as wireless media.

I. INTRODUCTION

This research paper proposes a combined technique of cryptography and steganography. The data to be transmitted is first encrypted using RC4 then the encrypted data is read as bytes and then broken into bits. The isolated bits are then placed at specific bit patterns of the digital image. The resulting image colour is changed by very small grayscale levels as compared to the original image. This change is not perceivable for any third party. Quality and dimension of carrier image used is directly proportional to efficiency of the designed system.

Use of only Cryptography however makes data meaningless but visible for cryptanalyst and is an invitation for attack to any intruder [1]. Use of steganography however makes data hidden but if the existence is sensed by any means, any intelligent steganalyst can find the secret data by some strong statistical analysis [2].The proposed technique can be cornerstone among future security trends in symmetric session key distribution. However the carrier file used in this scheme is the digital image but this technique can also be applied to other digital media .Next section gives an overview of both cryptography and steganography and some technical background of researches already made in this area. Third and fourth sections explain the proposed system regarding cryptography and steganography respectively. Fifth section describes the software implementation of our scheme. And sixth section describes the conclusion of our proposed system.

II. TECHNICAL BACKGROUND

The art of hiding information within digital data by a way that any third party cannot feel the existence of hidden communication is termed as Steganography[3]. The information that is to be concealed and the data that is used as carrier of that information can be of any digital format [4]. Information is embedded or encoded in the carrier digital file using a particular algorithm or technique [5]. The carrier digital file is transferred to second party and the hidden information is extracted using exactly the same technique as was used at the sending end, provided the encoded data is not transformed by any means while it is being transferred from sender to receiver. The encoding technique is designed in a way that the carrier digital file after and before encoding remains ostensibly same. This makes it different from cryptography in which data is deformed but not invisible.

In most simple way Cryptography might be termed as converting data into a form that is meaningless for any third party[6][7]. Encryption and Decryption are two main processes performed at sender and receiver end respectively. Encryption is just like a lock that is closed with the key and receiver needs the key to open that lock. The locked information known as cipher text is meaningless for third party.

Vikas Tyagi [8] proposed a technique of steganography in combination with cryptography in which the secret data is encrypted using symmetric key algorithm then the encrypted data is hidden into an image using LSB pixel processing. The combination of both these techniques provides a secure transmission of secret data. However this technique is combining both famous data security techniques but can be criticised by a limitation of data to be encoded because this technique is using only a single bit as carrier of information that is if a colour image is taken as carrier of information each pixel might carry only three bits of information.

Jagvinder Kaur and Sanjeev Kumar [9] propose a steganographic model in which secret message or data is embedded into a cover-object that can be text, image, or any multimedia digital file. The secret data is encrypted with a setgo-Key that is only known by sender or receiver. The message is embedded using the intensity of the pixel values directly. Image or cover-object is divided into blocks of bits and one message bit is embedded in every block of original image bits. This technique however makes minimum degradation of the original image but also provide a very small limit of data to be embedded since only one message bit is added to a block of image.

Samir Kumar and Indre Kanta [10] proposed a technique for hiding data in an 8-bit colour image file. This uses a lookup table or palette instead of 24-bit RGB image. In palette based steganography least significant bits are used to hide the data. A palette generation algorithm is used to quantize the image in different blocks then the colours in palette are sorted to minimize the difference between the colours. It uses Euclidian distance to choose the RGB values of 24-bit image compared to the RGB value of every colour in the palette [11] . Information will be hiding by changing the LSB of image with the bit values in palette. This technique provide a secure and fast system for internet and mobile communication due to light weight of image that can store small amount of data. Small amount of data again dictates the limitation of secret information that can be transmitted. Also the absence of

cryptography makes the carrier image vulnerable for attack.

Adnan Gutub [12] proposed a new merging technology of utilizing LSB within image and random pixel manipulation methods and stego-key. Pixel used for hiding data is selecting random fashion depends on stego-key .Two LSB of one colour channel used to indicate the existence of data in the other two channels. Security is improved because the selection of indicator channel is not fixed. Indicator channel is selected in sequence. The test of this technique shows attractive results in the storage capacity of data-bits that to be hidden in relation to RGB image. However the technique for hiding data is efficient but not using encryption can be a threat in case some statistical analysis is performed at the pixels' bits.

Tanvir and Adnan Abdul-Aziz [13] proposed a new technology for image based steganography. A comparison is represented between the previous technology (Pixel Indication) and new proposed technique that is Intensity Based Variable-bit by showing experiments. The variable numbers of bits are stored in the channel of RGB image. The number of data bit storage is decided on the bases of actual colours of the image. The data bits are stored in one of two channels of the image other than the indicator channel depends on the colour values. The lower colour value channel will store data in its LSB. The selection of colour scheme is at runtime and depends on the cover media. The technique might be efficient as the presence of data in each pixel is not sure for the attacker but processing each pixel in image can give required data as there is no encryption on data and the data is hidden but present in its original form.

Juan and Jeus [14] proposed a technique of steganography in spatial domain. Technique uses the LSB steganography by hiding data in only one of the three colours at each pixel of cover image. To choose the colour for hiding information Pair analysis is used then LSB Match method is applied so that the final colour is as close to possible to the original one in the scale of colours. The proposed technique is however immune to visual, statistical and histograms attacks but limitation of data to be hidden is demerit of the technique and also data is not encrypted so a good statistical analysis might easily give the secure data to the intruder.

III. RC4 CIPHER

Both sender and receiver use the RC4 cipher which is fast and easy to implement in software as well as in hardware. RC4 cipher has variable key length. In our scheme we use the minimum key length of 32 bytes or 256 bits.

First of all an array state S is declared of 256 bytes shown in Figure 1[15]. S[i] =i ,where i={0,1,2,3… 254,255}

Figure 1: State Vector S

After that a temporary array vector T is declared whose length is same as of S. T is initialized by replicating the K vector containing the user defined key shown in Figure 2[15].

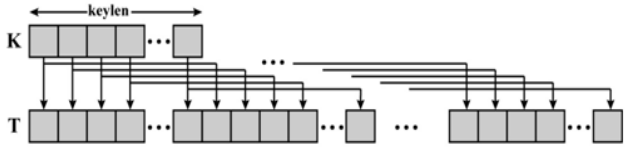

Figure 2: Initial State of T

Values of S are permuted by vector T. It is described by Figure 3[15]in which each ithbyte of S is swapped with jthbyte of S.

And j = (j + S[i] + T[i]) mod 256 [j initially set to zero]

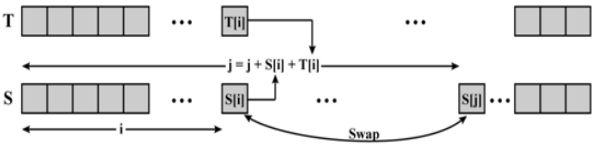

Figure 3: Initial Permutation of S

After the permutation, a temporary index t of S is generated by the ith and jth bytes of S which gives us the Random Key Stream Byte k given by algorithm:

$$k = S[t]$$

Where j& t are

$$j = (j + S[i]) \bmod 256$$

$$t = (S[i] + S[j]) \bmod 256$$

With generation of every k, S vector is again permuted at the end of each iteration as shown in Figure 4[15].

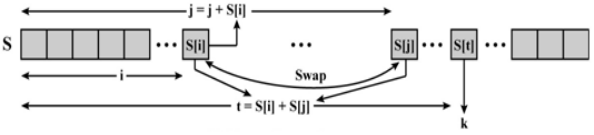

Figure 4: Stream Generation

Cipher byte is generated by the bitwise XOR operation between random key that is generated by above process and plaintext data. Figure 5 shows this procedure .In the same way at decryption end plain text is obtained from bitwise XOR of key (same key as was used at Encryption) with cipher text.

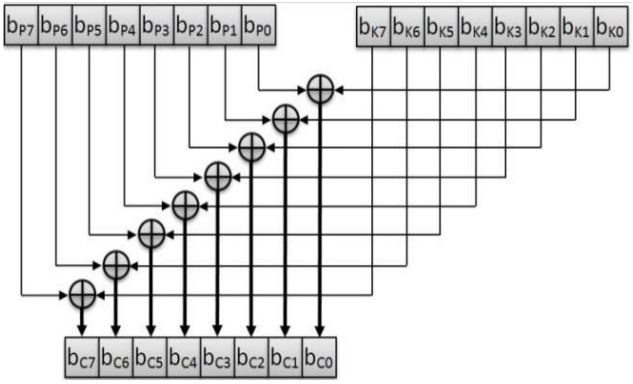

Figure 5: Cipher Text Generation

IV. STEGANOGRAPHY

The system reads the cipher text as a stream of bytes and for placement of different colour planes in the pixel, each byte is broken into group of bits. For the proposed system

there are 6 possible combinations of bits' groups by dividing a byte (8 bits).The designed system rely on these 6 combinations of bits' that have any value only as more combinations make grayscale value somewhat perceivable. Any combination of bits' groups constitutes a byte which is mapped to a pixel at its different colour planes (most probably red, green and blue).

Cipher Byte is broken into groups of bits in different ways. In all ways essentially there are three groups simply shown by Figure 6 where C_{g1}, C_{g2}& C_{g3} are chosen from set

C = {2, 3, 4} in a way that to complete a byte, that is

$$C_{g1} + C_{g2} + C_{g3} = 8 \quad \ldots 1$$

C_{g1}	C_{g2}	C_{g3}

Figure6: Cipher Byte Division

Choice of these numbers is explained by the following calculations. Let the chosen values for C_{g1}, C_{g2}& C_{g3}be

$$C_{g1} = 4$$

$$C_{g2} = 2$$

$$C_{g3} = 2$$

Then the change in grey levels of whole pixel due to C_{g1}willbe $C_{g1}' = 2^4 = 16$

Similarly

$$C_{g2}' = 2^2 = 4$$

$$C_{g3}' = 2^2 = 4$$

So the total change Δ_c in grey levels of the pixel due to these bits' change is given by

$$\Delta_c = C_{g1}' + C_{g2}' + C_{g3}'$$

$$\Delta_c = 24$$

Other possible combination for Figure 6 can be

$$C_{g1} = 3$$

$$C_{g2} = 3$$

$$C_{g3} = 2$$

Δ_c for this choice is 20 which is even a better choice. Value 4 cannot be chosen for any two of C_{g1}, C_{g2}& C_{g3}because it will not satisfy the Equation 1. In a similar fashion not all C_{g1}, C_{g2}& C_{g3}can be 3 or 2 at the same time. Hence it forms six possible combinations that are shown in Figure 7.

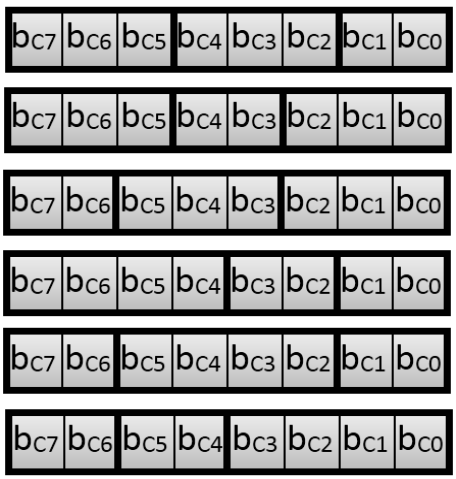

Figure 7: Possible Cipher Byte Division

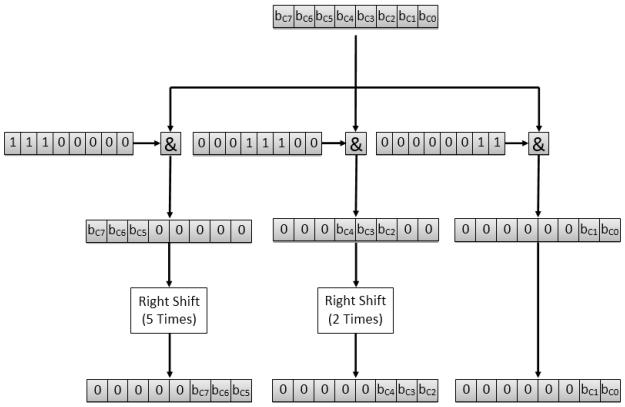

Figure 8: Isolation of Cipher Byte

A simple bitwise AND operation is performed to break the bits into groups ,for instance process of first possible bits-groups having 3, 3 and 2 bits is shown in Figure 8. First combination is result of bitwise AND operation of cipher byte Cb with 11100000 and then shifting it 5 bits-places towards right. The shifting is performed to move the meaningful bits at LSB positions and place 0 at rest of the bits which will help to map the value at desired place in colour plane of pixel using bitwise OR which are explained in next few lines. Group2 is result of bitwise AND operation of Cb with 00011100 and require shift of 2 bits-places to move the meaningful bits at LSB positions. Group3 is simply the result of bitwise AND of Cb with 00000011 without any shift. Brief overview of Steganographic process of above operation for 1st combination of Figure 7 is shown in Figure 9.

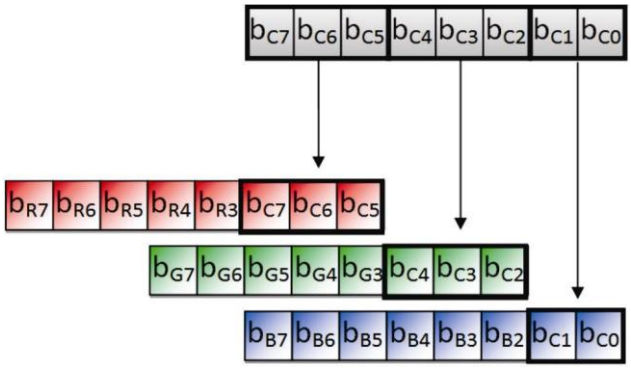

Figure 9: First Cipher Byte Division

Figure 10 shows overview of Steganographic process for second possible combination from Figure 7.

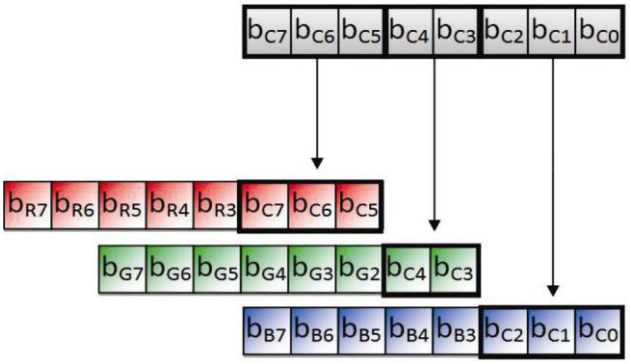

Figure 10: Second Cipher Byte Division

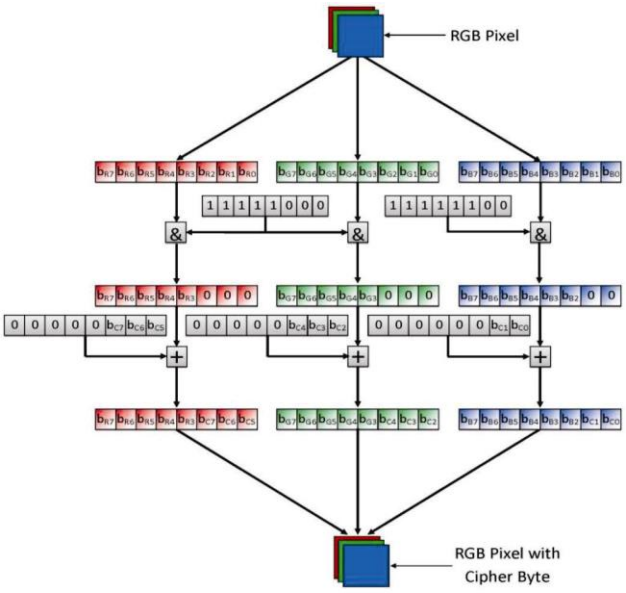

Figure11: Complete Process

The whole process shown in Figure 8 gives us isolated bits at LSB positions which are then mapped to respective color-bits of pixel by performing bitwise AND operation with color-bits of pixel .

Taking the above instance of groups in the RGB pixel, red and green color bits are performed bitwise AND operation with 11111000 (to place C_{g1} and C_{g2} respectively) and blue color bits with 11111100. This operation makes the last bits vacant so that the isolated bits of cipher text can be placed here which is done by performing bitwise OR of cipher with respective color bits. The whole process above is explained in the Figure 11.

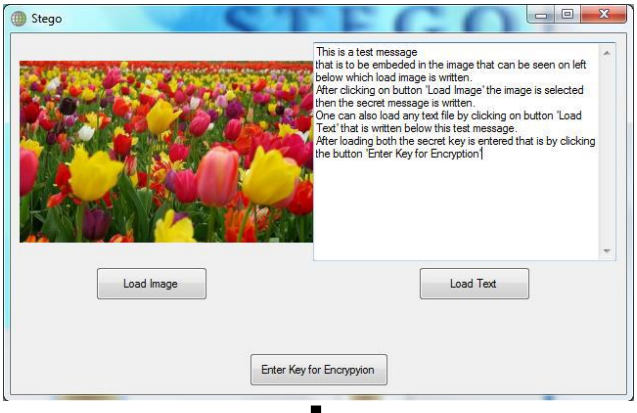

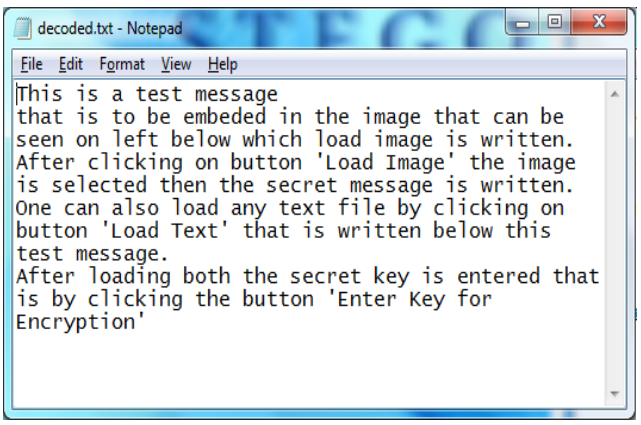

II. REFERENCES

[1]. Phad Vitthal S., Bhosale Rajkumar S., Panhalkar Archana R. "A Novel Security Scheme for Secret Data using Cryptography and Steganography" *I.J. Computer Network and Information Security*, 2, 36-42, 2012.

[2]. Shivendra Katiyar, Kullai Reddy Meka, Ferdous A. Barbhuiya, Sukumar Nandi, "Online voting system powered by Biometric security using Steganography", International conference on Emerging Applications of Information Technology, pp. 288-291, 2011.

[3]. Aniello Castiglione, Bonaventura D'Alessio, Alfredo De Santis, "Steganography and secure communication on online social networks and online photo sharing", International conference on Broadband and Wireless communication, Communication and applications, pp. 363-368, 2011.

[4]. D. Artz, "Digital Steganography: hiding data within data", IEEE Internet Computing, Vol. 5, Issue-3, pp. 75-80, 2001.

[5]. Piyush Marwaha, Paresh Marwaha, "Visual Cryptographic Steganography in Images", Second International conference on Computing, Communication and Networking, pp. 1-6, 2010.

[6]. S. Usha, "A secure triple level encryption method using cryptography and steganography", International Conference on Computer and Network Technology, Vol. 2, pp. 1017-1020, 2011.

[7]. K Suresh Babu, K B Raja, Kiran Kumar K, Manjula Devi T H, Venugopal K R, L M Patnaik, "Authentication in secret information in Image Steganography", TENCON, pp. 1-6, 2008.

[8]. Mr . Vikas Tyagi, Mr. Atul kumar, Roshan Patel, Sachin Tyagi, Saurabh Singh Gangwar, " Image Steganography using least significant bit with cryptography ", Journal of Global Research in Computer Science , Volume 3, No. 3, March 2012

[9]. Jagvinder Kaur, Sanjeev Kumar, "Study and Analysis of Various Image Steganography Techniques", IJCST Vol. 2, Issue 3, September 2011

[10]. Prof. Samir Kumar Bandyopadhyay, Indra Kanta Maitra, "An Application of Palette Based Steganography" , International Journal of Computer Applications (0975 – 8887) Volume 6– No.4, September 2010

[11]. Gao Hai-ying, Xu Yin, Li Xu, Liu Guo-qiang, "A steganographic algorithm for JPEG2000 image", International conference on Computer Science and Software Engineering, Vol. 5, pp. 1263-1266, 2008.

[12]. Adnan Gutub, Mahmoud Ankeer, Muhammad Abu-Ghalioun, Abdulrahman Shaheen, Aleem Alvi, "Pixel indicator high capacity technique for RGB image based Steganography" WoSPA 2008 – 5th IEEE International Workshop on Signal Processing and its Applications, University of Sharjah, Sharjah, U.A.E. 18 – 20 March 2008.

[13]. Mohammad Tanvir Parvez, Adnan Abdul-Aziz Gutub, "RGB Intensity Based Variable-Bits Image Steganography," apscc, pp.1322-1327, 2008 IEEE Asia-Pacific Services Computing Conference, 2008

[14]. Juan José Roque and Jesús María Minguet, "SLSB: Improving the Steganographic Algorithm LSB", 7th International Workshop on Security in Information Systems, 57-66, (2009).

[15]. William Stallings, "Cryptography and Network Security", 5th Edition, Publisher: Prentice Hall, 2005.

****

Performance Analysis of Conventional and Fuzzy Logic Controlled Automatic Voltage Regulator Systems in a Noisy Environment

Irfan Ahmed Halepoto, Imtiaz Hussain, Wanod Kumar, Bhawani Shankar Chowdhry
Department of Electronic Engineering, Mehran University of Engineering & Technology, Jamshoro, Pakistan.

Abstract:

The increasing demand for electric power is leading to complex interconnected power systems. As a result, generation units are being operated under stressed conditions with smaller stability margins. The power supplied by the generator involves active and reactive components and good control of active and reactive power is essential in order to maintain a satisfactory steady state as these components can disturb the parameters of the power system. To regulate the reactive power and voltage magnitude of generation unit, AVR (Automatic Voltage Regulation) system is used in the forward path of the closed loop system of the generator. The addition of a conventional Proportional Integral and Derivative (PID) controller in the forward path of the AVR system can improve the dynamic response significantly but this may be at the cost of additional noise (introduced by the derivative component) which may reduce the overall effectiveness of the controller and this is a matter of concern in practice.

This paper primarily focuses on the issue of noise vulnerability of PID controlled AVR systems. An alternative and more effective fuzzy logic controlled approach is proposed to tackle these issues encountered with conventional controllers. The proposed solution uses a Fuzzy Inference System (FIS) to control the magnitude and rate of change of error, while the two nonlinear fuzzy membership functions are used to mitigate the noise effects. Simulations models of the PID controlled AVR system and proposed fuzzy logic controlled AVR systems are developed and results are compared to demonstrate the potential of the proposed design. Simulation results confirm the superiority of the proposed fuzzy logic controlled AVR system under noisy conditions.

Key Words: Automatic Voltage Regulation, Proportional Integral and Derivative Controller, Fuzzy Logic, Synchronous Generator

1. INTRODUCTION

The prime objective of power system control is to deliver and generate power to an interconnected system as cost-effectively and securely as possible while maintaining the supply voltage and frequency within specified limits [1]. The power supplied by the generator involves active and reactive components. Good control of active and reactive power is necessary to keep the system in a satisfactory steady-state condition as these components can disturb the power system parameters [2]. The frequency of the system is mainly affected by changes in the real power demand whereas increase in the reactive power demand has a significant effect on system voltage [3]. Real and reactive powers are therefore controlled independently through separate AVR and Load-Frequency Control (LFC) loops. Primary control equipment are installed for each generator in a generation unit to provide the required stability and reliability in terms of the system frequency and voltage stabilization [4]. The real power and frequency are effectively controlled by LFC loop while the AVR system loop regulates the reactive power and voltage magnitude. When the generator is connected to the load, the real component of the power stresses the rotor in mechanical terms and opposes it rotation. This reduces the speed of the rotor and thus decreases the frequency of the generated voltage. Although reactive power lowers the frequency of the generated voltage this effect is small compared to the reduction of the e.m.f with increased reactive power. The active component is in the quadrature with the direction of the field but the reactive component directly opposes the excitation field. Thus, as the reactive power increases, the opposition to the excitation field increases which in turn reduces the generated e.m.f. This effect must be compensated so that the generator remains synchronized with the system.

In literature different approaches are used to achieve the regulation of reactive power and voltage magnitude of generation unit either using power system stabilizing (PSS) components [5], conventional PID controllers [6], fuzzy logic controllers [5] and hybrid controllers [10]. Techniques such as genetic algorithms [7] and other evolutionary algorithm [8] and particle swarm optimization methods [9] have also been considered for optimization and tuning of these controllers, but these control system design approaches usually consider only the ideal environmental conditions by neglecting the effect of noise which introduces high frequency disturbances, the effects of which are reflected in the overall system behavior.

This paper investigates the effect of PID controlled and fuzzy logic controlled AVR systems in terms of regulation of the reactive power and generated voltage while taking the noisy environment into account. Simulink models have been developed for both controllers and the performance characteristics are compared in terms of system output response and system response error.

The organization of the paper is as follows. In Section 2, the generator control loop configuration of the AVR is discussed. A state space representation and simulation model of AVR system using PID controller is detailed in Section 3. In Section 4, the fuzzy logic controlled AVR system is proposed. Conclusion and suggestions relating to future work are given in Section 5**.**

2. GENERATOR CONTROL LOOP BASED AVR SYSTEM

The reactive power demand and voltage magnitude of generation unit reduce the terminal voltage of the generator and control of this change in voltage is desired to ensure power system stability. This task is accomplished

by the generator excitation system using an AVR control loop through a closed loop system of the generator. The control loop of the generator continuously monitors the produced voltage level at the generator terminals and accordingly regulates the excitation level of the rotor using any appropriate type of controller (e.g. a microcontroller) system and firing circuit (based on thyristors, for example). The magnitude of the voltage is sensed and measured by a potential transformer which steps down the voltage and then measures its magnitude. This measured voltage is then rectified through a three-phase rectifier and then converted to the digital form to feed to the microcontroller where it is compared with the reference value set by the operator. The error signal, if exists, is then amplified to increase the excitation field which in turn increases the generated voltage until the error signal is reduced.

The terminal voltage is constantly sensed by a voltage level sensor, which is then rectified and regulated before comparing with DC reference signal in the comparator. Subsequently, if the comparison results in an error voltage signal, this will then be amplified and forwarded to the controller. In order to regulate the field windings of the generator, the exciter system can be used along with the output of the controller. For proper generator excitation, the AVR loop is configured to achieve the required reliability and the steadiness of the generator terminal voltage [11]. The AVR control loop configuration and sequence of events are illustrated in Fig.1.

The load voltage is first stepped down to a voltage suitable for measurement and then measured through a measuring device like voltmeter. The measured voltage is initially processed through an analog to digital converter (ADC) before being fed to the microcontroller for comparison. After conversion, the controller compares the ADC values with the terminal voltage set by operator. In case of any difference in the measured and the reference quantity, an error signal is generated from the controller's output. The error signal generated is in digital form and needs to be converted in its analog equivalent before feeding to the amplifier.

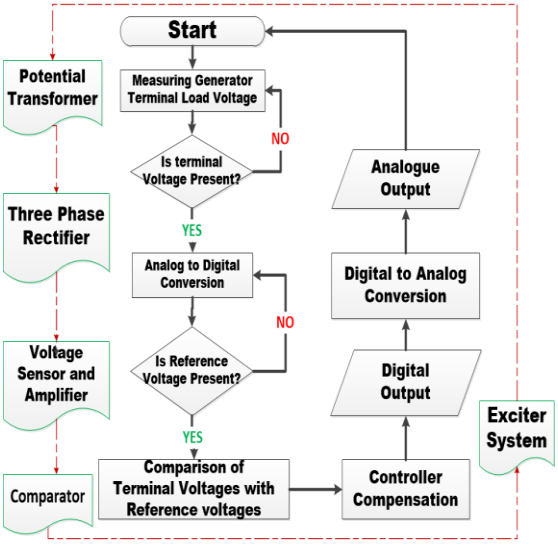

Figure1: AVR System Generator Control Loop Configuration and Event Flow Chart

Based on the generator control loop configuration of Figure 1, the AVR system can be designed to regulate and control the reactive power and voltage magnitude. The generalized AVR system is comprised of four basic units; i.e. Amplifier, Exciter, Generator and Sensor as shown in Figure 2. The system operating conditions and targeted set points are defined and are continuously monitored. Any abnormality in the system resulting in an error is amplified and forwarded to the controller. The controller can be of a conventional type like PID or an intelligent controller such as a fuzzy logic controller. The amplifier unit is responsible to strengthen the signal level without compromising on the shape of the signal [12]. The excitation can be achieved through solid state rectifiers (e.g. SCR or Thyristors). The rectifier's output is a nonlinear function of the field voltage due to magnetization created by overloaded saturation effects.

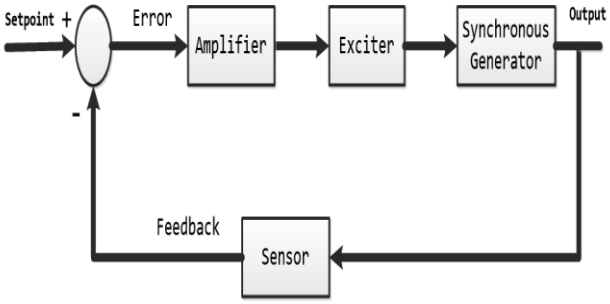

Figure 2: Generalized AVR System Model

For control system design, the saturation and nonlinearity effects of the system are usually ignored in the initial stages of the process and a linearized model is used. The e.m.f produced by the synchronous generator is closely related to the machine magnetization curve [13]. The terminal voltage of generator depends on the generator load. The voltage signal sensed by potential transformer is finally rectified into DC form.

3. SYSTEM MODELING

3.1 The state space representation model

The relationship between state variables of the system is typically non-linear; but for computational convenience a linearized state space model is used in the initial stages of design. The linearized mathematical model of system is given in equation (1). The detailed derivations of the model and system equations are given in [14, 15].

Where Δ is the change from nominal values, ω_r is the angular velocity of the rotor, ψ_{fd} is the magnetic field constant, K_D is the damping coefficient, v is the generator excitation voltage, L_{fd} is the field inductance, R_{fd} is the

field resistance, ω_0 is the initial rotor speed and T_m is the mechanical torque.

3.2 PID CONTROLLED AVR SYSTEM MODEL

A controller is the most important part of any system model, as it not only maintains the operating characteristics of the system but also effectively regulates, modifies and influences the process by remedying the abnormalities within defined limits. The simplest and most widely used conventional controller is the PID controller. The generalized transfer function of a PID controller [16] is given by

$$G_c(s) = K_p + \frac{K_I}{s} + K_D S \qquad (2)$$

Where K_p is the proportional gain factor, K_I is the integral gain factor, K_D is the derivative gain factor, and s is the Laplace operator. The values of K_p, K_I and K_D can be tuned through system optimization.

3.2.1 PID Simulation Model

As discussed earlier, an AVR system is used to regulate the reactive power and voltage magnitude which results in system stability in form of response errors. To eliminate the response error, the PID controller is added in the forward path of the AVR system to improve the dynamic response and minimize the error. A Simulink model from equation (1) is developed to demonstrate the potential of the idea. Figure 3 shows the designed Simulink model of PID controller to demonstrate the system response and error of the AVR. The basic units of AVR system i.e. amplifier, exciter and generator units are integrated in the Synchronous Generator Model. A Hall Effect sensor is used to measure the voltage and provides a feedback path back to the controller. It offers the exceptional linearity and accuracy, improved thermal drift and high tolerance to the external interference [17]. Using the characteristics of the synchronous generator, a set point is defined and the PID controlled system output response and system error are investigated by considering two scenarios. Initially it is assumed that the effect of noise is negligible, while in the second scenario, noise has been added.

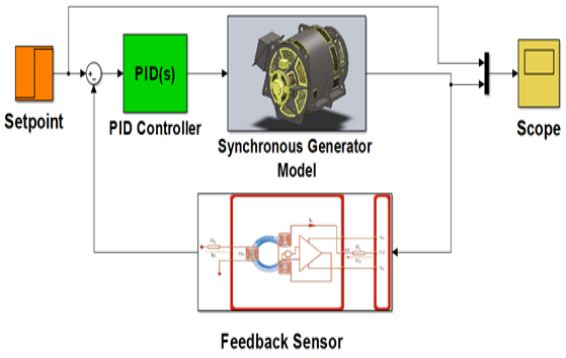

Figure 3: Synchronous Generator Model with PID Compensation

Figure 4 shows the output response of the PID controlled AVR system when noise effect is not considered. Although the overshoots produced by the PID controller during transients are very high but the response of the system after the transients is acceptable.

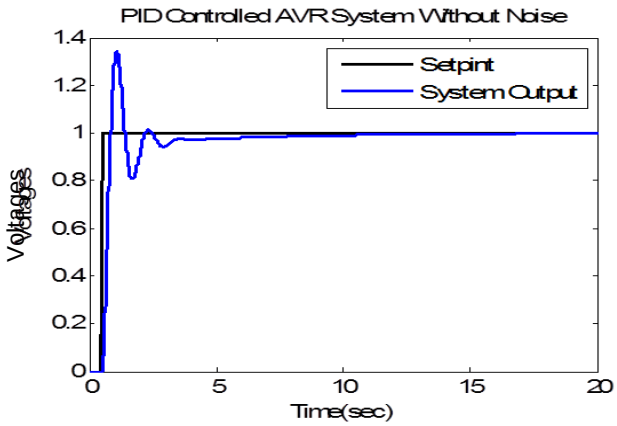

`Figure 4: Response of PID Controlled System without Noise

Figure 5 shows the error of the system without noise. It is evident from the figure that once the transients are over; the error converges to zero within acceptable time limits. However, in these simulation results (Figure 4 and Figure 5), the noise added by the feedback sensor is not considered. It is a well-known fact that the derivative component of the PID controller is vulnerable to noise. Therefore from practical aspects, the sensor noise is added in simulation model and simulation results are shown in Figure 6 and Figure 7 respectively.

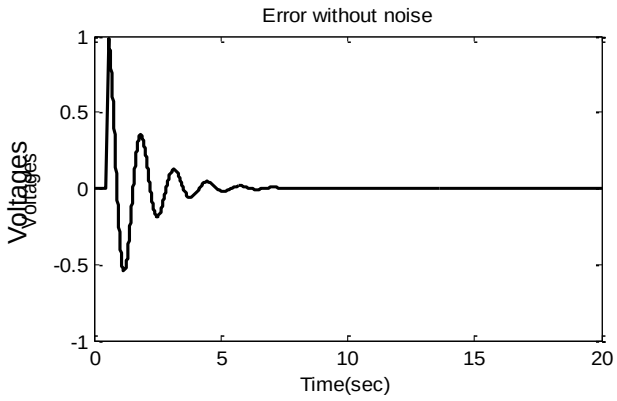

Figure 5: System Error without Sensor Noise

In Figure 6, the output of the PID controlled AVR system does not settle due to the presence of noise. The high frequency voltages fluctuations are induced in the output of the synchronous generator which cannot be removed completely using PID controller alone. Figure 7 shows the overall behaviour of the system error.

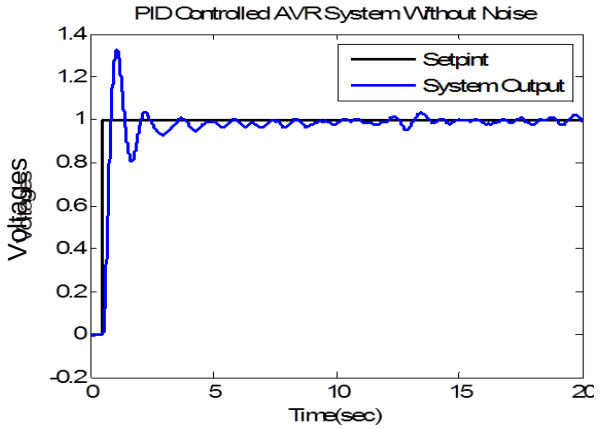

Figure 6: Output of PID Controlled AVR System with Sensor Noise

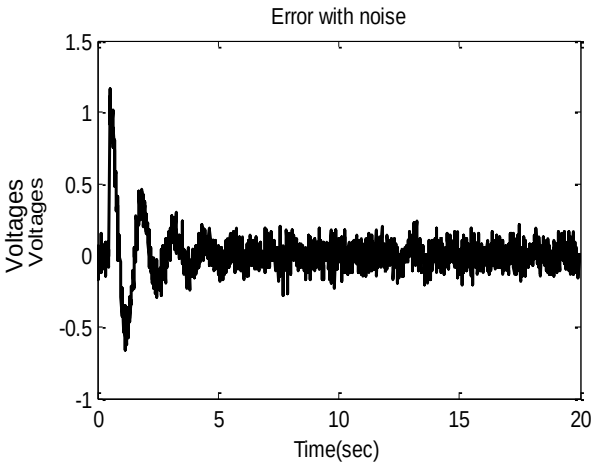

Figure 7: PID Controlled AVR System Error with Sensor Noise

During the steady state, the error is not able to converge to zero but it is continuously swinging around zero. These high frequency voltage fluctuations due to non-zero error state are harmful for electronic devices and may reduce the reliability of the system. It is therefore obligatory to have a regulated system output under varying load conditions. The limitations of PID controller are well proved in the above simulation results, so the need of an alternative and effective approach is evident.

4. FUZZY LOGIC CONTROLLED AVR SYSTEM

In this work, a fuzzy logic controller is designed to compensate for the limitations of the PID controller when it is operated in a noisy environment. The fuzzy logic controller is well known for its simplicity and effectiveness and this is why more research is being carried out specifically in industry aspects of fuzzy logic control [18, 19]. The designed Simulink model of fuzzy controlled AVR system is shown in Figure 8. In this work, for design of Fuzzy Inference System, we have used Memdani model [20] which is more suitable for non-linear application. The membership functions of Inputs and Output are shown in figure 9, 10 and 11 respectively. The inputs of the designed fuzzy controller are error and error rate, and the output of the controller is calculated using the centre of gravity method. This method is the most widely used defuzzification method [21].

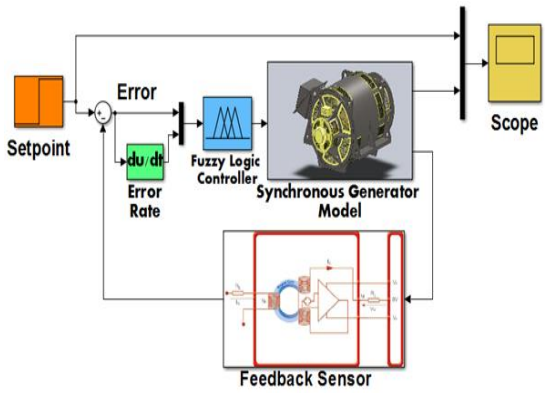

Figure 8: Simulation Model of Fuzzy Logic Controlled AVR System

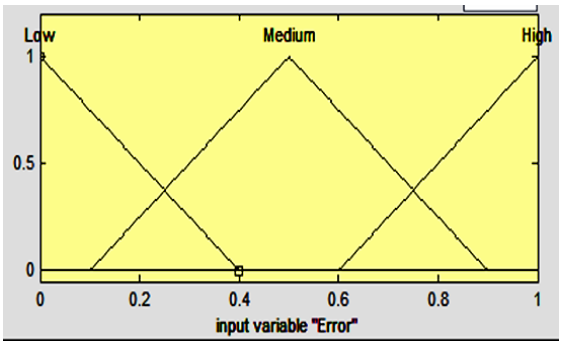

Figure 9: Membership Function of Error Input

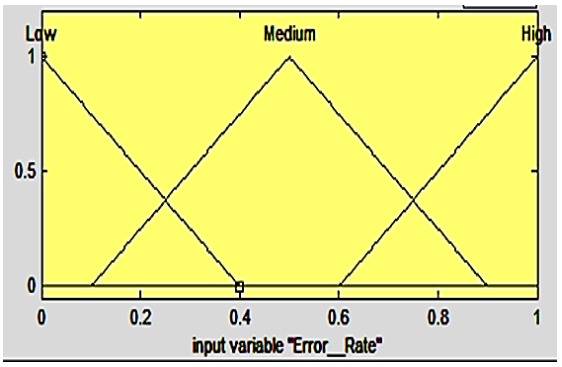

Figure10: Input Membership Function of Error Rate

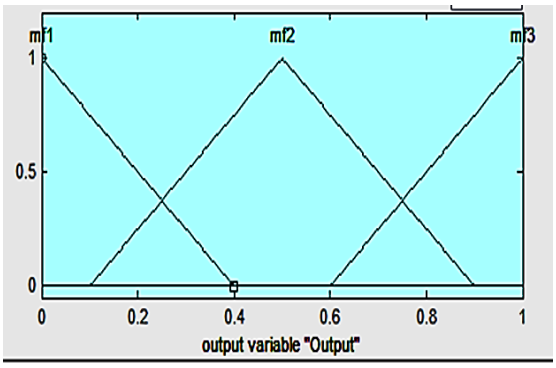

Figure 11: Output Membership Function

Figure 12 shows the surface plot of fuzzy logic rules with respect to error and error rate. When error and error rate are low, the output of the fuzzy logic controller is also low. When either of inputs is high, the fuzzy logic controller reacts accordingly to prevent the system error to exceed the bounded limits.

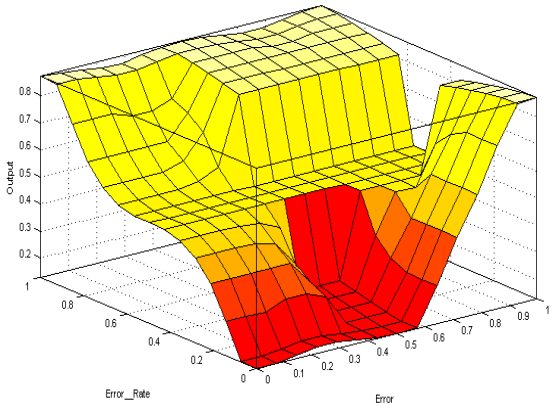

Figure 12: Surface Plot of Fuzzy Logic Rules

Figure 13 and Figure 14 show the system response of the fuzzy controlled AVR system and error without noise. The only difference between the fuzzy logic controlled AVR system and the PID controlled AVR system without noise is transient behavior. The response of fuzzy logic controlled AVR system varies smoothly until the steady state is achieved. On the contrary, the transient behavior of PID controlled AVR was observed as damped oscillations until the steady state is accomplished. The smooth variation in the output of the fuzzy logic controlled AVR system produces a smooth decay of error, as shown in Figure 14.

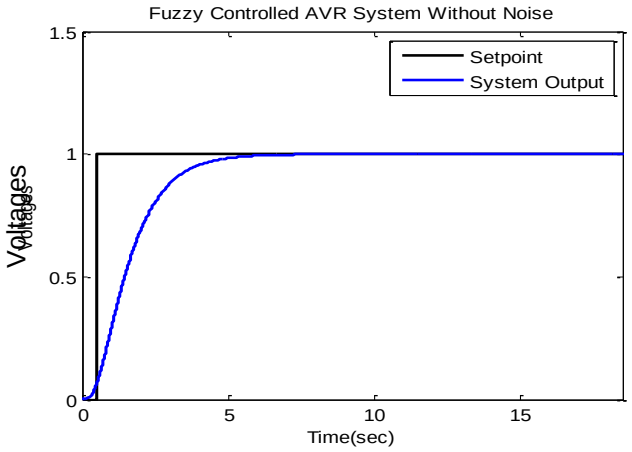

Figure 13: Response of Fuzzy Logic Controlled AVR System without Noise

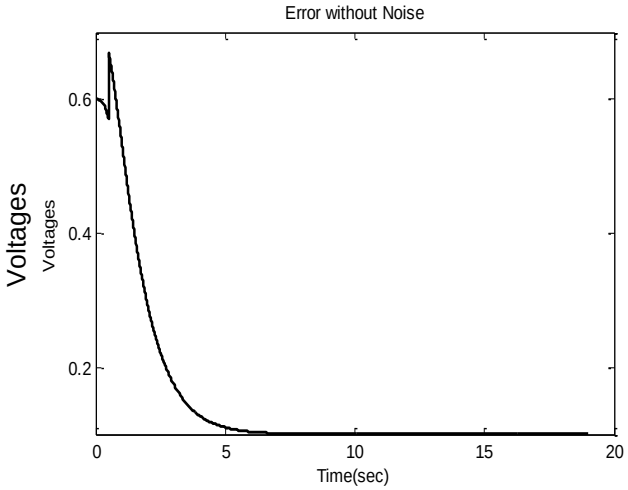

Figure 14: Error Response of Fuzzy Logic Controlled AVR System without Noise

When noise is added to fuzzy logic controller, the system response with noise and the corresponding system error are shown in Figure 15 and Figure16 respectively. It is evident from both figures that the system response and error of the fuzzy controlled AVR system stabilizes much earlier compared to PID controlled AVR system, even in the presence of noise.

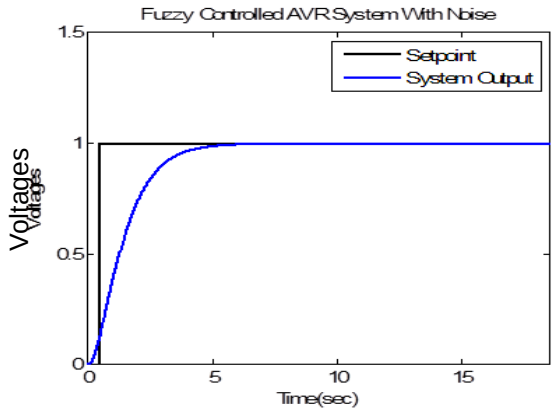

Figure 15: Response of Fuzzy Logic Controlled AVR System with Noise

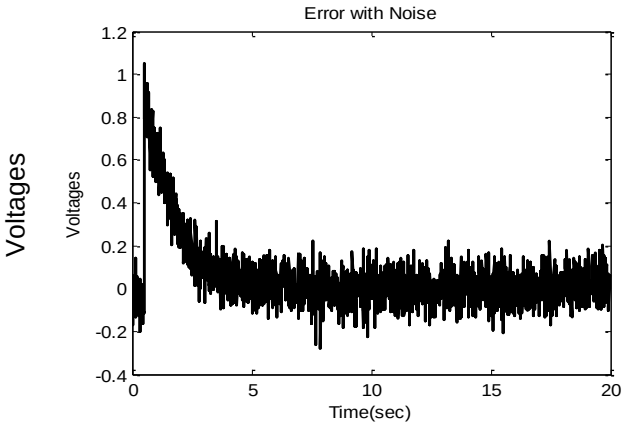

Figure 16: Error Response of Fuzzy Logic Controlled AVR System with Noise

The overall system response and error of the fuzzy controlled and PID controlled AVR systems are summarized in Figure 17 and Figure 18.

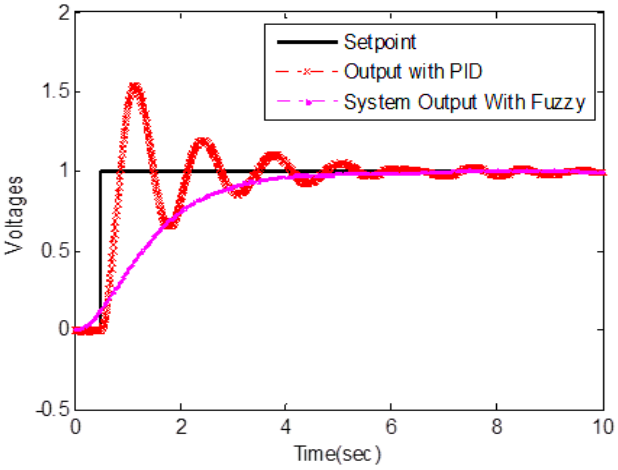

Figure 17: System Response Comparison of Fuzzy Logic and PID Controlled AVR System

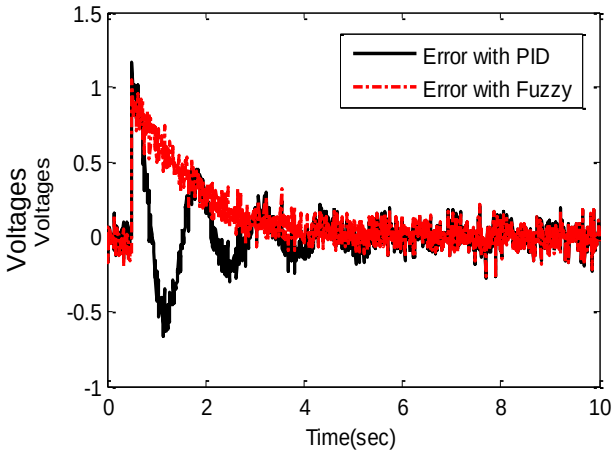

Figure 18: Error Response Comparison of Fuzzy Logic and PID Controlled AVR System

The simulation results confirm the suitability of the fuzzy logic approach to be used in a noisy environment. Even with the added noise, the response of fuzzy controlled AVR system is robust and quickly adjusts the system response. Hence, the system error converges to zero within acceptable time span. Thus, it is evident from the simulation results that the fuzzy logic controlled AVR system outperforms the PID controlled AVR system for these simulated test conditions.

5. CONCLUSION

Automatic voltage regulators with PID controllers do not perform well under varying load conditions. The noise added by system components further degrades the performance of PID controlled AVR systems. In order to solve this problem low pass filters can be used to filter the noise but that will require extra circuitry in the system which in turn will increase the cost and complexity of the system. Even after adding the extra circuits, the performance of the system is not guaranteed. Therefore, in this paper an alternative approach is proposed to solve this issue without adding extra signal conditioning components. The efficacy of the proposed solution is evident form the simulation results presented in this paper. Further work is planned to simulate the behaviour of fuzzy logic controllers under varying load conditions.

ACKNOWLEDGEMENT

The authors acknowledge the support of Mehran University of Engineering & Technology, Jamshoro, Pakistan, in providing the necessary laboratory and technical facilities to carry out this research work.

REFERENCES

[1] Halepoto, I.A., Uqaili, M.A., and Chowdhry, B.S., "Least Square Regression Based Integrated Multi-Parametric Demand Modeling for Short Term Load Forecasting", Mehran University Research Journal of Engineering & Technology, Jamshoro, Pakistan, Volume. 33, No. 2, pp. 215-226, 2014.

[2] Soares, F., Almeida, P.R., and Lopes, J.A.P., "Advanced Models and Simulation Tools to Address Electric Vehicle Power System Integration (Steady-State and Dynamic Behavior), Springer book chapter in Electric Vehicle Integration into Modern Power Networks, pp. 155-202, 2013.

[3] Hashmani, A.A., Uqaili, M.A. and Memon, R.A., "Delayed-Input Wide Area Power System Stabilizer for Mode Selective Damping of Electromechanical Oscillations", Mehran University Research Journal of Engineering & Technology, Jamshoro, Pakistan, Volume. 30, No. 2, pp. 289-296, 2011.

[4] Soundarrajan, A., Sumathi, S., and Sivamurugan, G., "Voltage and frequency control in power generating system using hybrid evolutionary algorithms", Journal of Vibration and Control, Volume 18, No. 2, pp. 214-227, 2012.

[5] Soundarrajan, A. and Sumathi, S., "Fuzzy-based intelligent controller for power generating systems. Journal of Vibration and Control, Volume. 17, No. 8, pp. 1265-1278, 2011.

[6] Wong, C.C., Li, S.A., and Wang, H.Y., "Optimal PID controller design for AVR system", Tamkang Journal of Science and Engineering, Volume. 12, No. 3, pp. 259-270, 2009.

[7] Kahouli, A., Guesmi, T., Hadj Abdallah, H., Ouali, A., "A genetic algorithm PSS and AVR controller for electrical power system stability, 6th IEEE International Multi-Conference on Systems, Signals and Devices (SSD'09), pp. 1-6, 2009.

[8] Iruthayarajan, M.W. and Baskar, S., "Evolutionary algorithms based design of multivariable PID controller, Expert systems with Applications, Volume. 36, No. 5, pp. 9159-9167, 2009.

[9] Gaing, Z.L., "A particle swarm optimization approach for optimum design of PID controller in AVR system", IEEE Transactions on Energy Conversion, Volume. 19, No. 2, pp. 384-391, 2004.

[10] Kim, D.H.," Hybrid GA–BF based intelligent PID controller tuning for AVR system", Applied soft computing, Volume. 11, No. 1, pp. 11-22, 2011.

[11] Galaz, M., Ortega, R., Bazanella, A.S., Stankovic, A.M., "An energy-shaping approach to the design of excitation control of synchronous generators. Automatica, Volume. 39, No. 1, pp. 111-119, 2003.

[12] Halepoto, I.A., Kumar, W., Memon, T.D., Ismaili, I.A., "Quantifying the effect of Look up Table Size and Coefficients Complexity for Non-Linearity Compensation in Power Amplifiers", Sindh University Research Journal (Science Series) Volume. 45, No. 2 pp. 447-452, 2013.

[13] Hallenius, K.E., Vas, P., and Brown, J.," "The analysis of a saturated self-excited asynchronous

generator", IEEE Transactions on Energy Conversion, Volume 6, No. 2, pp. 336-345, 1991.

[14] Ramya, R. and Selvi, K.," Simulation of Synchronous Generator with Fuzzy based Automatic Voltage Regulator", International Journal of Electrical & Computer Engineering, Volume.2, No. 6, pp. 2088-8708, 2012.

[15] Demiroren, A. and Zeynelgil,H.," Modelling and simulation of synchronous machine transient analysis using SIMULINK", International Journal of Electrical Engineering Education, Volume 39, No. 4, pp. 337-346, 2002.

[16] Schei, T.S., "Automatic tuning of PID controllers based on transfer function estimation", Automatica, Volume. 30, No. 12, pp. 1983-1989, 1994.

[17] Ramsden, E.," Hall-effect sensors: theory and application", Newnes Publishers, latest edition, ISBN: 13-978- 7506-7934-3, 2011.

[18] Hussain I, Patoli, A.A., Kazi, K., "Fuzzy Logic Based Effective Anti-Lock Braking System Adaptive to Road Conditions", 1st international conference on modern communication and Computing Technologies (MCCT'14), 2014.

[19] Hashmi, K., Graham, I., Mills, B., "Fuzzy logic based data selection for the drilling process", Journal of Materials Processing Technology, Volume. 108, No. 1, pp. 55-61, 2000.

[20] Mamdani, E.H., "Application of fuzzy logic to approximate reasoning using linguistic synthesis", IEEE Transactions on Computers, Volume. 100, No. 12, pp. 1182-1191, 1977.

[21] Hussain, I., Mei, T., Ritchings, R.," Estimation of wheel–rail contact conditions and adhesion using the multiple model approach", Vehicle System Dynamics, Volume. 51, No.1, pp. 32-53, 2013.

****

Quotations

- God gave burdens, also shoulders.
  Yiddish Proverb
- Going slowly does not stop one from arriving.
  West African saying
- A man's deeds are his life.
  West African saying
- Your food is close to your stomach, but you must put it in your mouth first..
  West African saying
- Don't call a man honest just because he never had the chance to steal.
  Yiddish saying
- A journey of thousand miles begins with a single step.
  Chinese Proverb
- The thoughtless strong man is the chief among lazy men.
  West African Saying
- If it isn't perfect, make it better.
  Japanese manufacturing slogan
- Modern is a tree with roots of contentment, and fruits of tranquility and peace.
  North African saying
- Nothing is achieved in a dream.
  West African saying
- You cannot prevent the birds of sorrow from flying over your head, but you can prevent them from building nests in your hair.
  Persian Proverb
- He who hates, hates himself.
  South African saying
- The man who is not jealous in love does not love.
  North African saying
- The opinion of the intelligent is better than the certainty of the ignorant.
  North African saying
- Not to know is bad; not to wish to know is worse.
  West African saying
- It's nice to be important, but it's more important to be nice.
  West African saying

Hollow Core Fiber Design with Ultimate Low Confinement Loss and Dispersion

Mamoona Khalid and Irfan Arshad
University of Engineering and Technology, Taxila, Pakistan.

Abstract

Secure and uninterruptable data communication is one of the most important requirements in telecommunication sector. Research is being done in the field of telecommunication in order to provide secure data to customers by reducing dispersion and confinement losses within an optical fiber. Photonic crystal fiber is a new technology of optical fibers which has provided secure and managed data transfer with low dispersion properties and confinement loss. In this paper we studied Hollow Core Photonic Crystal Fibers (HC-PCF) to reduce the dispersion and losses through the fibers. We presented different designs of HC-PCF and selected one design with reduced dispersion and confinement loss. The main purpose of this study was to develop a design that can be utilized in Wavelength Division Multiplexing Systems (WDM). In WDM systems we can only use a fiber that has low material dispersion and low confinement loss. The wavelength range for a WDM system is from 1300nm to 1550nm. So, we studied HC-PCF designs and calculated the confinement loss and dispersion within this range.

Index Terms—Hollow Core Fibers, Photonic Crystal Fibers, Confinement Loss, Dispersion, Wavelength Division Multiplexing Systems.

I. INTRODUCTION

Photonic Crystal Fiber (PCF) is a two dimensional fiber made up of a dielectric material such as silica. Latest trends of PCF show that they successfully replaced the conventional optical fiber in telecommunication sector. Two types of PCF have been reported in literature, Solid Core PCF (SC-PCF) and Hollow Core PCF (HC-PCF) [1]. Research is being done on both these fibers and it is expected that both of these types of PCF should propagate light with minimum losses and dispersion to fulfill the requirements of the customers.

Like conventional optical fibers, PCF also consist of a core that is surrounded by a cladding. The cladding of PCF is much different than the cladding of optical fiber. It consists of periodic air hole rings that sometimes make the refractive index of core smaller than that of the cladding. In conventional optical fibers the refractive index of core is greater than the refractive index of cladding due to which light is guided through the core because of Total Internal Reflection (TIR) [2]. In PCF light is guided through the core due to Total Internal Reflection (TIR) and also due to Photonic Band Gap effect (PBG) that is generated by the periodic air hole rings in the cladding. If the refractive index of core of PCF is greater than that of cladding, light guidance is due to TIR, and if the refractive index of core is smaller than the combined effect of air hole rings of cladding, light is guided due to PBG effect. In HC-PCF light guidance is mainly due to PBG effect. The Fig. 1 shows the difference between SC-PCF and HC-PCF [2].

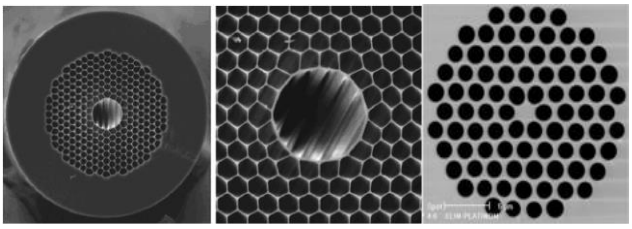

(a) (b) (c)

Fig.1: (a) Hollow Core PCF (b) Core of HC-PCF (c) Solid Core PCF

An SC-PCF propagates light using the air holes of cladding that runs down the entire fiber length [3]. These fibers are made up of a material commonly known as silica and consist of a core surrounded by a cladding made up of periodic air hole rings [4]. In SC-PCF, core is simply a region without an air hole. If we introduce an air hole in the core region of PCF then it becomes another important and useful form of PCF known as Hollow Core Photonic Crystal Fiber (HC-PCF). Presence of air holes in such fibers opens up a variety of potential applications ranging from small mode area for highly non-linear fibers for non-linear devices to large mode area fibers for high power delivery [5]. When we arrange large air-holes in the form of a periodic network, light propagation can be achieved through PBG effect. Literature Review shows that a band gap is only produced when the airholes are quite large. When a defect is established in such a structure, as large airhole in center of figure 1(a) and (b), a localization mode excitation is established in Photonic Band Gap region, and it is then possible for the PCF to direct light inside an air core along the entire length of the fiber. This new mechanism of light propagation within HC-PCF leads to a large number of useful applications such as, these fibers are used to deliver large amount of power, and they are also used as sensing elements in gas sensors [6].

II. Theoretical Discussion

Propagation through a Photonic Crystal Fiber requires the solution of Maxwell's equations. To solve the Maxwell's equations we assume a lossless and source free medium for convenience. The Maxwell's equations for such medium are given by Eq. (1-4) [7]

$$\nabla \times \boldsymbol{H} = \epsilon . \frac{\partial \boldsymbol{E}}{\partial t} \quad (1)$$

$$\nabla \times \boldsymbol{E} = -\mu . \frac{\partial \boldsymbol{H}}{\partial t} \quad (2)$$

$$\nabla . D = \nabla . \epsilon \boldsymbol{E} = \boldsymbol{0} , \quad (3)$$

$$\nabla . B = \nabla . \mu \boldsymbol{H} = \boldsymbol{0} \quad (4)$$

The normalized frequency V for a conventional step index fiber is given by Eq. 5

$$V = k_0 \rho \sqrt{n_{co}^2 + n_{cl}^2} \quad (5)$$

Where ρ is the core radius, k_0 is the wave number, n_{co} and n_{cl} are the refractive indices of the core and cladding respectively [8]. The smaller is the V number, the fewer guided modes are handled by the core. If for a given wavelength V < 2.405, fiber will only support a single mode for propagation of light and that fiber is simply a single mode fiber. The normalized frequency for a PCF is given by Eq. 6

$$V_{eff}(\lambda) = k_0 2\Lambda \sqrt{n_{silica}^2 + n_{eff}^2(\lambda)} \quad (6)$$

Where 2Λ is the core diameter [8]. A PCF with d/Λ $\leq$ 0.4 do not support higher order modes because for them $V_{eff}(\lambda) \leq 2.405$ for a given wavelength with d being the hole size.

As in this paper we are concentrating more on the losses and dispersion effects occurring within HC-PCF so we will now describe the spectral density $S_z(\kappa)$, as $S_z(\kappa)$ and the transverse overlap of modes at glass surfaces determine the strength of coupling and loss is calculated from power coupled to the modes [9]. $S_z(\kappa)$ is given by Eq. 7

$$S_z(\kappa) = \frac{k_B T_g}{4\pi\gamma\kappa} \coth\left(\frac{\kappa W}{2}\right) \quad (7)$$

Where T_g is glass transition temperature, k_B is the Boltzmann constant, γ is surface tension and κ is the spectral frequency and is given by Eq. 8

$$\kappa = \frac{2\pi}{\lambda} |n - n_0| \quad (8)$$

where n and n_0 are the mode index and the effective mode index respectively. The normalized field intensity is given by Eq. 9 [9]

$$F = \left(\frac{\varepsilon_0}{\mu_0}\right)^{1/2} \frac{\oint_{hole\ perimeters} dl |E|^2}{\int_{cross-section} dA |E \times H^*| \cdot \hat{z}} \quad (9)$$

Where **E** and **H** are the Electric and Magnetic fields. $\hat{z}$ is the unit vector along the direction of fiber. The air filling fraction f of air holes of HC-PCF is directly related to the hole parameters and is given by Eq. 10 [8]

$$f = \left(\frac{d}{\Lambda}\right)^2 \left[1 - \left(1 - \frac{\pi}{2\sqrt{3}}\right)\left(\frac{d_c}{d}\right)^2\right] \quad (10)$$

To obtain hexagonal holes we have to set $\frac{d_c}{d}$ = 0, and for circular holes we have $\frac{d_c}{d}$ = 1, where d is the hole size, d_c is the curvature at corners and Λ is the pitch (distance between two adjacent holes) [9].

For simulation purpose, we used Perfectly Matched Layer (PML) boundary conditions for which we selected an anisotropic material whose permittivity and permeability tensors are given by [9]

$$\varepsilon = \varepsilon_0 n^2 S \quad ; \quad \mu = \mu_0 S \quad (11)$$

with

$$S = \begin{bmatrix} s_x/s_y & 0 & 0 \\ 0 & s_x/s_y & 0 \\ 0 & 0 & s_x/s_y \end{bmatrix} \quad (12)$$

s_x and s_y are the components of S and are given in the following Table 1

TABLE I
PML PARAMETERS

PML Parameters	PML Region		
s_x	1	s_2	s_2
s_y	s_1	1	s_1

values of s_i (i = 1,2) are given by the formula

$$s_i = 1 - j\alpha_i \left(\frac{\rho}{d_i}\right)^2 \quad (13)$$

Here d is the distance from start of PML and d_i is the PML width in both horizontal and vertical directions, α_i is the attenuation [10].

Confinement loss L_c occurring within HC-PCF is due to finite number of air holes and is given by Eq. 14

$$L_c = 8.680\ k_0\ I_m \eta_{eff}$$

Where

$$\eta_{eff} = \eta_{material} + \eta_{eff,\ bandstructure} - \eta_{constant} \quad (15)$$

Dispersion is the combined effect of material dispersion and waveguide dispersion and is given by Eq. 16 [8]

$$D(\lambda) = -\frac{\lambda}{c} \times \frac{(d^2\ Re[\eta_{eff}])}{d\lambda^2} \quad (16)$$

Dispersion is basically the second derivative of propagation constant β i.e $\beta_2(\omega) = \frac{\partial^2 \beta}{\partial \omega^2}$ [8]

$$\beta(\omega) = \frac{n_{eff}(\omega)\omega}{c} = \sum_m \frac{1}{m!} \beta_m (\omega - \omega_0)^m; \quad \beta = \frac{\partial \beta}{\partial \omega}\Big|_{\omega = \omega_0} \quad (17)$$

III. Simulation and Results

In this paper we proposed a design for a Hollow Core Photonic Crystal Fiber through which light can be propagated with minimum confinement loss and dispersion. We designed this fiber in order to utilize it in wavelength division multiplexing systems where it is mandatory to minimize both the loss and dispersion for secure and uninterruptable transmission of light from one terminal to the other. In this paper we did the modal analysis of our proposed HC-PCF designs, to calculate the Electric Field intensity through the fundamental mode of the fibers and then calculated the dispersion and confinement loss through the proposed designs of HC-PCF using the formulas given in theoretical discussion. In WDM systems, wavelength range of operation is from 1300nm to 1550 nm [11]. So we analyzed our designs of HC-PCF over this range and calculated the dispersion and confinement loss for both the lower limit and upper limit

of the wavelength i.e at 1300nm and 1550nm. Using the technique given earlier in this paper we designed three different designs of HC-PCF and then compared them with each other as well as compared them with the designs available in literature and found a design with lowest possible loss and dispersion. For this purpose we used five layered model of HC-PCF which means that the cladding of the fiber contained five rings of periodic air holes. The following Table II shows the comparison between three designs we made:

In this table pitch is the distance between the two consecutive air holes. Radius R_1, R_2, R_3, R_4, R_5 is the radius of the air holes indexing from the inner ring. The first two designs are made by making the radius of air holes of all the rings equal and in the third design; radius of air holes of all the rings is different. We were supposed to find a design in which both dispersion and confinement loss should be kept in mind. We cannot select a design with low loss and high dispersion or vice versa. So, by comparing the designs given in table, design 3 is providing the best design with low loss and low dispersion. The following figure 2 shows the Electric Field intensity through HC-PCF designs.

TABLE II
SIMULATION PARAMETERS

Design	Pitch (µm)	Radius R1,R2,R3,R4,R5 (µm)	Core Dia (µm)	Loss at 1300nm (dB/cm)	Loss at 1550nm (dB/cm)	Dispersion at 1300nm (ps/nm/km)	Dispersion at 1550nm (ps/nm/km)
1	1.6	0.5	2.5	0	$3x10^{-7}$	45	65
2	1.6	0.3	1.5	0	17	− 100	− 160
3	1.6	0.25,0.29,0.32, 0.33,0.69	1.5	0	$4x10^{-9}$	− 4	− 38

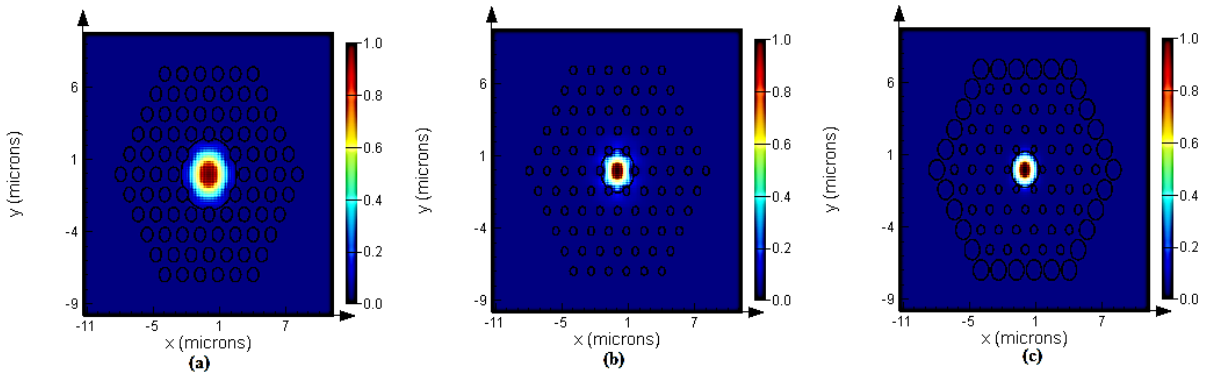

Figure 10: Electric field intensities through the fundamental mode for designs of HC-PCF

The following Figure 3 shows the confinement loss through the fiber designs presented above

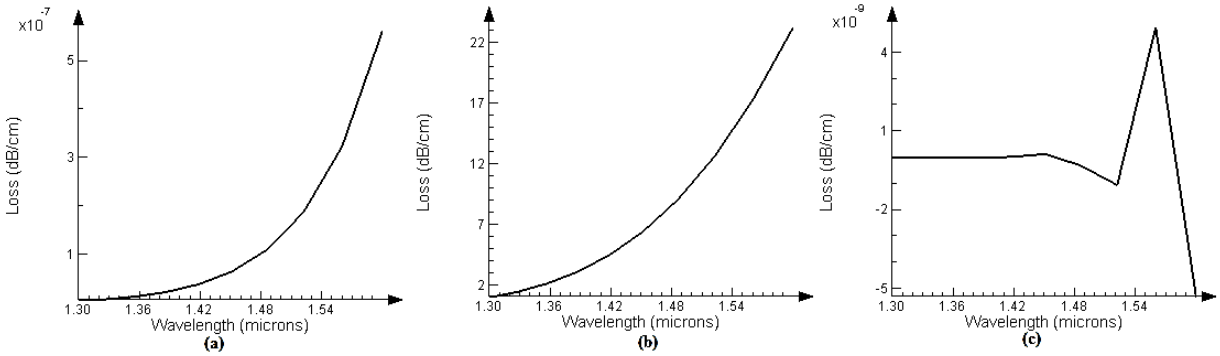

Figure 11: Comparison of confinement losses for the three designs of HC-PCF

The dispersion obtained through the three given designs is presented in the Figure 4

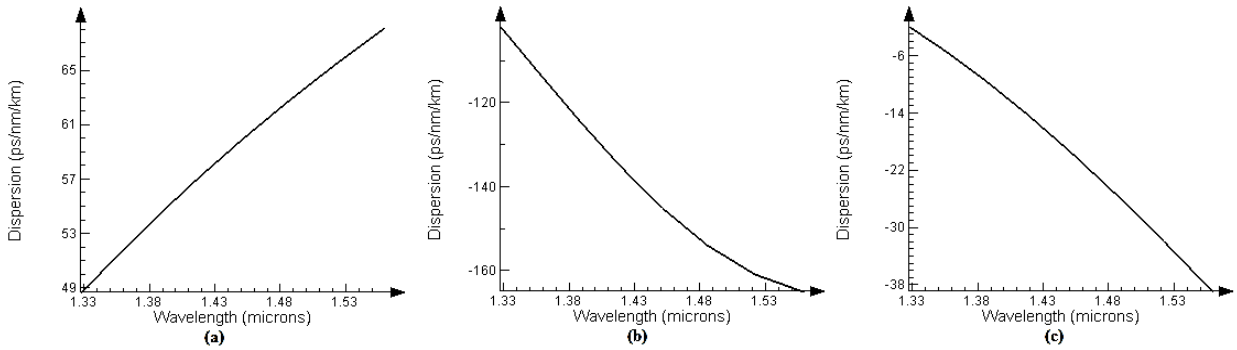

Figure 12: Comparison of dispersion for the three designs of HC-PCF

IV. Conclusions

In this paper, we studied the transmission properties of HC-PCF fiber so that it can be utilized in WDM systems. We have focused much on the confinement loss and dispersion properties occurring within the fiber. We first analyzed the three different designs to find their fundamental mode through which light passes more efficiently, and then compared these designs with each other to select the best design having lowest possible loss and dispersion. By looking at Table 1, we found that the Design 3 of HC-PCF is the best possible design having lowest possible loss and dispersion. The fiber of design 3 has a confinement loss of 4×10^{-9} dB/cm and dispersion of -38ps/nm/km at 1550nm. These three designs were made after having a thorough look at literature; we found that these three designs were a better option. Among these three designs, design 3 was chosen to be the one with minimum possible confinement loss and dispersion.

Reference

[1] P J Brown, Stephen H Foulger, "Photonic Crystal-Based Fibers" Project M02-CL06.Annual Report 2005.

[2] P. J. Roberts, F. Couny, H. Sabert, B. J. Mangan, D. P. Williams, L. Farr, M. W. Mason and A. Tomlinson, "Ultimate low loss of hollow-core photonic crystal fibres" *OPTICS EXPRESS*, vol 13. No.1, 2005.

[3] R. F. Cregan, B. J. Mangan, J. C. Knight, T. A. Birks, P. St.J. Russell, P. J. Roberts and D. C. Allan, "Single-mode photonic band gap guidance of light in air," *Science* 285, 1537-1539 (1999).

[4] Altaf Khetan, Ali Momenpour, T. Monfared, Vidhu S. Tiwari , Hanan Anis, "Hollow core photonic crystal fiber as a robust Raman biosensor" *Optical Fibers and Sensors for Medical Diagnostics and Treatment Applications* XIII, Proc. of SPIE Vol. 8576, 85760F.

[5] S. O. Konorov, C. J. Addison, H. G. Schulze, R. F. B. Turner, and M. W. Blades, "Hollow-core photonic crystal fiber-optic probes for Raman spectroscopy," *Opt. Lett.*31, 1911-1913 (2006).

[6] X. Yang, C. Shi, R. Newhouse, J. Z. Zhang, and C. Gu, "Hollow-Core Photonic Crystal Fibers for Surface-Enhanced Raman Scattering Probes," *International Journal of Optics*, vol. 2011, Article ID 754610, (2011).

[7] M. R. Albandakji, "Modeling and Analysis of Photonic Crystal Waveguides", PhD Dissertation submitted to the Faculty of the Virginia Polytechnic Institute and State University (2006).

[8] Rodrigo Amezcua Correa, "Development of Hollow Core Photonic Band Gap Fibers Free of Surface Modes" PhD Dissertation submitted to Faculty of Engineering, Science and Mathematics, Optoelectronics Research Center, University of Southampton (2009).

[9] F. BENABID, "Hollow-core photonic bandgap fibre: new light guidance for new science and technology" Philosophical Transactions, *The Royal Society* (2006).

[10] Sanjaykumar Gowre, SudiptaMahapatra, and P. K. Sahu "A Modified Structure for All-Glass Photonic Bandgap Fibers:Dispersion Characteristics and Confinement Loss Analysis" ISRN Optics, Volume 2013, Article ID 416537, (2013).

[11] Mamoona Khalid, I. Arshad, M. Zafrullah " Design and Simulation of Photonic Crystal- Fibers to Evaluate Dispersion and Confinement Loss for WDM Systems" accepted, The Nucleus 51, No.2, 2014.

***

Design and FPGA Implementation of Compositional Microprogram FIR Filter

Kamran Javed, Naveed Khan Baloch, Fawad Hussain, Dr. Muhammad Iram Baig
University of Engineering & Technology, Taxila, Pakistan

Abstract

FIR Filters on Field Programmable Gate Array (FPGA) are designed by different methods of Digital Design. Microprogramming based FIR filters are vastly used in Video and Image Processing application. Purpose technique is Compositional Microprogram Control Unit (CMCU) FIR Filter. CMCU is both time and area optimized filter than that of microprogram FIR Filter. Parallel architecture is used in Data path of design. Verilog Hardware Descriptive Language (HDL) is used to implement design. Results are evaluated on ModelSim SE Plus 6.1f and hardware optimization results are evaluated on Xilinx ISE web pack 10.1. As an example of synthesis, Compositional Microprogram Control Unit (CMCU) FIR Filter designed in this paper is also tested for real time Audio Filtering. Code is tested on FPGA XC3S700AN [14] using stereo audio codec (AKM AK4551) [13] on 50MHz clock frequency. Proposed filter is tested for third order but it can be extended for higher order which can be used for high speed applications like DSP applications e.g., Noise Cancelation, Video and Image Processing.

Index Terms— FPGA, Compositional Microprogram, Parallel Architecture, Audio Codec.

1. INTRODUCTION

Digital signal processing is very important process in many image and video applications. Finite impulse response (FIR) is a commonly used digital filter in many digital signals processing (DSP) [5]. FIR Filters are widely used because they have linear phase characteristics and guaranteed stability. Digital filters are mainly used for removing the undesirable parts of the input signal such as random noise or components of a given frequency content. FIR filters are commonly used in spectral shaping, motion estimation, noise reduction, channel equalization among many other applications. The simplest realization of an FIR filter is derived from.

In direct form mentioned above, $y(n)$ are the Outputs, $h(k)$ are Tap Coefficients, $x(n)$ are the Inputs and $x(n-k)$ are the delayed samples by time unit 'k'.

There are two type of implementation FIR Filters.

(i) Software

(ii) Hardware

In software implementation we used Matlab and Java to implement FIR Filter. In hardware implementation we use programmable Digital Signal Processors (DSPs) which are program according to FIR filter instructions which are write in programming language like C [15]. Another hardware implementation of FIR filter is by configuring hardware like Complex Programmable Logic Device (CPLD) or Field Programmable Gate Array (FPGA).

In software implementation we use general purpose computer for computing which is slow as compare to hardware implementations where we use dedicated hardware which provide fast computation as compare to general purpose computer [15]. Hardware implementation itself has two type in processor based implementation hardware is programed according to filter requirements which Fetch, Decode and Executes the instructions while configuration of FPGA for FIR filter is more faster implementation even as compare to processor based implementation. In FPGAs actually we design hardware as compare to processor based technique where we only program pre design hardware. This paper presents hardware implementation on FPGA. The architecture of FIR Filter is Compositional Microprogram.

$$y(n) = \sum_{k=0}^{N-1} h(k) \, . x(n-k) \qquad -(i)$$

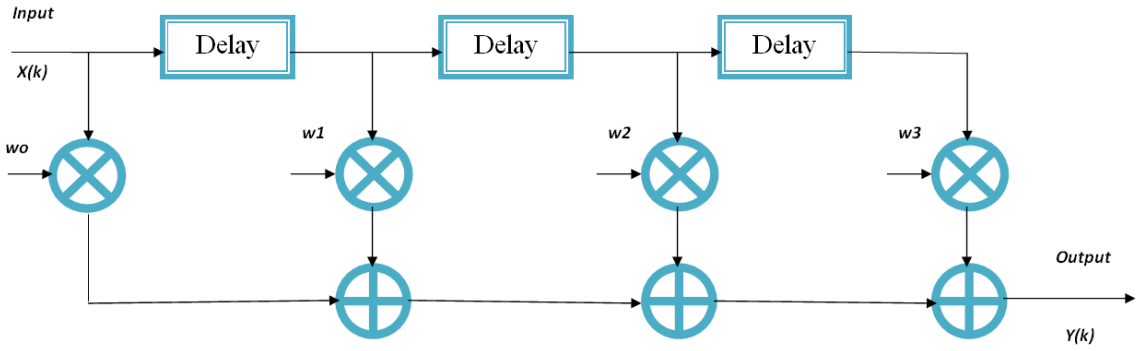

Fig.1 FIR Filter

2. DESIGN ARCHITECTURE OF FIR FILTER

The architecture of proposed FIR Filter is divided into two parts:

I. Control Logic (Control Unit)

II. Components that actually execute the Logic (Datapath)

Control Unit is controlling part of FIR Filter it undergoes different states, each state generates commands to Datapath which are executed as per direction of Control Unit in the Datapath of FIR Filter. Control Unit just think what are the control sequences and don't know how the design will operate on data, Datapath gets the signals from Control Unit and don't think what next, and execute the current control signals. So, the fig.2 clearly states that Control Unit is what which generates control signals and decides what to do, and Datapath is what which gets control signals from the Control Unit and executes the job.

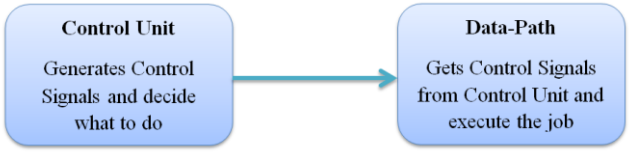

Fig 2. FIR Filter Design Partitioning

2.1 CONTROL UNIT

Control Unit takes decisions and produces control signals to Datapath. Control Unit doesn't have artificial intelligence to command operations. It goes through predefined sequence of operations. There are different ways of designing a Control Unit like Microprogram Control Unit and Hardwired Control Unit.

Flip-flops, decoders, gates and other digital circuits are used to implement the control logic in the hardwired architecture. One of benefits of hardwire organization is that it can be advanced to generate a fast mode of operation. On the other hand, Control memory is used to save the control information in the microprogram architecture [16]. The desired arrangement of micro-operations is programed in the control memory. Hardwired control is not beneficial since if there is a need to modify the design then modifying wiring among the various components is necessary [16]. Microprogram control is preferable because design can be modified easily by reprogramming the microprogram in the control memory.

Microprogram Control Unit consists of Control Memory which has microinstructions. Microinstructions in the control memory are addressed with the help of address register, which defines the address of corresponding microinstruction and as a result, control signals are produced. One of the most popular reasons to implement Control Unit by microprogramming is that it translates the hardware problems into programming problem, which makes it easy to control by a wider range of designers.

There is another way of designing Microprogram Control Unit i.e., Compositional Microprogram Control Unit (CMCU). In CMCU, Mealy machine is implemented. Program Counter is used to address microinstructions in the Control Memory [1], [2]. The advantage of proposed technique is that it permits to calculate the next address of control memory in one clock cycle of Control Unit operation. Because of which CMCU is efficient than MCU [1], [2].

The proposed design of CMCU is shown in Fig 3 and Algorithm State Machine of filter is shown in Fig 4.

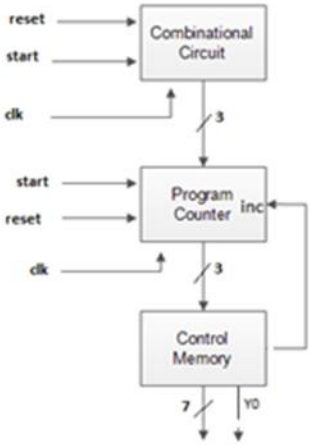

Fig. 3. FIR Filter Compositional Microprogram Control Unit

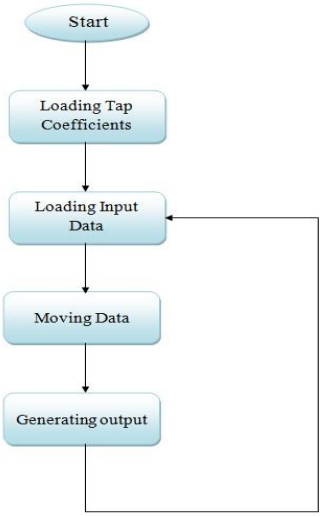

Fig. 4 Algorithm State Machine of Filter

The size of Control Memory is 8x8 having 8 microinstructions each of 8 bits. LSB 7 bit field of microinstruction includes the control signals for the Datapath where remaining single bit is used to increment or load the Program Counter. The Program Counter is of 3 bits to address 8 different microinstructions in the control memory. The Combinational Circuit is responsible for branching of Control Unit to capture new upcoming data.

The transition table of CMCU is shown in Table 1. The table shows the control signals are generated for Datapath which execute the job depending upon the control signals. According to Table 1, first microinstruction loads first tap coefficient, second microinstruction loads second tap

coefficient, third microinstruction loads third tap coefficient, fourth not only loads fourth tap coefficient but also clears the data registers, 5th microinstruction loads input data, 6th microinstruction moves the input data, 7th microinstruction latches the output. The first 4 steps are executed once at the start while step number 5, 6 and 7 are repeated again and again for each data.

2.2 FIR FILTER DATAPATH

The Datapath architecture of third order FIR Filter consists of the following sub modules: four 8-bit data registers, one 2-to-4 decoder, four 8-bit coefficient registers (ho, h1, h2, h3), four multipliers, three 16-bit adders and one 16-bit register for latching the output. The complete Datapath is obtained after coding each sub module in Verilog. The complete Datapath of four tap FIR filter with parallel architecture [3] is shown in Fig 5.

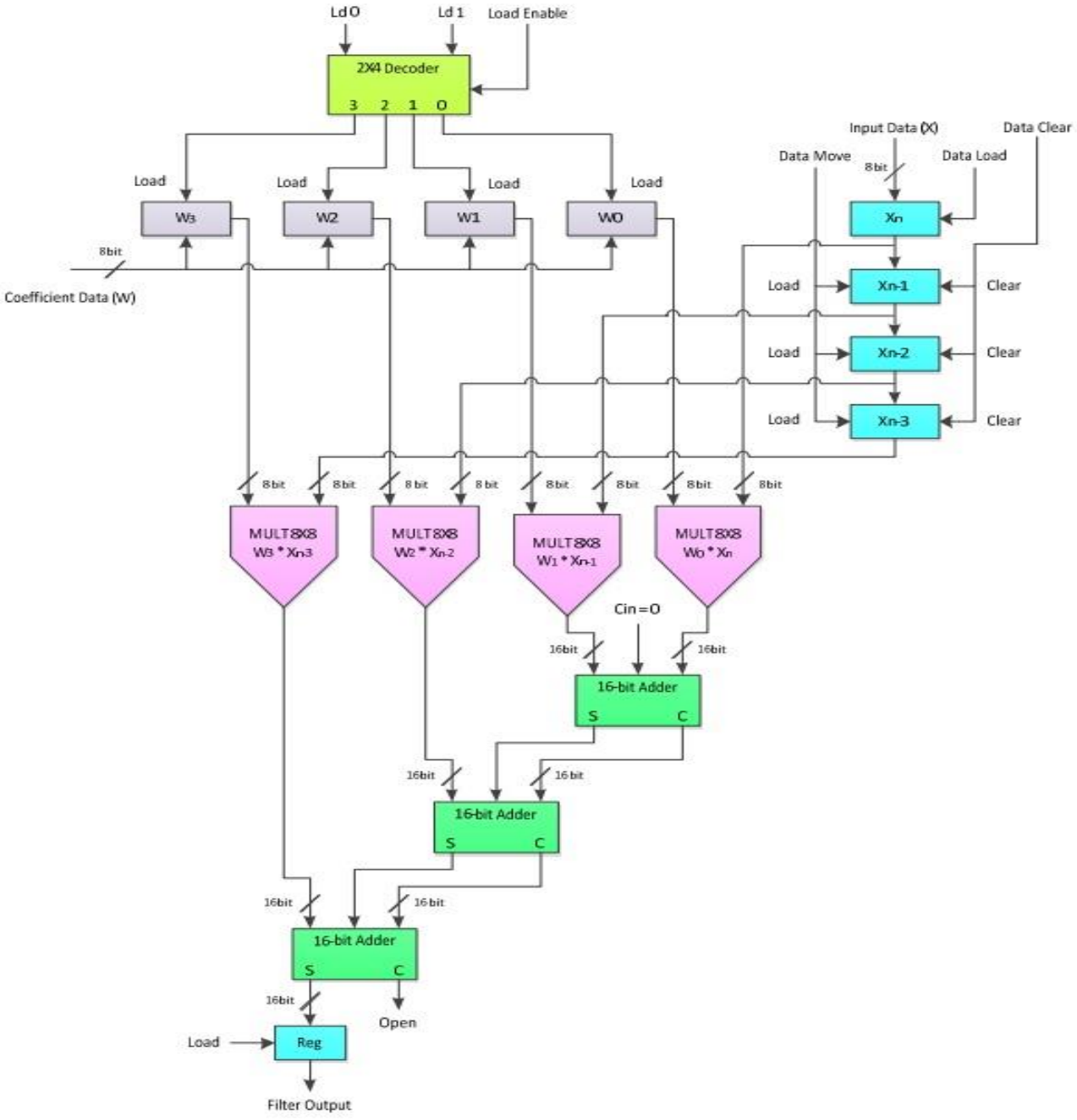

Fig.5 Datapath Architecture [3]

Sr #	Micro Operation		Increment	Load_en	Ld_1	Ld_0	D_clear	D_load	D_move	Y_L
1	Loading Tap Coefficients	*h0*	0	1	0	0	0	0	0	0
2		*h1*	0	1	0	1	0	0	0	0
3		*h2*	0	1	1	0	0	0	0	0
4		*h3*	0	1	1	1	1	0	0	0
5	Loading Input Data *x[n]*		0	0	0	0	0	1	0	0
6	Moving Input Data		0	0	0	0	0	0	1	0
7	Generating Output *y[n]*		1	0	0	0	0	0	0	1

TABLE.1 CMCU Transition Table

3. FPGA IMPLEMENTATION

To implement the proposed architecture, the FPGA device used is Spartan-3AN (xc3s700AN-4fg484). Table 2 shows the design summary of Resource Utilization of the device

Logic Utilization	**Used**	**Available**	**Utilization**
Number of Slice Flip Flops	44	11,776	1%
Number of 4 input LUTs	219	11,776	1%
Logic Distribution			
Number of occupied Slices	132	5,888	2%
Number of Slices containing only related logic	132	132	100%
Number of Slices containing unrelated logic	0	132	0%
Total Number of 4 input LUTs	219	11,776	1%
Number of bonded IOBs	35	372	9%
Number of BUFGMUXs	1	24	4%
Number of MULT18X18SIOs	4	20	20%

TABLE.2 Device Resource Utilization

4. RESULTS AND SIMULATIONS

The Compositional Microprogram FIR Filter code is tested for three different input vectors as described in the Table 3. The Tap Coefficients for a particular test are fixed while the input data is changed continuously. The output generated by the third order FIR Filter for each input vector is shown in output vector. The result of all three different tests is shown in Table 3.

Test Case	**Tap Coefficients (W)**	**Input Data (X)**	**Output Data (Y)**
1	{5,4,4,1}	{3,9,7,7}	{15,57,83,102}
2	{3,6,6,5}	{2,10,3,3}	{6,42,81,97}
3	{1,2,2,1}	{1,2,3,3}	{1,4,9,14}

TABLE. 3. CMCU Transition Table

5. CONCLUSION

In Micro-program Controller based Parallel Digital FIR Filter, each memory location was of 12 bits in order to save the control signals [3] while in proposed technique 8 bits are used in Compositional Micro-programmed Controller based Parallel Digital FIR Filter. So, memory width is reduced from 12 bits to 8 bits. Number of memory locations is also reduced from 16 to 8. Memory size is reduced from 16x12 (192 bits) [3] to 8x8 (64 bits). It has not only increased the access time but also the overall speed is increased. Moreover, branching instruction for each pair of data is reduced. Now, each pair of data require 12 clock cycles instead of 16 clock cycles which were required by Micro-programmed Controller based Parallel Digital FIR Filter. So, overall speed is increased. Filter is tested on FPGA XC3S700AN using stereo audio codec (AKM AK4551) [13] on 50MHz clock frequency. As a future work, this FIR Filter can be optimized by using Xilinx IP Core and implementing Control Memory on dedicated FPGA BRAM.

REFERENCES

[12] Alexander Barkalov, Larysa Titarenko "Logic Synthesis for FSM-Based Control Units," vol. 5 3, Springer-Verlag, Berlin, 2009

[13] Alexander Barkalov, Larysa Titarenko "Logic Synthesis for Compositional Microprogram Control Units," vol. 5 3, Springer-Verlag, Berlin, 2008

[14] Mohammed S. BenSaleh, Syed Manzoor Qasim, M. Bahaidarah, H. AlObaisi, T. AlSharif, M. AlZahrani, and H. AlOnazi.'"Field Programmable Gate Array Realization of Microprogrammed Controller based Parallel Digital FIR Filter Architecture "' Proceedings of the World Congress on Engineering and Computer Science 2012 Vol II WCECS 2012, October 24-26, 2012, San Francisco, USA

[15] Bruce W. Bomar, Senior Member, IEEE '"Implementation of Microprogrammed Control in FPGAs."', IEEE Transactions On Industrial Electronics, Vol 49, No. 2, April 2002

[16] Yajun Zhou, Pingzheng Shi. 'Distributed Arithmetic for FIR Filter implementation on FPGA.', 978-1-61284-774-0/11 ©2011 IEEE

[17] Remigiusz Wiśniewski, Monika Wiśniewska, Marek Węgrzyn, Norian Marranghello.'Design of Microprogrammed Controllers with Address Converter implemented on Programmable Systems with Embedded Memories', 978-1-4577-1958-5/11 ©2011 IEEE

[18] Monika Wiśniewska, Remigiusz Wiśniewski, Marek Węgrzyn, Norian Marranghello.'Reduction of the Memory Size in the Microprogrammed Controllers', 978-1-4577-1958-5/11 ©2011 IEEE

[19] Syed Manzoor Qasim, Mohammed S. BenSaleh,Mazen Bahaidarah, Hesham AlObaisi And Tariq AlSharif, Mosab AlZahrani and Hani AlOnazi."Design and FPGA Implementation of Sequential Digital FIR Filter using Microprogrammed Controller."', 978-1-4673-2015-3/12 ©2012 IEEE

[20] Shoab Ahmed Khan.' Digital Design Of Signal Processing Systems A Practical Approach', John Wiley and Sons, United Kingdom, 2011.

[21] Dr. Shoab A. Khan And Hamid M. Kamboh.'An Algorithmic Transformation for FPGA Implementation of High Throughput Filters', 978-1-4577-0768-1/11 ©2011 IEEE

[22] Remigiusz Winiewski.'Synthesis of Compositional Microprogram Control Units for Programmable Devices.', Ph.D. Thesis University of Zielona Góra Zielona Góra, Poland, 2008

[23] Ms. Aye Thi Ri Wai and Ms. Phyu Phyu Tar "Translating A Microprogram To Hardwire Control" Proceedings of ECTI-CON 2008

[24] Dave Vandenbout. "S tereo loopback circuit" available at: *http://www.xess.com/static/media/projects/loopbk.zip*

[25] Xilinx Development Team. "Spartan-3AN Documentation." available at:

http://www.xilinx.com/support/index.html/content/xilinx/en/supportNav/silicon_devices/fpga/spartan-3an.html

[26] Pieter Abbeel Assistant Professor UC Berkeley "Signals and Systems- Implementation of FIR filters" available at:

http://ptolemy.eecs.berkeley.edu/eecs20/week12/implementation.html

[27] CADENTI "Hardwired control" available at:

http://www.cadenti.com/hardwired.html

[28] Shih-Lien lu and Hubert Stier " Design of Pipelined FIR Filter with MSB-First Multiplier" Dept. of Electrical and Computer Engineering , Oregon State University ,Corvaliis, Or 97331 USA

[29] Joseph B. Evans.'"Efficient FIR Filter Architectures Suitable for FPGA Implementation,", ISCAS '93 in Chicago,Illinois.

[30] Remigiusz Wi´Sniewski , Alexander Barkalov , Larisa Titarenko Wolfgang A. Halanl: '"Design Of Microprogrammed Controllers To Be Implemented In FPGAs."', Int. J. Appl. Math. Comput. Sci., 2011, Vol. 21, No. 2, 401–412 DOI: 10.2478/v10006-011-0030-1

[20] Alexander Barkalov, Larysa Titarenko "Logic Synthesis for Compositional Microprogram Control Units" Donetsk National Technical University,Poland

****

Improved Dynamic Frame Size with Grouping Slotted Aloha (IDFSG)

Usman Hayat, Naveed Khan Baloch, Fawad Hussain, Malik Muhammad Asim
Department of Computer Engineering, University of Engineering and Technology Taxila, Pakistan

Abstract:

Radio Frequency Identification (RFID) system is an emerging technology in field of automatic identification and object tracking. It's a wireless communication between sender tag and receiver via radio frequency. One of the challenges it faces is tag collision at reader. It's an important factor that determines the performance of RFID system. Different approaches and algorithms have been developed to reduce collision and to efficiently read the RFID tags. The basic concept is the best utilization of time slots between reader and tag during data transmission. DFSG algorithm improves EDFSA by implementing dynamic group sizing technique. However it is dependent upon initial frame-length. The proposed algorithm removes initial frame-length dependency. The proposed algorithm is compared with previous techniques. Identification time, iteration taken to read group and system efficiency comparison is included in this research work. The proposed algorithm shows improved results for Identification time, iteration taken to read group and system efficiency is much closer to possible ideal values.

4. Keywords: RFID Algorithm, Passive UHF RFID, RFID Anti -collision, EPC class 1 Gen 2, grouping approach, maximum system efficiency

1. Introduction:

RFID system is a result of an effort to have a low cost radio frequency system to communicate between two or more equipment. It consists of Reader (which send query) and a Tag (Accept the query and reply with its ID. In response of the reader broadcast query message all tags within range tries to reply and some replies arrive at the reader at same time resulting a misconception at reader end i.e collision. Aloha protocol [1] (better known as pure Aloha) was the first successful algorithm to cater this problem. However pure Aloha had very less successful transmission rate of 18.4%.

1.1 Related work

Slotted Aloha [2, 3] was improved version of Pure Aloha. A communicator can send only at the timeslot beginning and not during the transmission of data. Slotted Aloha was further enhanced by N. Abramson [3] deciding frame size dynamically on the bases of tag estimation. This greatly improved Aloha and become bases of other anti-collision algorithms such as, An Enhanced Dynamic Framed Slotted ALOHA Algorithm (EDFSA) by S. Lee et al [4], Dynamic Grouping Frame-slotted Aloha (DGFS) by Mian Hammad Nazir at al [5] and Dynamic Frame Sizing with Grouping Slotted Aloha (DFSG) by Sobia Arshad et al [6].It was quite noticeable fact in RFID system that higher the numbers of tags available within the reader range greater the number of collision exists. The main requirement of any anti-collision algorithm is to efficiently read all the tags in minimum possible time.

In following sections frame-length and time slot concept is discussed. A comparison of proposed technique with previously developed techniques is described.

2. Material and Methods

RFID anti-collision algorithms can be categorized into two groups: Tree-based and Aloha based algorithms. A tree-based algorithm organizes tags identities in a binary search tree. Tree-based algorithms are considered accurate and have low computational cost but they are limited to few applications because of identification delay. Tree-based algorithms are examined by Hush et al [7] and by Myung et al [8]. Aloha based algorithms are less accurate and have low performance however they are more attractive because of less identification delay. EPC class 1 Generation 2protocolis based upon Dynamic Frame Size Slotted Aloha. It restricts the frame-length to 2^k {where k =0 - 15}[9] where frame-length is time slices to read a tag and each time slice is known as slot . The identification delay increases and the throughput suffers badly when the number of available tags are much larger than the number of available slots in frame or *vice versa*. Commercial readers can be categorized as fixed frame-length non-customizable, fixed frame-length user-customizable and, variable frame-length readers [10]. Fixed frame-length readers have fixed frame size so same number of slots are available in each identification cycle [5]. Those readers which can change (increase or decrease) number of slots per frame without human interaction is known as variable frame-length readers [5]. In readers with fixed frame-length, non-customizable [11-15] frame length is pre-set by manufacturer. In Readers with fixed frame-length, user-customizable [10][15,16] frame length value {k= 0 -15} can be manually set by user . In most of the variable frame-length readers users can configure frame-length only for the first time[10][15,16].Frame Slotted Aloha, Binary Frame size Aloha, Dynamic Frame size Aloha[1,2], Enhanced Dynamic Framed Slotted ALOHA[4], Dynamic Grouping Frame-Slotted Aloha[5] and Dynamic Frame Sizing with Grouping Slotted Aloha[6] are some of the examples.

2.1FSA and EPCGLOBAL CLASS-1 GEN-2 STANDARD

EPC Global Gen 2 or Class 1 Generation 2 defines the physical and logical requirements of RFID systems [17]. It operates between 860MHz ~ 960 MHz frequency. RFID systems comprised of electronic chips known as tags and reader. EPC global provides standards for RFID. It is mainly based on DFSA [18]. The EPC global Gen2 defines protocol to interaction between reader and tag using three procedures [18] as shown in figure 1.

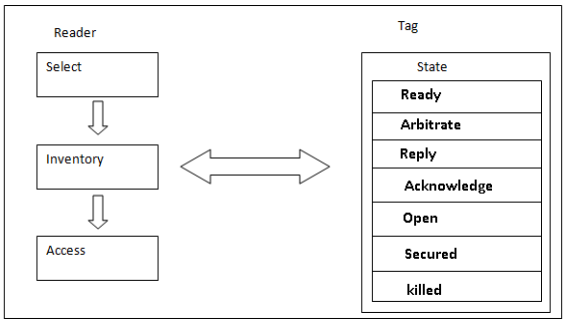

Figure 1: Read Procedure between RFID Reader and Tag [18]

During Select procedure reader selects the frame length for inventory. The frame has number of slots. The frame-length is defined by DFSA algorithm and its value is between k=0-15. During Inventory process reader identifies all the tags available in his range by sending a query command. All the available tags will reply with their own 16 bit random number. During access procedure reader will read tags and for remaining tags reader will start again from Select procedure. The complete inventory procedure is shown in figure (2).

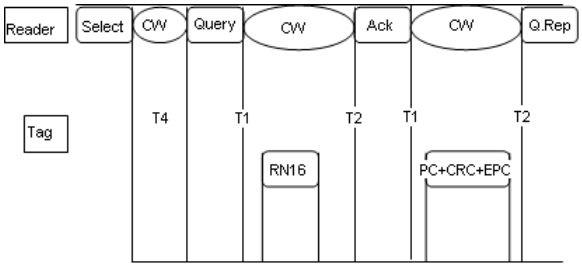

Figure 2: Generation 2 for Single tag reading

2.2 Mathematical analysis of DFSA

The maximum throughput of DFSA algorithm is approximately 37%. If *t* is the total number of tags available in reader's range and *S* is total number of slots available in frame-length then the maximum efficiency (E_{max}) can be defined using following equation [6].

$$E_{max} = \begin{cases} 1, & t = 1 \\ \left(1 - \frac{1}{S}\right)^{S-1}, & t > 1 \end{cases} \quad (1)$$

t	1	2	4	8
E_{max}	1	0.5	0.42	0.393
t	16	32	64	128
E_{max}	0.38	0.374	0.371	0.369
t	256	512	1024	2048
E_{max}	0.368	0.368	0.368	0.371

Table1. Maximum RFID Efficiency using DFSA

Table1 shows the efficiency DFSA for different frame-lengths using equation (1)

2.3 Improvement of DFSA in DFSG

Dynamic frame sizing with grouping Slotted Aloha [6] (DFGS) adjusts frame-length dynamically along with tag grouping. DFGS shows efficiency around 0.368. DFGS is a grouping technique, we examine group tagging technique in next section.

2.4 Group tagging technique with variable frame sizing

Frame-length is limited to maximum size of 2^{15}.When reading very large or infinite number of tags, tag grouping is necessary because of the limitation of frame-length. Static and dynamic grouping are two main methods of tag grouping. Division of large number of tags into equal number of groups is known as Static grouping [4]. Enhanced Dynamic Frame Slotted Aloha (EDFSA) [4] is an example of Static grouping. The number of groups is determined by dividing total number of unread tags by maximum frame-length. EDFSA performance depends upon the initial frame-length selected since it does not adjust frame-length and frame size determines the number of groups. In dynamic grouping frame-length is variable and tags read in particular frame are categorized as one group. Select and Inventory steps shown in figure (1) are repeated for the remaining tags [19].

3. Result and Discussion

3.1 FSG algorithm and its limitation

DFSG improved DFSA performance by dividing tags into groups but with limitations. The number of iteration DFSG takes to read a group depends upon initial frame size. While the frame-length is adjusted before tag reading, it gets reset to initial frame-length after every group reading which may or may not be the best choice for next group. Frame-length cannot be reduced than the initial frame size during group reading.

3.2 Proposed algorithm

We proposed an algorithm which is independent of initial frame size. The pseudo code is shown in figure (3).

```
N= number_of_Tags
Total_slots = 0 , Frame_size=0 ,
Tag_succ =0
While N > 256
Frame size = 2 ^ ceil (log2(N));
Tag_succ = ceil (N * (1 – 1/N)^(N-1)) ;
N=N – Tag_succ ;
Total_slots= Total_slots+ Frame_size
End
```

Figure 3: Pseudo code for proposed Algorithm

3.3 Proposed algorithm Comparison

MATLAB is used for simulation of proposed algorithm. Comparison of BFSA, DFSG and Proposed algorithms is described in detail.

For the number of Tags less than 256 we use same scheme as of DFSG i.e. frame length is selected from following table.

n	Q	Frame-length
2-5	2	4
6-11	3	8
12-22	4	16
23-44	5	32
45-88	6	64
89-176	7	128
177-255	8	256

Table 2. Frame size selection for Tags <256

3.4 Identification time

Identification time is associated with number of iterations and total slots taken to read all tags. Comparison result from MATLAB of proposed scheme with DFSG and BFSA is shown in Figure (4)

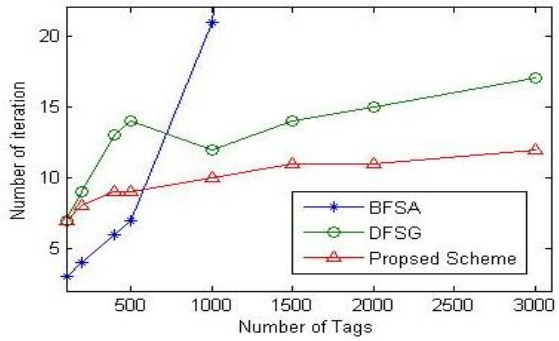

Figure4: Comparison of BFSA, DFSG and Proposed Scheme with respect to Number of iteration

Figure 4 shows that proposed algorithm takes less number of iterations for reading tags as compared to both BFSA and DFSG. When tags are less than 256 number of iteration are same for both DFSG and proposed scheme but for larger number of tags proposed scheme take less number of iteration.

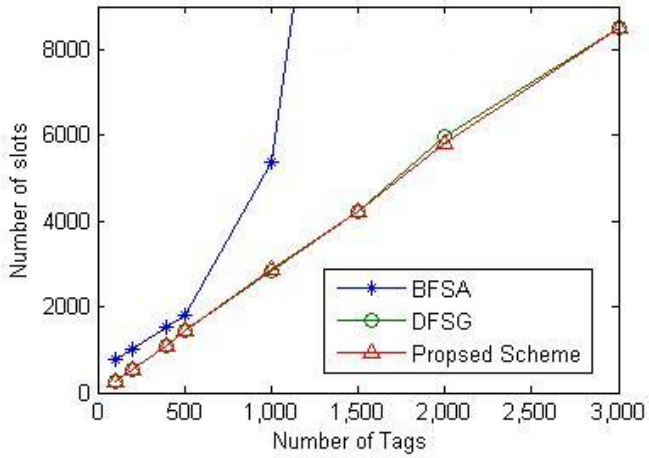

Figure 5: Number of slot comparison of BFSA, DFSG and Proposed Scheme

Figure 5 shows that proposed scheme takes less number of total slots than BFSA. We observe that number of slots for both proposed scheme and DFSG are very close. Proposed scheme take slightly less number of slots than DFSG.

3.5 Iteration and Efficiency of Proposed Scheme

From the above proposed scheme we found that it uses less number of iteration to read all the tags. The system efficiency is given by following equation.

$$\text{System Efficiency} = \frac{\text{No. of Successful Slots}}{\text{Total No. of Slots}} \quad (2)$$

Comparison of iteration and efficiency between BFSA, DFSG and proposed scheme is shown in Table 3.which shows that results obtained from proposed scheme are better than previous techniques. All results were obtained using MATLAB.

Tags	BFSA with 256 Frame-length		DFSG with 256 Frame-length		Proposed Scheme	
	Iteration	Efficiency	Iteration	Efficiency	Iteration	Efficiency
100	3	0.130	7	0.384	7	0.384
200	4	0.195	9	0.369	9	0.369
400	6	0.260	13	0.361	9	0.361
500	7	0.279	14	0.342	9	0.348
1000	21	0.186	12	0.354	10	0.346
1500	77	0.076	14	0.355	11	0.354
2000	313	0.024	15	0.335	11	0.345
3000	1313	0.008	17	0.352	12	0.353

Table 3. Comparison of BFSA, DFSG and Proposed Scheme

4 Conclusion

DFSG [6] is based upon EDFSA [4] and it improves system efficiency to a great deal as compared to BFSA and EDFSA. Improved Dynamic Frame size with tag grouping algorithm that we have just presented above further extends the performance of DFSG by reducing the number of iteration. Also it removes the dependency of algorithm on initial frame-length. The comparison of iteration, system efficiency and identification time between BFSA, DFSG and proposed algorithm is shown in above figure (4), figure (5) and table (3). Result obtained for proposed algorithm is much closer to possible optimal values.

References:

[1] Alohanet, http://en.wikipedia.org/wiki/ALOHAnet#The_ALOHA_protocol

[2] Multiple Access protocols in Computer Networks, Aloha vs Slotted aloha documentation available at: http://enggpedia.com/computer-engineering-encyclopedia/dictionary/computer-networks/1615-multiple-access-protocols-pure-aloha-vs-slotted-aloha-a-throughput

[3] N. Abramson (1970). "The ALOHA System - Another Alternative for Computer Communications"(PDF). Proc. 1970 Fall Joint Computer Conference. A

[4] S. Lee, S. Joo, C. Lee, “An Enhanced Dynamic Framed Slotted ALOHA Algorithm for RFID Tag Identification,” in the Proc. of International Conference on Mobile and Ubiquitous Systems: Networking and Services (MOBIQUITOUS), pp. 166-174, 2005.

[5] Mian Hammad Nazir , Nathirulla Sheriff “Dynamic Grouping Frame-slotted Aloha” , International Journal of Computer Applications (0975 – 8887) Volume 37– No.4, January 2012

[6] Sobia Arshad , Syed Muhammad Anwar, Mian Hammad Nazir, Shumaila Khan, “Dynamic Frame Sizing with Grouping Slotted Aloha for UHF RFID Networks” , International Journal of Computer Applications (0975 – 8887) Volume 61-No.18, January 2013

[7] Hush, D.R, Wood, C., “Analysis of Tree Algorithms for RFID Arbitration”. In Proc. of International Symposium on Information Theory, pp. 107-114, Cambridge, Massachusetts, USA, 1998.

[8] Myung, J., Lee, W., “Adaptive Splitting Protocols for RFID Tag Collision Arbitration”, MobiHoc’06, Florence, Italy, pp. 203-213, 2006.

[9] Class 1 Generation 2 UHF Air Interface Protocol Standard Version 1.0.9: “Gen 2”. Documentation available online at: http://epcglobalinc.org/standards/

[10] Samsys, RFID Reader. Documentation available on-line at: http://www.samsys.com

[11] Caen, RFID Reader. Documentation available on-line at: http://www.caen.it/rfid/

[12] ThingMagic Mercury4, RFID Reader. Documentation available at: http://thingmagic.com/

[13] Symbol, RFID Reader. Online documentation at: http://tecno-symbol.com

[14] Awid, RFID Reader. Documentation available on-line at: http://awid.com/

[15] Intermec, RFID Reader. Documentation available on-line at: http://www.intermec.com

[16] Development kit Alien 8800. Documentation available on-line at: http://alientechnologies.com/

[17] http://www.skyrfid.com/RIFD_Gen_2_What_is_it.

php

[18] A Novel Q-algorithm for EPCglobal Class-1

[19] X Huang, “An Improved ALOHA Algorithm for RFID Tag Identification”, Knowledge-Based Intelligent Information and Engineering Systems [Book] Berlin Heidelberg, Springer-Verlag, vol. 4253, pp. 1157-1162, 2006.

[20] Abraham, C., Ahuja, V., Ghosh A.K., Pakanati, P., “Inventory Management using Passive RFID Tags: A survey”, Department of Computer Science, The University of Texas at Dallas, Richardson, Texas, USA, pp. 1-16, 2002.

[21] Shih, D-H., Sun, P-L, Yen, D.C., Huang, S-M, “Taxonomy and survey of RFID anti-collision protocols”. Computer and Communications, vol. 29, pp. 2150-2166, 2006.

****

Fixed order robust Controller Design by using H_∞ Loop Shaping and Immune Algorithm for Ball and Hoop System

Faizullah Mahar
Department of Electrical Engineering, Balochistan
University of Engineering and Technology, Khuzdar, Pakistan

Abstract

This work presents an innovative design practice for determining the fixed order robust proportional-integral-derivative (PID) controller for ball and hoop system using the immune algorithm (IA). The paper demonstrates how to make use of the IA to search the optimal PID-controller gains. This approach has much better characteristics, including easy to implement, sure convergence attribute and fine computational efficacy. The optimum PID-controller tuning yields high-class solution. To support the predicted performance of the proposed IA based scheme a performance criterion i.e. cost function is also defined, and the preferred practice was more proficient and robust in getting better step response of ball and hoop system.

The simulation results demonstrate that IA- based PID controller be able to compensate the effect and improve the performance of control system. Additionally, the proposed design practice overcomes the weakness of conventional practices and improvement has been accomplished in terms of time domain performance.

Keywords

PID controller; optimization; immune algorithm and cost function.

1. Introduction

In recent times, industrial process control techniques have made great progress. Various control techniques have been developed such as adaptive control, neural control, and fuzzy control [1-2]. Amongst them, the top recognized is the proportional-integral-derivative (PID) controller, which has been widely used in the process industry for the reason that it holds simple structure and robustness in performance in wide range of operating conditions [3].

Regrettably, it became relatively hard to tune PID controller gains since several industrial plants are often hampered with problems like high order and time delay [4]. Several techniques have been proposed for the tuning of PID controller gains. The first method used the classical tuning rule proposed by Ziegler and Nichols. Mostly, which is safe to find out optimal or near optimal PID gains with Ziegler-Nichols for several industrial plants [5].

To design a controller means select the proper gains. The major point to note is that if calculated values of gains are too large, the response will fluctuate with high frequencies. On the other hand, having too small gains would mean longer settling time. Consequently, finding the best possible values gain is a significant concern in a controller design [6]. In general, the controller design practice is iterative among controller design and cost function (CF)[1] appraisal [7].

The design of controller to stabilize complex plant and to achieve specific performance is became an open problem. The researchers proposed approaches to make simpler the controller design practices. While alternative is to minimize the closed loop CF. But, there are certain difficulties essential to the fixed order robust controller design, such as to compute the best optimal value of controller gains and minimization of (CF) [8].

The fixed order robust controllers can be achieved by using H_∞ loop shaping procedure (LSP). The drawback of this design practice is the order of controller cannot be fixed a priori. The typical requirements are: little settling time, little overshoot and minimal value of CF [9].

Recent studies have proposed an IA to resolve optimization problems in the field of control systems and computer sciences [10]. The use of IA in optimization problems have been engorged owing its significance, capability in terms of implementation and robustness to perturbation.

An IA based PID controller was designed to improve the time domain performance of ball and hoop system. The IA will be used to determine the optimal controller gains [*kp*, *ki*, kd], and minimize the CF so that the controlled system could obtain good performance and robustness.

1.1 Original Plant

The original plant is given in Eq.1 has been used in [6, 7]. Ball and Hoop system, fourth order with the transfer function as given in Eq.1

$$G(s) = \frac{1}{(S^4 + 6S^3 + 11S^2 + 6S)} \qquad (1)$$

Fig.1 shows the pole zero plot of plant Eq.1. The four real poles are S=0, S=-1, S=-2 and S=-3, system is stable.

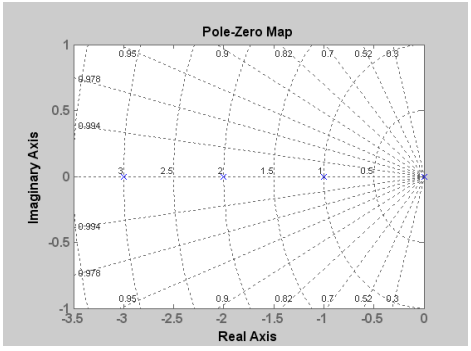

FIG. 1 SHOWS THE POLE ZERO PLOT OF NOMINAL PLANT

1 measure of performance

Perturbed plant

The perturbation to the original system transfer function has been measured in percentage. The plant poles are perturbed by 5% of the original value. Generally, perturbation in small percentage will not shift the poles in right hand side. If that is the case the plant is first needed to be stabilized by an additional local loop and then the proposed algorithm can be applied.

The plant parameters have been perturbed by 5% of the original value. The resultants transfer function is given in Eq. (2)

$$G(s) = \frac{1}{(S^4 + 6.3\,S^3 + 12.127\,S^2 + 6.9457\,S)} \qquad (2)$$

Fig.2 shows the pole zero plot of plant Eq. (2). The four perturbed poles are S=0, S=-1.0500, S=-2.100 and S=-3.1500 while system remains stable.

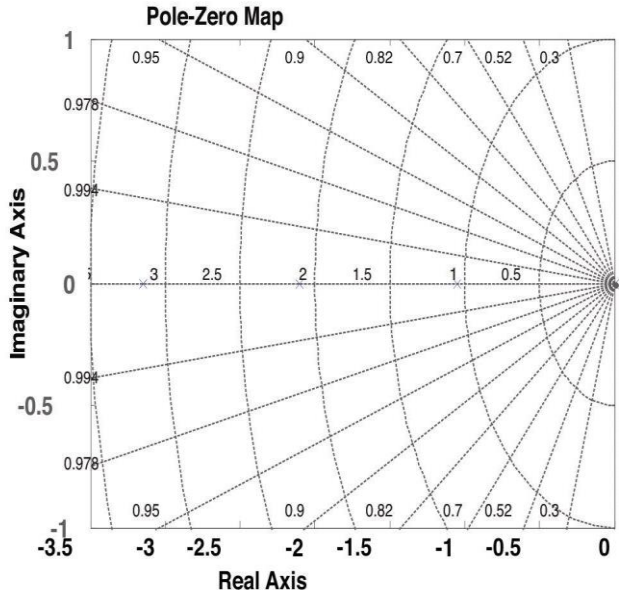

FIG. 2 SHOWS THE POLE ZERO PLOT OF PERTURBED PLANT

The paper is arranged as follows: Desired performance specifications are given in Section 2, A brief overview of $H\infty$ control design is presented in section 3, H_∞ loop shaping procedure is discussed in Section 4, Section 5 gives brief overview of immune algorithm, the deign aspects of IA based procedure is presented in Section 6, Section 7 presents experimental results and the conclusions are summarized in Section 8.

2. Desired Performance Specification

The main purpose of control system design is to provide good time domain performance of the controlled system. The best possible controller has to be designed such that the desired time domain performance specifications are meeting up. The desired specifications are given in Table.1

TABLE 1 DESIRED PERFORMANCE SPECIFICATION

H_∞- norm	≤ 2
Settling time	≤ 2 sec.
Rise time	≤ 1 sec
Stability margin	≤ 1
Steady state error	1

3. The H_∞ Control Design

Consider a system *P(s)* of Fg.3, with inputs *w* and outputs *z* measurement *y* control *u* and controller *K(s).* If *P(s)* is used to devise a design problem, then it will also incorporate weighs [9].

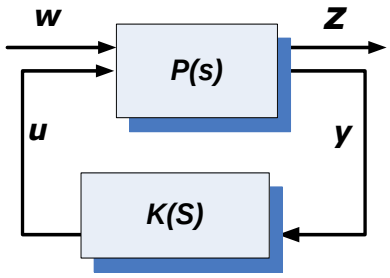

FIG.3 GENERAL H ∞ CONFIGURATION [8]

For minimizing the $H\infty$-norm of the transfer function from *w* to *z*, *P(s)* may be partitioned as given in Eq. [3]:

$$P(s) = \begin{bmatrix} P_{11}(s) & P_{12}(s) \\ P_{21}(s) & P_{22}(s) \end{bmatrix} \qquad (3)$$

The closed loop transfer function from *w* to *z* can be obtained directly as given in Eq. [4]:

$$Z = F_l(P,K)w \qquad (4)$$

Where, $F_l(P,K) = P_{11} + P_{12}K(I - P_{22}K)^{-1}P_{21}$ is called the lower fractional transformation of P and K. Therefore, the optimal H_∞ control problem is to minimize the H_∞ norm of $F_l(P,K)$, i.e, $\left\|F_l(P,K)\right\|_\infty$

4. The H∞ Loop Shaping Procedure

H_∞ loop shaping procedure (LSP) is an efficient method used for robust controllers design and has been efficiently used in a variety of applications. Two main phases are implicated in LSP [12].

In first phase the singular values of original plant are shaped by choosing proper weights W_1 and W_2. The original plant G_0 and weights are multiplied to form a shaped plant G_s as shown in Fig. [4]. The weighs can be chosen as:

$$W_1 = K_w \frac{s+\alpha}{s+\beta} \qquad (5)$$

Where K_w, α, β are positive integers, β is selected as smallest number (<< 1).

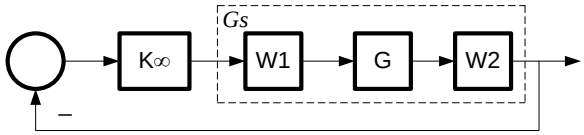

FIG. 4 BLOCK DIAGRAM OF SHAPED PLANT

In second phase the controller K_∞ is synthesized and stability margin is computed. The final controller is constructed by multiplying K_∞ with weights W_1 and W_2 as given in Eq. (6) and depicted in Fig. 5.

$$K(s)_{final} = W_1 K_\infty W_2 \tag{6}$$

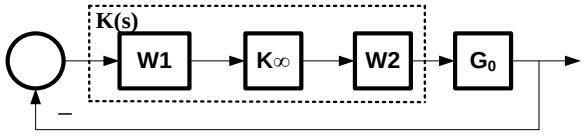

FIG.5 BLOCK DIAGRAM OF FINAL CONTROLLER

This step by step method has its groundwork in [10, 12]. After achieving the desired loop shape, H_∞-norm is minimized to find the overall stabilizing controller $K(s)_{final}$

4.1 PID Controller Background

The structure of PID controllers is very simple it works in a closed-loop system as given in Fig.6; the controller operates on the error signal that is the difference between the desired output and the actual output, and generates the actuating signal *(u)* that drives the plant. The output of a PID controller, equal to the control input to the plant, in the time-domain is as given in Eq. (7)

$$u(t) = K_p e(t) + K_i \int e(t)dt + K_d \frac{de}{dt} \tag{7}$$

The transfer function of a PID controller is found by taking the Laplace transform of Eq. (9).

$$K_p + \frac{K_i}{s} + K_d s = \frac{K_d s^2 + K_p s + K_i}{s} \tag{8}$$

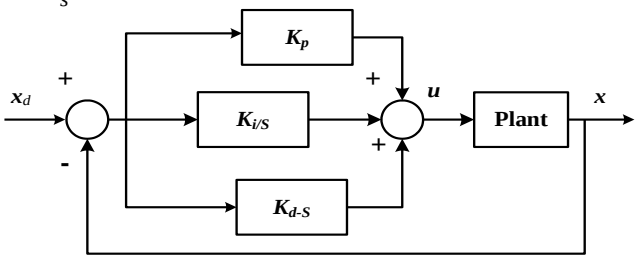

FIG. 6 STRUCTURE OF A SISO-PID CONTROLLER

4.2 H_∞ Robust Stabilization

The normalized co-prime factor of the shaped plant is $G_S = W_1 G_O W_2 = NM^{-1}$, then a perturbed plant G_Δ is written as:

$$G_\Delta = (N + \Delta_N)(M + \Delta_M)^{-1} \tag{9}$$

Where, Δ_M and Δ_N are stable unknown transfer functions representing the uncertainty in the original plant Go. Satisfying $\left\| \Delta_M \quad \Delta_N \right\|_\infty \leq \varepsilon$, here $\in$ is uncertainty boundary called stability margin [13].

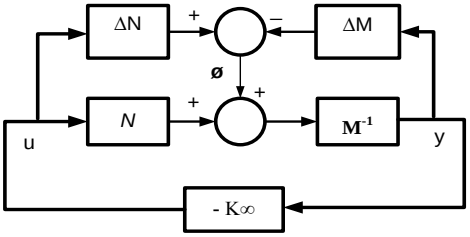

FIG.7 CO-PRIME FACTOR ROBUST STABILIZATION

Configuration shown in Fig. 7, a controller K_∞ stabilizes the original closed loop system and minimizes γ is given in Eq. (10)

$$\gamma = \inf_{stab_k} \left\| \begin{bmatrix} I \\ K_\infty \end{bmatrix} (I + G_s K_\infty)^{-1} M^{-1} \right\|_\infty \tag{10}$$

Where, γ is the H_∞-norm from γ to v and $(I + G_S K_\infty)^{-1}$ is the sensitivity function, the lowest achievable value of γ and correspondent maximum stability margin is computed by Eq. (11)

$$\gamma = \varepsilon_{\max}^{-1} = \sqrt{1 + \lambda_{\max}(XZ)} \tag{11}$$

Where λ_{max} denotes maximum Eigen value, *Z* and *X* are the solution to the Riccati equation [10-11]:

$$\begin{aligned} &(A - BS^{-1}D^T C) + Z(A - BS^{-1}D^T C)^T \\ &-ZC^T R^{-1} CZ + BS^{-1}B^T = 0 \end{aligned} \tag{12}$$

$$\begin{aligned} &(A - BS^{-1}D^T C)^T + X(A - BS^{-1}D^T C) \\ &-XBS^{-1}B^T X + C^T R^{-1} C = 0 \end{aligned} \tag{13}$$

Where, A, B, C, and D are state-space matrices of G, $S = I + D^T D$ and $S = I + D^T D$.

5. Overview of Immune Algorithm

An IA is a search method, starts with randomly initialization of antibodies. Then the fitness of each individual antibody is calculated. The transmission of one population to next takes place by means of immune aspects such as selection, crossover and mutation. The process chooses the fittest individual antibody from the population to continue in the next generation [2]. Moreover, an affinity is the fit of an antibody to the antigen. The role of antibody is to eliminate the antigen [9].

5.1 Modeling of gain matrix

The specified controller gain matrix consists of *n* elements:

$$\theta = \left[k_1, \; k_2, \; k_n \right] \qquad (14)$$

The aim of IA is to implement heuristic search for best grouping by the these *n* elements that identify the antigen form CF Fig. 8, immune aspects includes, selection, cross over, colonial affinity and mutation are engaged to implement in the algorithm [13]

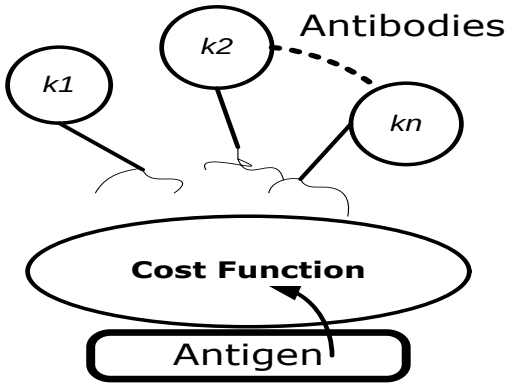

FIG.8 COST FUNCTION

6. Design Aspects of IA-PID Controller

By assuming that $K(\theta)$ is specific controller. The structure of controller has been specified previously starting the optimization procedure. The θ controller structure has been taken as vector is given by θ = [k_p, k*i*, k_d]. A set of controller parameters θ has been appraised to minimize the CF, by using Eq. (7) a controller $K(\theta)$ can be written as given in Eq. (15)

$$K(\theta) = W_1 \, K_\infty \, W_2 \qquad (15)$$

Again by assuming that W_1 and W_2 are invertible, hence,

$$K_\infty = W_2^{-1} \, K(\theta) \, W_1^{-1} \qquad (16)$$

W_2 has been selected as an identity matrix; mean that sensor noise is insignificant? By substituting Eq. (15) in Eq. (9), the H_∞-norms of the transfer functions matrix from disturbances to states, which has to be, minimized that is CF can be written as:

$$\left\| T_{zw} \right\|_\infty = \left\| \begin{bmatrix} I \\ W_1^{-1} K(\theta) \end{bmatrix} (I + G_S W_1^{-1} K(\theta)(I \quad G_S) \right\|_\infty \qquad (17)$$

5.2 Proposed approach using IA

The main steps for implementing the IA to design of robust controller are:

Step-1 calculate gamma using Eq. (11), returned variable γ is the inverse of the magnitude of uncertainty so the $\gamma \leq 4$ is requisite. If γ is > 4, it means weights are unsuitable with robust stability; the weights are to be adjusted.

Step-2 Generate initial population of antibodies as sets of parameters θ

Step-3 calculate CF of each antibody using Eq. (17) by considering θ as each string of antibodies as a vector of controller gains.

Step-4 the colonial affinity of each antibody can be calculated by using Eq. (17), best antibody in the present problem is chosen as an antigen, which has minimum CF.

$$Affinity = \frac{f(antigen)}{f(antiboby)} \qquad (18)$$

Flowchart for the above steps is depicted in Fig. 9.

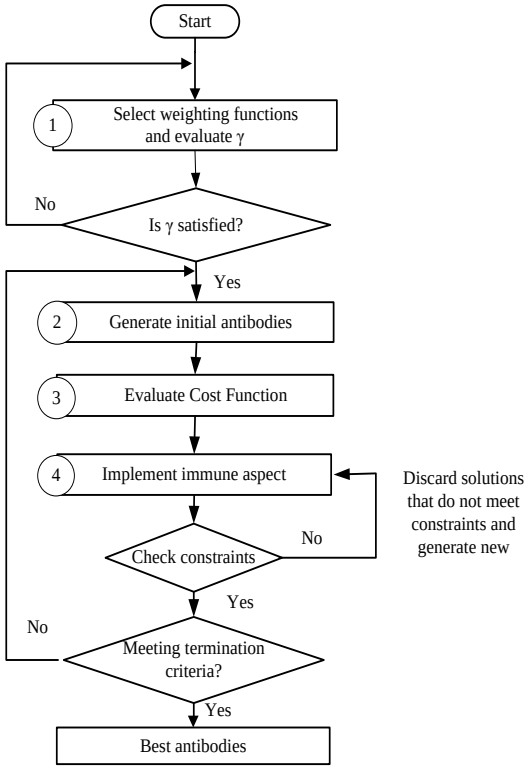

FIG. 9 FLOW CHART OF PROPOSED SCHEME

7. Simulation Results

The proposed controller and their performance evaluation criteria in time domain were implemented by MATLAB. The fixed order controller design by using IA has been set in MATLAB environment to predict performance of the proposed approach. All the simulations are performed by using MATLAB codes.

Model parameters of the nominal plant are shown in the Eq. (1) as transfer function. First, we design a controller by using LSP the weights are chosen as:

$$W_1 = \frac{0.30 + 1.0}{S + 0.001} \qquad (19)$$

Where $W_2$is the identity matrix, with these weighting functions the shaped plant is computed as?

$$G_S(s) = \frac{0.30 \, S + 1}{S^4 + 11.6 \, S^3 + 6.0 \, S^2 + 0.06 \, S} \qquad (20)$$

The stabilizing controller K_∞ is obtained by using MATLAB code is as:

$$K_\infty(s) = \frac{2.66e^{-015} S^4 + 5.32e^{-015} S^3 - 8.88e^{-016} S^2 + 0.3 \, S + 1}{S^5 + 6.01 \, S^4 + 11.06 \, S^3 + 6.1 \, S^2 + 0.06 \, S}$$

(21)

By using the LSP the final controller is obtained as:

$$K(s)_f = \frac{7.99e^{-016}S^5 + 4.26e^{-015}S^4 + S^3 + 0.09S^2 + 0.6S + 1}{S^{10} + 12S^9 + 58.2S^8 + 145.2S^7 + 195.9S^6 + 135.9S^5 + 38.6S^4 + 0.7S^3 + 0.3S^2 + 6S + 1} \quad (22)$$

The controller achieved by LSP given in Eq. (22) has very complex structure and is of 10th order controller; it appears that it would be not easy to implement that controller for practical applications.

Hence, an advantage of fixed order controller design can be gained from recommended method. An IA based PID controller has been considered fixed order robust controller; k_p, k_i and k_d are parameters of the controller that would be evaluated using IA. The exact controller structure is stated in Eq. (23)

$$K(\theta) = K_p + \frac{K_i}{s} + K_d s \quad (23)$$

The Mat lab based simulations has been carried out with representation of antibodies. The size of initial population was set as 100 antibodies. Colonial affinity was computed and single bit mutation was recycled, the IA parameters are shown in Table 2, on 52nd iteration of IA the optimum values for PID gains has been accomplished.

TABLE 2 SPECIFIED PARAMETERS FOR THE IA

Parameters	**Immune Algorithm**
Initial Population of antibodies	100
Selection Type	tournament
Crossover	one point
Crossover Probability	0.80
Mutation Type	single bit mutation

As for as convergence algorithm is concerned the IA converged after 52nd iteration, and provided minimal value of CF of 1.416 Fig.10 shows the plot of convergence of CF versus iterations of IA. This fulfils the stability margin of 0.872. The calculated optimal gains of IA-based controller are presented in Eq. (24)

$$K(\theta)^* = 0.301 + \frac{0.847}{S} + 0.42S \quad (24)$$

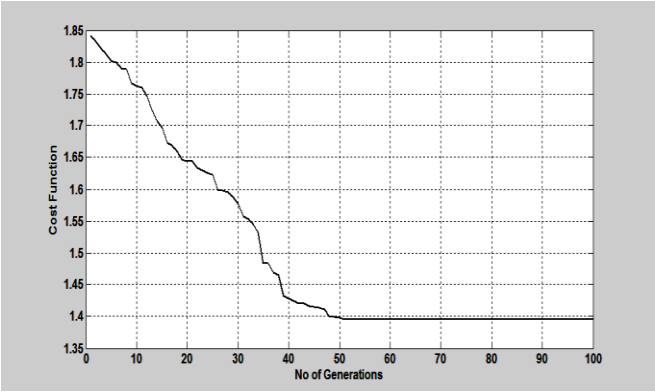

FIG. 10 CONVERGENCE OF CF VERSES ITERATIONS OF IA

The closed loop step response of the control system with IA-based controller is presented in Fig.11which presents 1.5 sec rise time, 2% overshoot, about 2 sec. settling time and zero steady state error.

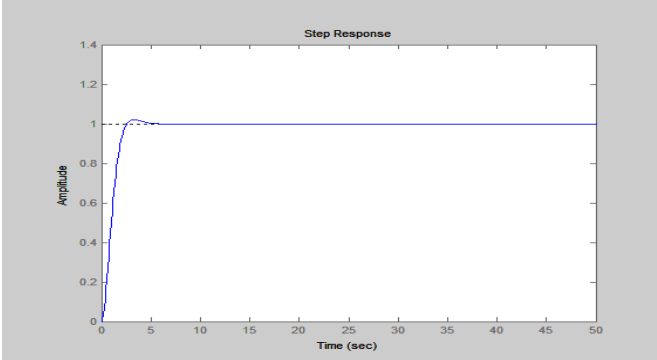

FIG. 11 CLOSED LOOP RESPONSE WITH IA CONTROLLER

7.1 Robustness Analysis

In order to validate the robustness performance of IA PID controller as given in Eq. (24) were implemented to perturbed plant Eq. (2). The closed loop step response of perturbed plant is presented in Fig.12 which presents rise time 1.5 sec., 2.2% overshoot, settling time is about 2 sec. and zero steady state error, which validates that the proposed scheme have reasonably good robustness performance.

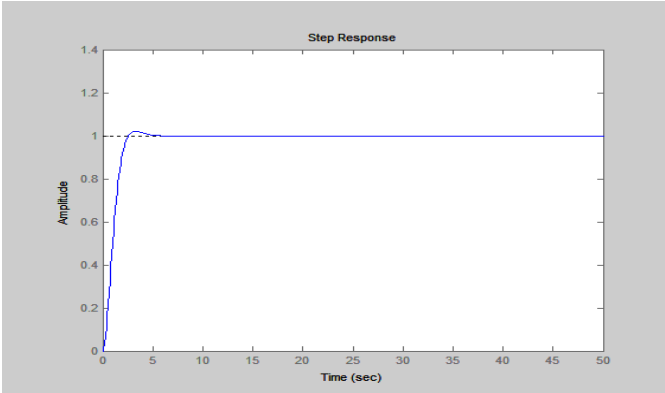

FIG. 12 ROBUSTNESS CHECK OF IA-PID CONTROLLER

8. Conclusions

In this manuscript an IA based innovative methodology has been presented. The IA has been suggested for optimization of PID controller parameter and minimization of cost function. Primary investigation demonstrates that the suggested approach can supply an optimal solution for fixed order robust PID controller.

Moreover, conventional approach used for this application experiences large settling time, large overshoot and oscillations. Henceforth, when an IA is applied to control system problems, their typical characteristics demonstrates quicker and smoother response.

REFERENCES

[1] A. Visioli, Tuning of PID controllers with fuzzy logic, Proc. Inst. Elect. Eng. Contr. Theory Applicat., 2001, 1–8

[2] T. L Seng, M. B Khalid, & R. Yusof Tuning of a neuro-fuzzy controller by genetic algorithm," IEEE Trans. Syst., Man, Cybern, *29*(1), 1999, 226–236.

[3] R. A. Krohling & J. P. Rey, Design of optimal disturbance rejection PID controllers using genetic algorithm, IEEE Trans. Evol. Comput., 5 2001, 78–82.

[4] Zwe-Lee Gaing, A Particle Swarm Optimization Approach for Optimum Design of PID Controller in AVR System, ieee transactions on energy conversion, *19*(2), 2004,

[5] Y. Mitsukura, T. Yamamoto & M. Kaneda, A design of self-tuning PID controllers using a genetic algorithm, Proc. Amer. Contr. Conf., San Diego, CA, 1999,1361–1365.

[6] Morkos S. and H. Kamal, 2012. Optimal Tuning of PID Controller using Adaptive Hybrid Particle Swarm Optimization Algorithm, International Journal of Computers, Communications Control, pp. 101–114,

[7] M. El-Said and E. Telbany, Employing Particle Swarm Optimizer and Genetic Algorithms for Optimal Tuning of PID Controllers: A Comparative Study, ICGST-ACSE Journal, vol. *7*, 2007, 49–54,

[8] T. Kawabe, & T Tagami., A real coded genetic algorithm for matrix inequality design approach of robust PID controller with two degrees of freedom, Proc. 12th IEEE Int. Symp. Intell. Contr., Istanbul, Turkey, 1997, 119–124.

[9] F. Mahar & A .A. Saad, PSO Based Fixed Order Controller Design and System Simulation," International Conference on Soft Computing and Pattern Recognition (SoCPaR 2010), Vol.*1* 2010,71-78,

[10] F. Mahar and A. A. Saad & K. Abid, Design of fixed order robust controller by using evolutionary optimization techniques: Comparison and Performance Analysis, journal of engineering and applied science. vol.*29*, 2010, 131-139

[11] D. Hai-bin, Novel Approach to Nonlinear PID parameter optimization using Ant Colony Optimization Algorithm, Journal of Bionic Engineering, 2006,73-78

[12] F. Mahar and A. A. Saad, Immune Algorithm Based Fixed Order Controller Design and System Simulation, IEEE International Symposium on Signals, Systems and Electronics, Nanjing, China, 2010, 18-24.

[13] M. Mori, M. Tsukiyma & T. Fukuda, Immune algorithm with searching diversity and IA applications to resource allocation Problem, Transactions on Instrumentation Electronics Engineering, Japan, 1993,

Quotations

- Don't tell other people your troubles. Half of them aren't interested, and the other half'll think you deserved it

  West African saying

- An intelligent enemy is better than an ignorant friend.

  North African saying

- The tyrant is only the slave turned inside out.

  North African saying

- If you wait for tomorrow, tomorrow comes. If you don't wait for tomorrow, tomorrow comes

  West African saying

- Rivlry is better than envy.

  Central African saying

- Hate has no medicine.

  West African saying

- Bitter truth is better than sweet falsehood.

  East African saying

- One pound of common sense requires ten pounds of common sense to apply it.

  Persian proverb

- Deal with the faults of others as gently as with you own.

  Chinese proverb

- Every good partnership is based on trust.
- Never trust a man who says, "Trust me."
- Trust is hard earned, and easily lost..
- Religions gretest miracle is the survival of faith.
- A man's faith, more than his house, is his castle.
- All are not saints that go to church.
- |Laughter is God's gift to mankind," proclaimed the preacher ponderously. "And mankind," responded the cynic, "is the proof that God has a sense of humor."
- All great deeds and all great thoughts have a ridiculous beginning. Great works are often born on a street corner or in a restaurant's revolving door.
- Think today and speak tomorrow
- Tomorrow is often the busiest day of the week.

LIST OF REFERES FROM ABROAD

S.#	Name	From
1	Engr. Prof. Dr. Akhtar Kalam	Professor-School of Electrical Engineering Victoria University, Melbourne, Australia Email:akhtar.kalam@vu.edu.au
2	Engr. Prof. Dr. Mahmood Nagrial	Sydney, University Australia m.nagrial@uws.edu.au
3	Engr. Prof. Dr. D. Kothari	Former Director I/C, IIT Delhi and Ex-Dy.Director (Admn) Prof. Center for Energy Studies, India Institute of Tech. Delhi New Delhi-110016, India Email:dpkvits@gmail.com
4	Dr. Muhammad Tajammal Chughati	Project Officer William Lee Innovation Centre Textiles and Papers School of Material, Manchester University, UK Email:muhammad.chughtai@manchester.ac.uk

LIST OF LOCAL REFEREES

1	Engr. Prof. Dr. K.E. Duranni	U.E.T Lahore, Pakistan Email:kedurrani@uet.edu.pk
2	Engr. Dr. Tabreez Aslam Shami	Central Punjab University, Lahore Pakistan Email:drshami@ucp.edu.pk
3	Engr. Prof. Dr. Noor M. Sheikh	U.E.T Lahore, Pakistan Email:omanchair@uet.edu.pk
4	Engr. Prof. Dr. M. Saleem Mian	U.E.T Lahore, Pakistan Email:drmsaleem@uet.edu.pk
5	Engr. Prof. Dr. Bawani Shankar Ch	U.E.T Mehran University Hyderabad Jamshroo, Pakistan. Email:bsc_itman@yahoo.com
6	Engr. Dr. Abdur Rasheed	Comsat, Abbotabad, Pakistan Email:drarashid@ciit.net.pk
7	Engr. Prof. Dr. Intesar Ahmed	Lahore College for Women University Lahore, Pakistan Email:intesart2000@yahoo.com

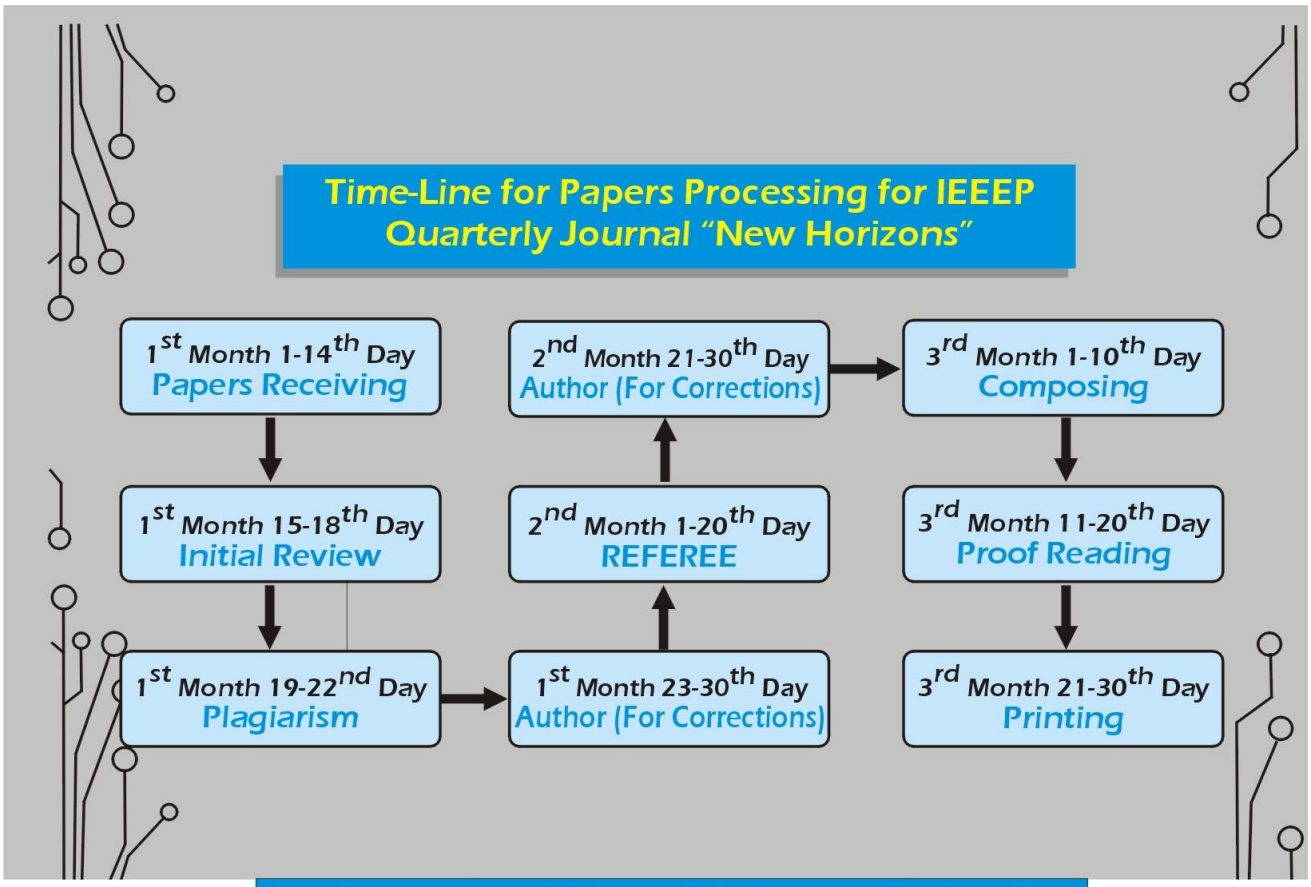

CALL FOR RESEARCH PAPERS FOR "NEW HORIZON"

Research Papers from engineers in the Disciplines of Electrical, Electronics (Including Information Technology and Telecommunications), Controls, Mechatronics, Avionics, Computers and Medical Engineering are invited for publication in "New Horizons", HEC recognized Y-Category, quarterly research journal of the Institution of Electrical & Electronics Engineers Pakistan. A soft copy of the paper may please be sent to ieeep1969@gmail.com or info@ieeep.org.pk in the following format:-

1. The research paper should be prepared in MS Word Software in Two-Column Format.
2. Select A-4 size, 1 inch margins on all four sides, 1.0 line spacing, Times New Roman Font with size 12 and justification on both sides.
3. All headings should be in capital bold letters.
4. All figures and diagrams must be properly numbered and labeled.
5. All diagrams, tables, graphs and photographs must be in Black & White.
6. All text within diagrams must be bold enough for readable clarity.
7. The papers must not contain more than 6 pages.
8. Complete references must be provided at the end of the paper.
9. The format to be followed for all references is given below:

   N.E. Nilsson and J. Mercurio "Synchronous generator capability curve testing and evaluation" IEEE. Trans. Power. Del., Vol: 9, no: 1, pp 414. 424, Jan 1994.

PLEASE NOTE: You are requested to provide a brief Resume of yourself and of the co-authors (if any) alongwith the paper(s). Also please provide contact numbers and email addresses of all authors. Kindly note that papers/material as PDF Files will not be accepted.

The Institution of Electrical & Electronics Engineers Pakistan Ph: +92 (42) 36305289 Fax: (042) 36360287
4 Lawrence Road, Lahore-54000, Pakistan. Email: info@ieeep.org.pk Website: www.ieeep.org.pk